Bayesian chronological analyses consistent with synchronous age of 12,835–12,735 Cal B.P. for Younger Dryas boundary on four continents

James P. Kennett[a,1], Douglas J. Kennett[b], Brendan J. Culleton[b], J. Emili Aura Tortosa[c], James L. Bischoff[d], Ted E. Bunch[e], I. Randolph Daniel Jr.[f], Jon M. Erlandson[g], David Ferraro[h], Richard B. Firestone[i], Albert C. Goodyear[j], Isabel Israde-Alcántara[k], John R. Johnson[l], Jesús F. Jordá Pardo[m], David R. Kimbel[n], Malcolm A. LeCompte[o], Neal H. Lopinot[p], William C. Mahaney[q], Andrew M. T. Moore[r], Christopher R. Moore[j], Jack H. Ray[p], Thomas W. Stafford Jr.[s,t], Kenneth Barnett Tankersley[u], James H. Wittke[e], Wendy S. Wolbach[v], and Allen West[w,2]

[a]Department of Earth Science and Marine Science Institute, University of California, Santa Barbara, CA 93106; [b]Department of Anthropology, Pennsylvania State University, University Park, PA 16802; [c]Departament Prehistoria i Arqueologia, Universitat de Valencia, E-46010 Valencia, Spain; [d]Berkeley Geochronology Laboratory, Berkeley, CA 94709; [e]Geology Program, School of Earth Science and Environmental Sustainability, Northern Arizona University, Flagstaff, AZ 86011; [f]Department of Anthropology, East Carolina University, Greenville, NC 27858; [g]Museum of Natural and Cultural History, University of Oregon, Eugene, OR 97403; [h]Viejo California Associates, Joshua Tree, CA 92252; [i]Lawrence Berkeley National Laboratory, Berkeley, CA 94720; [j]South Carolina Institute of Archaeology and Anthropology, University of South Carolina, Columbia, SC 29208; [k]Instituto de Investigaciones Metalúrgicas, Departamento de Geología y Mineralogía, Universidad Michoacana de San Nicolás de Hidalgo, 58060 Morelia, Michoacán, Mexico; [l]Santa Barbara Museum of Natural History, Santa Barbara, CA 93105; [m]Departamento de Prehistoria y Arqueología, Facultad de Geografía e Historia, Universidad Nacional de Educación a Distancia, E-28040 Madrid, Spain; [n]Kimstar Research, Fayetteville, NC 28312; [o]Center of Excellence in Remote Sensing Education and Research, Elizabeth City State University, Elizabeth City, NC 27909; [p]Center for Archaeological Research, Missouri State University, Springfield, MO 65897; [q]Quaternary Surveys, Thornhill, ON, Canada L4J 1J4; [r]College of Liberal Arts, Rochester Institute of Technology, Rochester, NY 14623; [s]AMS [14]C Dating Centre, Department of Physics & Astronomy, University of Aarhus, 8000 Aarhus C, Denmark; [t]Centre for GeoGenetics, Natural History Museum of Denmark, Geological Museum, DK-1350 Copenhagen, Denmark; [u]Departments of Anthropology and Geology, University of Cincinnati, Cincinnati, OH 45221; [v]Department of Chemistry, DePaul University, Chicago, IL 60614; and [w]GeoScience Consulting, Dewey, AZ 86327

The Younger Dryas impact hypothesis posits that a cosmic impact across much of the Northern Hemisphere deposited the Younger Dryas boundary (YDB) layer, containing peak abundances in a variable assemblage of proxies, including magnetic and glassy impact-related spherules, high-temperature minerals and melt glass, nanodiamonds, carbon spherules, aciniform carbon, platinum, and osmium. Bayesian chronological modeling was applied to 354 dates from 23 stratigraphic sections in 12 countries on four continents to establish a modeled YDB age range for this event of 12,835–12,735 Cal B.P. at 95% probability. This range overlaps that of a peak in extraterrestrial platinum in the Greenland Ice Sheet and of the earliest age of the Younger Dryas climate episode in six proxy records, suggesting a causal connection between the YDB impact event and the Younger Dryas. Two statistical tests indicate that both modeled and unmodeled ages in the 30 records are consistent with synchronous deposition of the YDB layer within the limits of dating uncertainty (~100 y). The widespread distribution of the YDB layer suggests that it may serve as a datum layer.

Younger Dryas | comet | Bayesian | radiocarbon | synchroneity

A ccording to the Younger Dryas Impact Hypothesis (YDIH) (1), a major cosmic episode of multiple airbursts/impacts occurred at 12,800 ± 300 calendar years before 1950 (Cal B.P. represents calendar years before A.D. 1950, unless otherwise noted; 95% probability) or 12,950–12,650 Cal B.P. at 68% probability. This event produced the Younger Dryas boundary (YDB) layer, displaying peaks in a variable assemblage of spherules (glassy and/or magnetic—inferred to be impact ejecta and therefore, for simplicity, referred to below as impact-related spherules), high-temperature minerals and melt glass, nanodiamonds, charcoal, carbon spherules, glass-like carbon, aciniform carbon (soot), nickel, iridium, platinum, and osmium. The event may have triggered the Younger Dryas episode of abrupt climate change, contributed to the end-Pleistocene megafaunal extinctions, and initiated human population reorganization/decline across the Northern Hemisphere (1–5). Because a temporally singular event is proposed, the YDIH requires dates on the YDB layer to be essentially isochronous across four continents within the limits of dating methods.

In a test of synchroneity, it is ideal to have numerous, highly accurate, and precise dates to develop robust chronological models (6). The term "date" represents a measured value, and "age" refers to real or modeled calendar years. However, when developing high-precision chronologies, there are multiple challenges that are amplified in Pleistocene age deposits. Modern accelerator mass spectrometry (AMS) radiocarbon (^{14}C) measurements are typically very precise, with uncertainties of ±20 y to ±30 y at 11,000 ^{14}C years B.P., but high precision does not mean high accuracy. Numerous problems can produce erroneous ages

Significance

A cosmic impact event at ~12,800 Cal B.P. formed the Younger Dryas boundary (YDB) layer, containing peak abundances in multiple, high-temperature, impact-related proxies, including spherules, melt glass, and nanodiamonds. Bayesian statistical analyses of 354 dates from 23 sedimentary sequences over four continents established a modeled YDB age range of 12,835 Cal B.P. to 12,735 Cal B.P., supporting synchroneity of the YDB layer at high probability (95%). This range overlaps that of a platinum peak recorded in the Greenland Ice Sheet and of the onset of the Younger Dryas climate episode in six key records, suggesting a causal connection between the impact event and the Younger Dryas. Due to its rarity and distinctive characteristics, the YDB layer is proposed as a widespread correlation datum.

and age reversals in stratigraphic sections (2, 7–9). For example, ^{14}C concentrations have varied unevenly over time for many reasons, including from carbon turnover in the deep oceans, fluctuations in Earth's magnetic field, the release of ^{14}C from biomass burning, influx of ^{14}C from long-period comets, and variations in cosmic radiation (solar and galactic and from supernovae; for details, see *SI Appendix, Dating Information*). In addition, there can be considerable uncertainty about the association of charcoal ages with paleontological and archaeological assemblages, caused by the vertical transport of charcoal in sedimentary sequences through many processes, including plant bioturbation (especially roots), animal bioturbation, and redeposition by wind, water, and ice. Furthermore, a measured ^{14}C date may be inaccurate for multiple reasons, including the old wood effect, or inbuilt age (7), as, for example, when burning a 200-y-old tree causes the fire's age to appear to be 200 y too old. Accuracy also may be affected by improper handling and pretreatment of samples before dating and by uncertainties in the current ^{14}C calibration curves. All of these problems currently make it impossible to date an end-glacial event with better than multidecadal to centennial accuracy, whether it is a Clovis campfire, mammoth kill site, or cosmic impact event. Regardless, dating uncertainties must be carefully addressed to obtain the best possible age estimates (see *SI Appendix, Dating Information and Figs. S1 and S2*).

Meltzer et al. (10) rejected 26 of 29 YDB sites, claiming that the ages of those sites do not fall within the previously published YDB age span of 12,950–12,650 Cal B.P. and thus could not have resulted from a single impact event (table 3 of ref. 10). Those authors criticized previous YDB age–depth models (11–13), but in doing so, they often improperly compared YDB dates by using median ages without considering inherent uncertainties, as discussed in site descriptions below and in *SI Appendix*.

In this contribution, we model the age of YDB deposits at 23 locations, chosen primarily because independent workers at all 23 sites had previously identified the stratum that corresponds in age to the Younger Dryas onset. In addition, at 17 of 23 sites, two or more independently published radiocarbon or optically stimulated luminescence (OSL) dates were already available, and the other 5 sites were previously dated by YDIH proponents (see *Methods* and *SI Appendix*, Tables S1 and S2 and Fig. S3, for details and map). Using Bayesian analyses, we address the following questions. (*i*) At each YDB site investigated, what is the best age estimate for the proxy-rich YDB layer? (*ii*) Do these modeled ages fall within the previously published YDB age range of 12,950–12,650 Cal B.P. (11–13)? (*iii*) What is the probability that the collective ages of the YDB layer resulted from a single isochronous event? (*iv*) If so, what is a revised probability age distribution for that event? (*v*) Is the modeled age of the YDB event consistent with the Younger Dryas onset, as determined by dates from the Greenland Ice Sheet, speleothems (cave deposits), lake cores, ocean cores, and tree rings? (*vi*) Have other researchers raised valid age-related issues (10, 14–17)?

To explore a climate connection, we modeled six records that report the age of earliest onset for the Younger Dryas, proposed to be coeval with the YDB cosmic impact event (1). We also compared all records to the age of the platinum peak reported in the Greenland Ice Sheet, interpreted by Petaev et al. (18) to mark a cataclysmic extraterrestrial impact event exactly at the earliest onset of the Younger Dryas climate episode. In addition to the 23 YDB sites, 9 sites display a variable assemblage of impact-related proxies, but they lack sufficient temporal and/or stratigraphic resolution for Bayesian statistical analysis and will be discussed only briefly.

The YDB chronology is the focus of this contribution, so, for further information about site descriptions, geological settings, archaeological and paleontological significances, and additional references, see individual sites discussed in *SI Appendix*. Previous papers have addressed the nature and origin of YDB impact-related proxies in detail, and, therefore, we consider these issues only briefly here. For more information, see the table that lists representative contributions by YDIH proponents, opponents, and independent researchers (*SI Appendix*, Table S2).

Results and Discussion

Calibrating Direct [14]C Dates. The process of radiocarbon calibration produces probability density functions, meaning that some unknown true age will fall within a specified age range at a certain percentage probability, e.g., 68%. In traditional statistics, those percentages are variously known as SDs or sigma (σ), but in Bayesian statistics, they are referred to as credible intervals, abbreviated here as CI. (19). Here, we use 68%, 95%, and 99% CI to represent degrees of uncertainty. A single calibrated calendar year is insufficient to represent the dating uncertainties involved, and thus, a probability, such as 68% or 95% CI, should always be assigned to each date (19, 20). Michczynski (21) observed that many researchers continue to present a single point date without reporting the uncertainties, due to convenience and simplicity, but doing so yields poor estimates of true ages. This is because there is only a very small statistical likelihood, typically <0.5%, that the median or mean date of a probability distribution represents the true calendar year for an event (Fig. 1).

Meltzer et al. (page 9 of ref. 10) ostensibly agreed with the criticism of point estimates and wrote, "Using just a single point estimate—whether a median, midpoint, or weighted mean—fails to account for uncertainties in the age estimate and thus leads to questionable regression results." Later, referring to their table 3 (10), they claimed, "9 of the 11 sites in this group have predicted ages for the supposed YDB that fall outside the YD onset time span." However, they contradicted their stated position by comparing YDB single dates without using the appropriate 68% or 95% probability. Furthermore, they did not use established principles of "chronological hygiene," meaning that, for example, they sometimes used an average age calculated from multiple charcoal dates from a single stratum. That practice is inappropriate when an old wood effect has been identified, in which case, short-lived samples (twigs, seeds, etc.) or the youngest dates from a single stratum should be given priority (*SI Appendix, Dating Information*) (2, 22).

For the nine YDB sites rejected by Meltzer et al. (10), one or more dates were acquired directly from the layer containing YDB impact proxies, in accordance with Telford et al. (8), who concluded that the age of any short-term event is best constrained by using dates from directly within or as close as possible to the event layer. To investigate, we used the IntCal13 curve within OxCal to calibrate the dates with uncertainties and
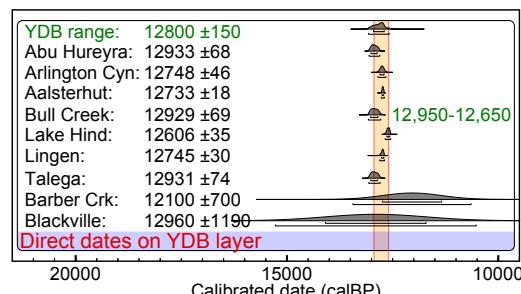
Fig. 1. Radiocarbon dates from directly within the YDB layer at nine localities. The published YDB age range is in green text; the vertical gold bar denotes the YDB age range of 12,950–12,650 Cal B.P. at 68%, which overlaps the age range distributions from all nine sites. Dates are from Kinzie et al. (9), except for Aalsterhut (15), Barber Creek (13), and Talega (13).

compared them with the previously published YDB age range. For these nine sites from four countries (United States, Canada, Germany, and Syria), geographically separated by ∼12,000 km, all nine YDB ages fall within the previously published YDB range of 12,950–12,650 Cal B.P. (Fig. 1). This finding contradicts Meltzer et al. (10) and agrees with previously published YDIH contributions (1, 9, 11–13).

Background for YDB Bayesian Analyses. Previously, proponents and opponents of the YDIH produced age–depth models using various types of regression algorithms. Even though widely used, regression models suffer from limitations, and, therefore, the use of Bayesian analyses to produce age models has become increasingly common (23–25). Such analyses can (*i*) calculate and compare millions of possible age models (iterations), unlike regression algorithms that calculate only one; (*ii*) integrate prior external information relevant to dating, e.g., the law of superposition (deepest is oldest); (*iii*) identify outlying dates that are too young or too old [e.g., the old wood effect (7)]; (*iv*) efficiently merge disparate data sets, e.g., from stratigraphy, archaeology, palynology, and climatology; (*v*) evaluate a cluster of dates for contemporaneity; (*vi*) overcome some of the inherent biases of various dating methods that tend to favor some calendar dates over others (26); and (*vii*) present a robust statistical model that

explicitly represents all modeling assumptions and data input. Because of these advantages, Bayesian age–depth modeling is considered more robust and flexible than other types (23, 24), and, therefore, multiple disciplines now commonly use Bayesian analytical programs [e.g., BCal (27), BChron (28), OxCal (23, 24), and Bacon (25)]; see *SI Appendix, Dating Information* and *Methods*.

Bayesian Models for 23 Sites. For this paper, we used the IntCal13 calibration curve in the OxCal computer program for Bayesian statistical analysis (v4.2.4) (23, 24), which has three principal pertinent routines: ^{14}C calibration, calibrated age modeling, and contemporaneity testing. OxCal produces a modeled age distribution that is summarized in multiple ways, including as a mean age with uncertainties (±68% CI) and as a distribution of ages at 68%, 95%, and 99% CI. We used three different types of OxCal coding: (*i*) P_Sequence code, in which dates are associated with depths; (*ii*) Sequence code with Boundaries, for placing dates into groups with specified boundaries, between which the stratigraphic order is known, but exact depths are unknown or unclear; and (*iii*) Sequence coding with Phases, for placing dates into chronological groups, because the stratigraphic order is unknown or unclear.

All modeled ages were rounded to the nearest 5 y. For every site, we report the age ranges at 95% CI, along with the mean age and ±68% CI, because reporting both formats provides

LOCATION	AGE	Uncertainty (68%)	RANGE (upper 95%)	RANGE (lower 95%)	# Total dates	# Rejected dates	# Accepted dates	Quality ranking	STRENGTHS						DISADVANTAGES					
Abu Hureyra	12825	55	12935	12705	37	8	29	High	● ● ● · ● ·						· · ● · ·					
Arlington Cyn	12805	55	12925	12695	16	0	16	High	● ● ● ● ● ●						· · ● · ●					
Aalsterhut	12780	35	12845	12725	14	0	14	High	● ● ● · · ●						· · · · ·					
Big Eddy	12770	85	12935	12580	30	2	28	High	· ● ● · ● ·						· · · · ·					
Bull Creek	12840	75	12995	12710	12	0	12	High	● ● ● ● · ·						· · · · ·					
Daisy Cave	12730	320	13320	12050	20	10	10	High	· ● · · · ·						· ● · · ●					
Lake Hind	12745	180	13190	12550	12	1	11	High	· · · · ● ·						· · · ● ●					
Lingen	12735	85	12910	12520	2	0	2	HIgh	● · ● · ● ●						● · · · ·					
Sheriden Cave	12840	120	13110	12625	30	1	29	High	· ● · ● ● ●						· · · · ●					
Barber Creek	12865	535	13945	11865	14	1	13	Med	● · ● · · ·						· ● · · ·					
Blackwater	12775	365	13510	12090	29	1	28	Med	· ● · ● · ●						· · ● · ●					
Indian Creek	12750	425	13495	11805	8	0	8	Med	· · · · ● ·						· · · · ·					
Lindenmeier	12775	180	13195	12440	11	1	10	Med	· ● · · ● ·						· · · · ·					
Murray Spgs	12750	235	13195	12255	33	6	27	Med	· ● · ● ● ●						· · ● · ·					
Santa Maira	12785	295	13265	12070	11	0	11	Med	· · · · · ·						● · · · ·					
Talega	12860	150	13075	12545	12	0	12	Med	● · ● · · ·						· · · · ·					
Topper	12785	185	13085	12365	11	0	11	Med	· · · ● · ●						· ● · · ·					
Blackville	12820	1080	15015	10705	5	2	3	Low	● · · · · ·						● ● ● ● ·					
Lake Cuitzeo	12850	570	14265	12195	22	11	11	Low	· · ● ● · ·						● ● ● · ●					
Lommel	12735	790	14410	11325	17	1	16	Low	· · ● · ● ●						● ● · · ·					
Melrose	12255	2405	17185	7710	3	1	2	Low	● · · · · ·						● ● ● ● ●					
Mucunuque	12845	630	13550	11335	3	0	3	Low	· · ● · · ·						● · · · ·					
Ommen	12750	560	13605	11425	2	0	2	Low	· · ● · · ●						● · · · ·					
Chobot	·	·	·	·	3	·	·	x	· · ● · · ·						● ● ● ● ·					
Gainey	·	·	·	·	5	·	·	x	· · ● · · ·						● ● ● ● ·					
Kangerlussuaq	·	·	·	·	2	·	·	x	· · ● · · ·						● ● · · ·					
Kimbel Bay	·	·	·	·	7	·	·	x	· · ● · · ·						● · ● · ·					
Morley	·	·	·	·	·	·	·	x	· · ● · · ·						● · · ● ·					
Mt.Viso	·	·	·	·	·	·	·	x	· · ● · · ·						● · · · ·					
Newtonville	·	·	·	·	2	·	·	x	· · ● · · ·						● · · ● ·					
Paw Paw Cove	·	·	·	·	1	·	·	x	· · ● ● · ·						● · · · ●					
Watcombe	·	·	·	·	2	·	·	x	· · ● · · ·						● · · · ·					

Fig. 2. YDB site details. LOCATION column lists sites. AGE columns show Bayesian modeled ages at 68%; RANGE is at 95% CI. DATE columns list total dates used, dates accepted, and dates rejected by OxCal as outliers. QUALITY ranks as high, medium, low, and not modeled. STRENGTHS and DISADVANTAGES are listed by category.

greater clarity. After analyses of 354 dates at 23 YDB sites, the chronology for each site was ranked according to estimated quality, ranging from high to low, as discussed below (summarized in Fig. 2; for OxCal's coding, see *SI Appendix, Coding*).

High-Quality Chronologies. Bayesian statistical models for 9 of 23 sites are discussed in this section and in *SI Appendix*. These sites are considered high quality because they (*i*) mostly have ^{14}C dates from directly within the proxy-rich sample extracted from the YDB layer; (*ii*) have a high total number of dates per site (avg. 19 dates); (*iii*) have lower uncertainties than lesser quality dates (avg. 112 y); (*iv*) typically contain multiple temporally diagnostic indicators, including sedimentary and paleobiological records; and/or (*v*) usually contain temporally diagnostic cultural artifacts and megafaunal remains.

Abu Hureyra, Syria. This site was located on an archaeological mound, or "tell," ~14 km west of Al Thawra, Syria, and is now inundated by Lake Assad (29). The 5-cm-thick YDB sample was at a depth of 402.5–407.5 cm below surface (cmbs) and contained peaks in impact-related spherules, carbon spherules, nano-diamonds, and high-temperature melt glass and minerals (9, 12, 13).

For this site, the sequence of human cultural traditions is represented as Phases 1, 2, and 3 (the latter is the youngest), with the YDB layer occurring between Phases 1 and 2 (*SI Appendix, Fig. S4*). Based on changes in pollen and seeds, the YDB layer at Abu Hureyra is coeval with the Younger Dryas onset, which initiated significant cultural changes, including the adoption of early cultivation practices that later led to the emergence of agriculture in the Middle East (5, 29).

From a 7 × 7 m excavated pit, Moore et al. (29) acquired 37 ^{14}C dates, and OxCal generated a sequence-phase stratigraphic model using 29 of those dates and rejecting 8 dates as outliers (dates that appear either too young or too old for the statistical model). For details on rejection of outliers, see *SI Appendix, Prior Information in OxCal*. One ^{14}C date acquired from directly within the proxy-rich YDB sample has a modeled range of 12,935–12,705 Cal B.P. at 95% (12,825 ± 55 Cal B.P. at 68%). That date overlaps the previously published YDB age of 12,950–12650 Cal B.P. (*SI Appendix, Fig. S4 and Table S3*) (12, 13). For Abu Hureyra, Meltzer et al. (10) modeled a date of 13,044 Cal B.P. and claimed the YDB to be 144 y too old. However, they overlooked the presence of one age of 12,825 ± 55 Cal B.P. at 68% CI that is directly from the proxy-rich layer and falls within the YDB age range. Also, they presented a modeled YDB age as a point date without considering dating uncertainties.

Arlington Canyon, CA. This site is located on the northwest coast of Santa Rosa Island, one of California's Northern Channel Islands, ~52 km southwest of Santa Barbara (2, 13). Kennett et al. (2) sampled a 5.03-m-thick profile that includes the YDB layer, concluding that the sequence formed within a catchment basin that underwent rapid deposition at ~12,800 cal BP. The 111-cm-thick YDB stratigraphic section from 392 to 503 cmbs contains abundance peaks of impact-related spherules, nanodiamonds, carbon spherules, and aciniform carbon.

Kennett et al. (2) provided 16 dates, 12 of which are from directly within the proxy-rich YDB horizon. From these, OxCal modeled the dates in the proxy-rich YDB interval to obtain a YDB age of 12,805 ± 55 Cal B.P. at 68% (12,925–12,695 Cal B.P. at 95%) (Fig. 3 and *SI Appendix, Table S4*). Meltzer et al. (10) presented a median point date of 13,106 Cal B.P. and rejected the age of the Arlington Canyon YDB layer as being 308 y too old. However, their conclusion is incorrect, because they did not consider the uncertainties for their date and overlooked the substantial old wood effect from long-lived conifers that were widespread on the Channel Islands until ~12,800 y ago (2, 9).

Aalsterhut, Netherlands. Extending across northwestern Europe, the Usselo horizon is a buried eolian soil with high concentrations of charcoal at its upper boundary (15). The Usselo layer is buried by
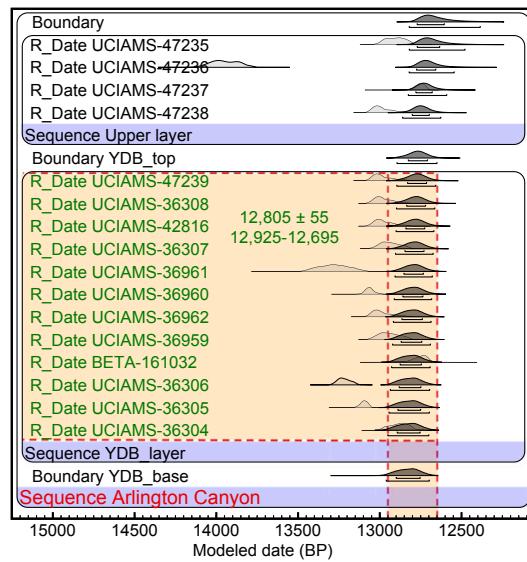

Fig. 3. Age sequence model for Arlington Canyon, CA. For this and chronological figures below, the vertical dashed lines represent the previously published YDB range of 12,950–12,650 Cal B.P. (9, 13). Horizontal red dashed lines represent the bounds of the proxy-rich sample. Laboratory numbers of dates are along the left side, with dates falling within the YDB interval shown in green text. R_Date represents ^{14}C dates, and C_Date, when present, represents OSL, varve, and ice layer calendar dates. OxCal's individual unmodeled probability distribution curves are shown in light gray, and modeled probability distributions are shown in dark gray. Boxed areas represent separate chronostratigraphic Phases or Sequences, and the probability distributions between phases represent the likely ages of transition. Phases mainly were identified by earlier site investigators in stratigraphic order, and dates within each Phase typically are in chronological order.

an overlying regional horizon, the Coversands, and the boundary between these lithologic units marks the onset or early years of the Younger Dryas episode (15). At the Aalsterhut site, van Hoesel et al. (15) reported nanodiamonds embedded in glass-like carbon from the top of the Usselo layer at a depth of 8.25–10 cm below the top of their sampled interval (they did not report the measured depth below surface).

Combining 14 ^{14}C dates, van Hoesel et al. (15) used OxCal to calculate an average median age for the entire 10-cm-thick section of 12,733 ± 18 Cal B.P. (recalibrated with IntCal13). However, 11 of the 14 dates are from the upper 8.25 cm, which contain no reported nanodiamonds. Because it is inappropriate to mix dates from nonproxy layers with those from the proxy-rich layer when dating a potential YDB layer, the average date reported by van Hoesel et al. (15) is incorrect, so we developed a new age model for the site using the same dates. OxCal used the three dates on the nanodiamond-rich interval from 8.25 cm to 10 cm to model an age range of 12,845–12,725 Cal B.P. at 95% (12,780 ± 35 Cal B.P. at 68%) (*SI Appendix, Fig. S5 and Table S5*).

van Hoesel et al. (15) compared their Aalsterhut age with that from Arlington Canyon and concluded that their nanodiamond-rich layer was not the YDB but instead postdated it by 200 y. However, that conclusion is contradicted by their own observation that the age of the Aalsterhut nanodiamond layer overlaps the age of the YDB layer at Murray Springs. Also, they did not consider the old wood effect, which makes their average age for Arlington Canyon too old (see *Arlington Canyon, CA*). Finally, they compared three YDB sites, but those had been calibrated with different ^{14}C calibration curves and had not been recalibrated, as is standard practice. To investigate the purported age difference, we obtained a Bayesian age range for Aalsterhut of 12,813–12,724 Cal B.P. at 95% CI that falls completely within
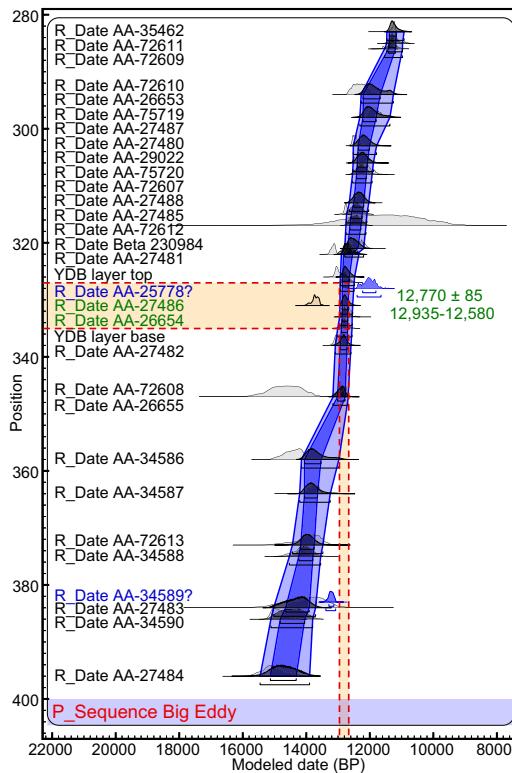
Fig. 4. Age–depth model for Big Eddy. The lighter blue continuous curve represents 95% probability, and the darker blue represents 68%. OxCal rejected the dates in blue text as outliers, meaning that they were statistically too old or young for the model.

the range for Arlington Canyon at 12,925–12,695 Cal B.P. at 95% CI. Thus, there is no 200-y age difference.

Big Eddy, MO. This site is located ~4.5 km north of Stockton in the lower Sac River valley (13). The 8-cm-thick YDB sample contains a peak in YDB impact-related spherules at a depth of 327–335 cmbs. This site contains well-stratified, culturally rich deposits that include Clovis-age ^{14}C dates on a hearth feature and associated stone tools (13). To develop an age–depth model, we used 28 ^{14}C dates (10, 13) (Fig. 4 and *SI Appendix*, Table S6) and rejected 2 ^{14}C dates, consistent with the previous observation of redeposited charcoal (13). The age range for the YDB interval is 12,935–12,580 Cal B.P. at 95% (12,770 ± 85 Cal B.P. at 68%), matching the previously published YDB age.

Bull Creek, OK. This site lies along Bull Creek, an intermittent stream located in the panhandle of Oklahoma, where the 9-cm-thick YDB sample (298–307 cmbs) contained peaks in impact-related spherules, aciniform carbon, and nanodiamonds, which have been independently confirmed (9, 30). Of 12 available ^{14}C dates, 1 is reported at a depth of 307 cm from within the interval that included the nanodiamond-rich YDB sample (298–307 cmbs). The OxCal program generated a modeled YDB age of 12,995–12,710 Cal B.P. at 95% (12,840 ± 75 Cal B.P. at 68%), falling within the published YDB age range (*SI Appendix*, Fig. S6 and Table S7).

Daisy Cave, CA. Located ~15 km west of Arlington Canyon, this cave–rockshelter complex is on the northeast coast of San Miguel Island, off the Southern California coast (9, 31). The YDB layer is at a depth of 79–81 cmbs and contains carbon spherules, glass-like carbon, and nanodiamonds. That layer's stratigraphic position is consistent with the palynological record, showing the transition from pine-dominated to oak-dominated forests in the area beginning at the Younger Dryas onset (31).

More than 20 AMS ^{14}C dates (10 on charcoal and 10 on shells) were acquired from a sample pit less than 1 m away from the stratigraphically correlated YDB profile. Only the 10 high-quality charcoal dates on short-lived samples (charred twigs) from this finely stratified sequence were used to generate a stratigraphic model for the YDB at the top of a darker layer, providing an age range of 12,730 ± 320 Cal B.P. at 68% (range of 13,220–12,050 Cal B.P. at 95%) (Fig. 5 and *SI Appendix*, Table S8).

Murray Springs, AZ. This well-known Clovis site is located 10 km east of Sierra Vista in a dry stream channel in the San Pedro Valley (13, 32, 33). The YDB layer is immediately beneath a black mat layer (33) at a depth of 246–247 cmbs and contains peaks in impact-related spherules, carbon spherules, aciniform carbon, nanodiamonds, melt glass, iridium, and nickel (1, 9, 13, 34).

We used 27 of 33 ^{14}C dates, acquired <40 m away from the sampling site, to produce a modeled age for the YDB of 12,750 ± 235 Cal B.P. at 68% (13,195–12,255 Cal B.P. at 95%). Previously, Haynes (33) reported an average calibrated age of 12,771 ± 47 Cal B.P. (recalibrated with IntCal13) based on eight dates associated with Clovis campfires from Unit F1, which is stratigraphically equivalent to the YDB layer. Likewise, Waters and Stafford (35) reported an average calibrated age of 12,761 ± 42 Cal B.P. (recalibrated with IntCal13) for the Clovis occupation layer. All these modeled ages closely correspond to each other and to the published YDB age (*SI Appendix*, Fig. S7 and Table S9).

Sheriden Cave, OH. This deeply stratified karst cavern is 4 km northwest of Carey, OH (13), where the YDB is a 1.5-cm-thick, charcoal-rich layer at a depth of 44.5–46.0 cmbs containing peaks in impact-related spherules, carbon spherules, and nanodiamonds. The YDB is closely associated with bones of the youngest known specimens of two extinct megafaunal species, the giant beaver (*Castoroides ohioensis*) with an age of 12,745 ± 45 Cal B.P. and the flat-headed peccary (*Platygonus compressus*) with a calibrated age of 12,920 ± 80 Cal B.P. The YDB layer is also closely associated with a Clovis flaked-stone projectile point and two Clovis bone projectile points that date to 12,765 ± 30 Cal B.P. Based on 29 of 30 AMS ^{14}C dates from across the 18-m-wide cave complex, the modeled age for this site is 12,840 ± 120 Cal B.P. at 68% (13,110–12,625 Cal B.P. at 95%) (Fig. 6 and *SI Appendix*, Fig. S8 and Table S10).

Medium-Quality Chronologies. Bayesian age–depth models for 8 of 23 sites are discussed in this section (see also *SI Appendix*). The chronologies for these sites are considered medium quality because the sites have (*i*) lower stratigraphic resolution, (*ii*) fewer


Fig. 5. Age sequence model for Daisy Cave, CA.

Fig. 6. Age sequence model for Sheriden Cave, OH.

Blackwater Draw, NM. Clovis projectile points were first discovered at this site, ~18 km southeast of the city of Clovis. Sixteen sediment samples collected inside the South Bank Interpretive Center included a 1-cm-thick YDB sample at a depth of 250 cmbs (1237.55 m elevation). The YDB contained peak abundances in impact-related spherules, glass-like carbon, polycyclic aromatic hydrocarbons (PAHs), iridium, and nickel (1, 13, 36, 37). The YDB layer is located between Level C, the Clovis occupation surface, and Level D1, a diatomite layer that correlates with the black mat at >50 other sites across North America (33).

Based on stratigraphic relationships between 28 of 29 ^{14}C dates, we generated a Bayesian age model, in which the transition at the top of the YDB layer dates to 12,775 ± 365 Cal B.P. at 68% (13,510–12,090 Cal B.P. at 95%) (*SI Appendix*, Fig. S9 and Table S12). A YDB age is supported by abundant Clovis artifacts and mammoth bones in the layer immediately below the diatomite and by Folsom artifacts ~20 cm above the diatomite. YDB impact-related spherules also were distributed across the original spoil from a hand-dug Clovis-age well (38) ~50 m from the South Bank site, supporting the modeled age of the YDB layer.

Indian Creek, MT. Located ~10 km west of Townsend, Indian Creek is a well-documented archaeological site, exhibiting a black mat layer containing Folsom cultural artifacts (33). A peak in nano-diamond-rich carbon spherules was found at a depth of 790–820 cmbs in the Clovis horizon immediately below the Folsom artifacts (9). Based on eight ^{14}C dates for the sequence, the age–depth model dates the top of the YDB layer to 12,750 ± 425 Cal B.P. at 68% (13,495–11,805 Cal B.P. at 95%), falling within the published YDB age span (*SI Appendix*, Fig. S10 and Table S13).

Lake Hind, Manitoba, Canada. Located in a cutbank along the Souris River in southwestern Manitoba, this site was once part of Glacial Lake Hind, an end-Pleistocene proglacial lake. At or near the Younger Dryas onset, ice dams on the lake failed in a regional pattern of meltwater flooding, transforming the lake from deep to shallow water (ref. 1 and references therein). The top of the YDB layer at a depth of 1,096–1,098 cmbs (avg., 1,097 cm) contains peaks in nanodiamonds, carbon spherules, nickel, and iridium. Eleven AMS ^{14}C dates were accepted and one was rejected in computing an age model that includes one date from directly within the proxy-rich YDB sample (*SI Appendix*, Fig. S11 and Table S14). The modeled age of the YDB layer is 12,745 ± 180 Cal B.P. at 68% (13,190–12,550 Cal B.P. at 95%), falling within the published YDB age range.

Lindenmeier, CO. Located in Larimer County, Colorado, ~45 km north of Fort Collins (9), this site contains multiple Folsom-age

dates per site (avg. 17 dates), (*iii*) larger uncertainties (avg. 295 y), and/or (*iv*) fewer temporally diagnostic indicators compared with the high-quality chronologies.

Barber Creek, NC. This next site is located ~5.7 km east of Greenville, along a paleobraidplain near the confluence of the Tar River and Barber Creek (13). The YDB layer contained a peak in impact-related spherules at a depth of 97.5–100 cmbs, immediately above an abrupt stratigraphic change from alluvial to eolian deposition that marks the Younger Dryas onset. The stratigraphic position of Archaic and Woodland cultural artifacts is consistent with the age of the YDB layer.

Wittke et al. (13) reported an OSL date of 12,100 ± 700 Cal B.P. from directly within the YDB layer, but Meltzer et al. (10) rejected Barber Creek as a YDB site, because its median age is 700 y younger than the YDB. This conclusion is unfounded, because the probability distribution of that date (12,800–11,400 Cal B.P.) overlaps the published YDB range of 12,950–12,650 Cal B.P. (Fig. 7). We used 13 of 14 AMS ^{14}C and OSL dates from two excavation pits ~10 m apart to produce an age model (*SI Appendix*, Table S11). The modeled age of the proxy-rich YDB layer is 12,865 ± 535 Cal B.P. at 68% (13,945–11,865 Cal B.P. at 95%), a span that falls within the previously published YDB range and has greater statistical certainty than the original OSL date as the result of Bayesian modeling.


Fig. 7. Age sequence model for Barber Creek, NC.

encampments, associated with a black mat layer just above a peak in nanodiamonds found at a depth of 100–102 cm. The stratigraphic age model is based on 10 of 11 ^{14}C dates, producing a YDB age of 12,775 ± 180 Cal B.P. at 68% (13,195–12,440 Cal B.P. at 95%), which overlaps the published YDB range (*SI Appendix*, Fig. S12 and Table S15).

Lingen, Germany. Located along the Ems River in Germany, this site is approximately 1 km downstream from the bridge to Lingen (1, 13). As is typical of northwestern Europe and Aalsterhut, the Usselo layer at this site is enriched at the top in charcoal, signifying widespread biomass burning at the Younger Dryas onset. The YDB layer at a depth of 42–45 cmbs contained peaks in impact-related spherules and carbon spherules. One new ^{14}C date on charcoal from directly within the YDB layer calibrates to 12,735 ± 85 Cal B. P. at 68% (12,910–12,520 Cal B.P. at 95%), overlapping the YDB age range (*SI Appendix*, Fig. S13 and Table S16).

Lommel, Belgium. This site is 3 km west of the Lommel town center and exhibits a lithologic succession that includes the Usselo horizon, as discussed above for Aalsterhut and Lingen (1, 13). The charcoal-rich YDB layer at a depth of 47–50 cmbs contains peaks in impact-related spherules, carbon spherules, nano-diamonds, nickel, osmium, and iridium. Using 16 of 17 dates (16 OSL and 1 AMS ^{14}C), OxCal calculated a YDB age of 12,735 ± 790 Cal B.P. at 68% (14,410–11,325 Cal B.P. at 95%), within the published YDB age range (*SI Appendix*, Fig. S14 and Table S17).

Santa Maira, Spain. This limestone cave complex is ~22 km from the Mediterranean Sea in the Alicante Province of eastern Spain (9). The YDB layer exhibits peaks in carbon spherules and nanodiamonds at a depth of 4–10 cmbs. Identification of the YDB layer is supported by the presence of temporally diagnostic changes in plant remains and cultural artifacts at the Younger Dryas onset (ref. 9 and references therein). Using 11 ^{14}C dates, OxCal generated an age sequence with a YDB age of 12,785 ± 295 Cal B.P. at 68% (13,265–12,070 Cal B.P. at 95%), which overlaps the YDB age range (*SI Appendix*, Fig. S15 and Table S18).

Talega, CA. Located ~5 km northeast of San Clemente in the Santa Ana Mountains of Southern California, this site was sampled for an archaeological study using a platform-mounted auger to collect samples from deep boreholes (13). The proxy-rich YDB sample came from within a 30-cm interval (1,485–1,515 cmbs) that contained abundance peaks in impact-related spherules and carbon spherules. For Talega, Meltzer et al. (10) modeled an age of 13,030 ± 150 Cal B.P. (range: 13,180–12,880 Cal B.P.) and claimed that the date "does not fall within the temporal target of 12,800 ± 150 cal BP [range: 12,950 to 12,650]," even though it clearly does overlap. Using 12 spatially separated dates from the site, OxCal generated an age-sequence model with a YDB age of 12,860 ± 150 Cal B.P. at 68% (13,075–12,545 Cal B.P. at 95%), consistent with the published YDB age range (13) (*SI Appendix*, Fig. S16 and Table S19).

Topper, SC. This well-known Clovis-age quarry lies 17 km west of Allendale near the Savannah River (13). The YDB layer is a 5-cm-thick interval at a depth of 57.5–62.5 cmbs, exhibiting peaks in impact-related spherules, carbon spherules, nanodiamonds, nickel, chromium, and iridium intermixed with temporally di-agnostic Clovis artifacts. LeCompte et al. (37) showed that YDB impact-related spherules were abundant in the sediment directly above and in contact with the chert artifacts but were absent directly beneath these artifacts. The sequence indicates that quarry use was interrupted for ~600 y, beginning near the time the impact proxies were deposited, consistent with a major population decline/reorganization at the site (3). One AMS ^{14}C date from the layer containing abundant Clovis artifacts was used with 10 spatially separated OSL dates to determine a modeled age of 12,785 ± 185 Cal B.P. at 68% (13,085–12,365 Cal B.P. at 95%), which fall within the published YDB range (Fig. 8 and *SI Appendix*, Table S20).

Lower-Quality Chronologies. Bayesian age models for the remaining 6 of 23 sites are discussed in this section and are illustrated in *SI Appendix*. The sites are considered of lower quality because they (*i*) often include OSL dates, (*ii*) have larger uncertainties (avg. 1006 y), (*iii*) have fewer dates per site (avg. 9 dates), (*iv*) display more bioturbation and redeposition, and/or (*v*) contain fewer temporally diagnostic indicators.

Blackville, SC. This site is ~3.2 km northwest of the town of Blackville (12, 13). The YDB layer occurs at a depth of 174–190 cmbs and exhibits peak abundances in impact-related spherules, high-temperature melt glass, carbon spherules, aciniform carbon, nanodiamonds, and iridium. Wittke et al. (13) reported an OSL date of 12,960 ± 1190 Cal B.P. from directly within the proxy-rich YDB layer. This age range (14,150–11,770 Cal B.P.) fully overlaps the published YDB age range, but Meltzer et al. (10) overlooked that range of uncertainties and claimed that Blackville is too old to be a YDB site. In OxCal, we used two of three OSL dates and one of two AMS ^{14}C dates to develop an age sequence with a modeled YDB age of 12,820 ± 1080 Cal B.P. at 68% (15,015–10,705 Cal B. P. at 95%) (*SI Appendix*, Fig. S17 and Table S21).

Lake Cuitzeo, Mexico. Israde-Alcántara et al. (11) analyzed samples in a 27-m-long core from the second largest lake in Mexico, covering 380 km² ~26 km north of Morelia in the state of Michoacán. They found peaks in impact-related spherules, carbon spherules, and nanodiamonds at a depth of 277.5–282.5 cmbs. Kinzie et al. (9) acquired a new AMS ^{14}C date from a nearby shoreline sequence with a black mat layer and several tephra layers that were stratigraphically correlated with the lake core. OxCal used 11 of 22 ^{14}C dates to model a YDB age of 12,850 ± 570 Cal B.P. at 68% (14,265–12,195 Cal B.P. at 95%) (*SI Appendix*, Fig. S18 and Table S22). This site has a lower rank because of nine anomalously old outlier dates near the YDB layer that form two unusual, coherently linear age clusters of unknown origin.

Geochemical and paleolimnological evidence shows a signifi-cant climatic transition from warm temperatures, corresponding to the Allerød warm period, to cool temperatures, corresponding to the Younger Dryas (11). At Lake Cuitzeo, the transition oc-curred between two ^{14}C dates of 9,911 Cal B.P. and 18,755 Cal B.P., consistent with the age–depth model of Israde-Alcántara et al. (11). This warm-to-cool transition is identified as the onset of the Younger Dryas climatic episode, corresponding to evi-dence at other regional sites (11). We also investigated two al-ternate age–depth models, one of which excluded the shoreline date from Kinzie et al. (9) and produced a modeled YDB age of
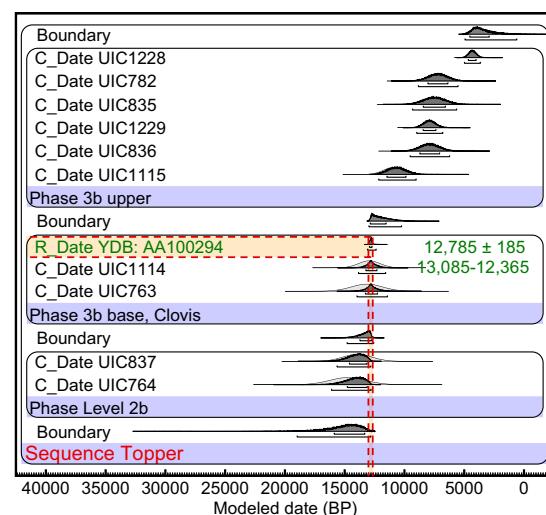

Fig. 8. Age sequence model for Topper, SC.

~15,300 Cal B.P. The other model that included the nine outliers produced a modeled YDB age of ~27,100 Cal B.P. However, both of these alternate YDB ages are inconsistent with the local and regional paleoclimatic record, and, hence, even though the lake is poorly dated, it is likely that the proxy-rich layer at Lake Cuitzeo is the same age as the YDB layer at well-dated sites.

Melrose, PA. This site is approximately 1 km southwest of Melrose in northeastern Pennsylvania (12, 13). The YDB layer spans an interval from 15 cmbs to 28 cmbs and contains a remarkable array of high-temperature impact proxies, including peaks in impact-related spherules, carbon spherules, aciniform carbon, nanodiamonds, high-temperature melt glass, nickel, and osmium (9, 12, 13, 39). The YDB age sequence model was based on one new AMS ^{14}C date and an OSL date of 11,701 ± 1846 Cal B.P. (equivalent to 11,640 y before 1950), taken from directly within the proxy-rich YDB sample. The modeled YDB age is 12,255 ± 2,405 Cal B.P. at 68% (17,185–7,710 Cal B.P. at 95%) (*SI Appendix*, Fig. S19 and Table S23).

Mucuñuque (MUM7b), Venezuela. This site is at an elevation of ~4,000 m in the Merida Province on the northwestern slope of the Cordillera Sierra de Santo Domingo in the Venezuelan Andes (40) and is farther south than any other well-studied YDB site. Recessional moraines and outwash fans representing the advance of area glaciers are undated at the site but are dated to the Younger Dryas nearby. The YDB layer lies at a depth of 210–213 cmbs beneath one of the Younger Dryas outwash fans and contains peaks in impact-related spherules, carbon spherules, quartz with planar features, and high-temperature melt glass. Using three dates directly from the site, OxCal generated an age sequence model with a YDB age of 12,845 ± 630 Cal B.P. at 68% (13,550–11,335 Cal B.P. at 95%), within the published YDB range (*SI Appendix*, Fig. S20 and Table S24).

Ommen, Netherlands. Located 3 km west of Ommen in the province of Overijssel, this site displays the Usselo Horizon, accepted to mark the Younger Dryas onset, as at Aalsterhut, Lingen, and Lommel (1, 13). The charcoal-rich YDB layer occurs at the top of the Usselo horizon at a depth of 115–120 cmbs and contains peaks in impact-related spherules, carbon spherules, and nanodiamonds. OxCal used two AMS ^{14}C dates to model the age of the YDB layer as 12,750 ± 560 Cal B.P. (13,605–11,425 Cal B.P. at 95% confidence interval), consistent with the previously published YDB range (*SI Appendix*, Fig. S21 and Table S25).

Other Sites. Nine other proxy-rich sites currently lack sufficient dating for robust Bayesian analysis. Even so, the stratigraphic context of a proxy-rich layer or samples at these sites supports a YDB age. These sites are Chobot, Alberta, Canada; Gainey, MI; Kangerlussuaq, Greenland; Kimbel Bay, NC; Morley, Alberta, Canada; Mt. Viso, France/Italy; Newtonville, NJ; Paw Paw Cove, MD; and Watcombe Bottom, United Kingdom. For further discussion, see *SI Appendix, Unmodeled Sites*.

Modeled vs. Unmodeled Ages. By design, Bayesian models alter some dates to produce statistically stronger age models. Therefore, the question arises of whether such changes cause errors by shifting the unmodeled YDB dates too old or too young. To investigate this for each of the 23 YDB sites, we selected the date closest to the median age of the YDB layer (12,800 ± 150 Cal B.P.) and calibrated each date with IntCal13 without using any Bayesian modeling (*SI Appendix, Methods*, Fig. S22 and Table S26). Of the 23 dates, 22 (96%) fall within the YDB range at 99% CI, and 19 (83%) overlap from 12,840–12,805 Cal B.P., a 35-y interval. These results indicate that Bayesian modeled ages are not substantially different from unmodeled calibrated ages.

Onset of Younger Dryas Climatic Episode. The YDIH posits that the Younger Dryas climate episode was triggered by the cosmic impact, and, therefore, the two should be contemporaneous (1).
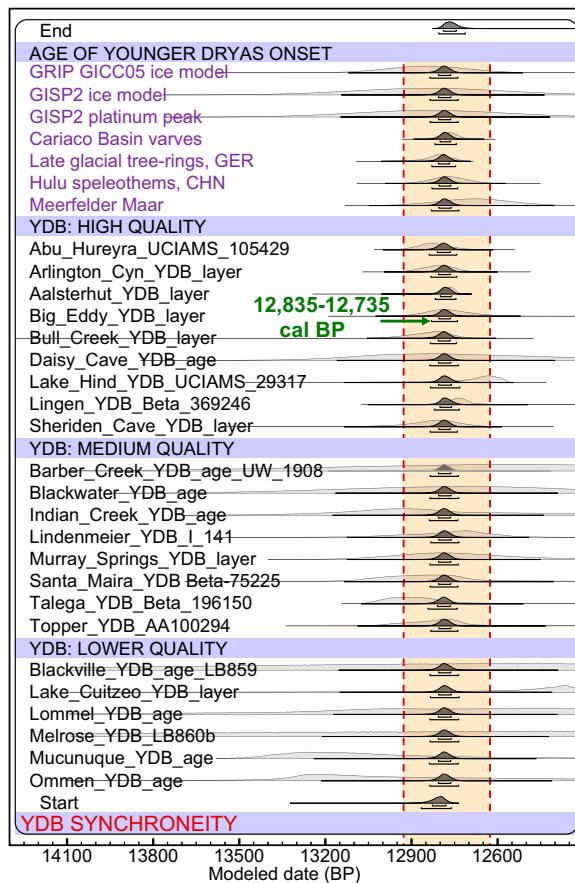
Fig. 9. Bayesian synchroneity tests of 30 records: 23 YDB sites with 1 GISP2 platinum peak and 6 independently dated climate records marking the Younger Dryas onset (purple text). For the 30 records, Sequence and Difference codes calculated the common age interval as ranging from 12,835 Cal B.P. to 12,735 Cal B.P. at 95% probability, as represented by the bottom black bar (at green arrow). Light gray probability distributions represent the individual modeled YDB ages for each record. Both light and dark gray distributions fall within the YDB age range of 12,950–12,650 Cal B.P. (yellow vertical bar).

Sometimes, multiple climate proxies are available for determining the onset of the Younger Dryas in a given record, and, if so, we used the earliest date in our Bayesian analyses, as others have done (41) (see *SI Appendix, Onset of Younger Dryas and Table S27*). The onset of the Younger Dryas has been independently dated in multiple records, representing a wide range of paleoenvironments in the Northern Hemisphere, including ice cores, tree rings, lake and marine cores, and speleothems, as follows [ice core dates are reported here as b2k (calendar years before base year AD 2000), consistent with glaciological convention; when compared with Cal B.P. dates (base year 1950), OxCal automatically adjusted b2k dates to Cal B.P. dates to be chronologically consistent]: (*i*) 12,896 ± 138 b2k (13,034–12,758 b2k), from several ice cores, Greenland Ice Core Project (GRIP), North Greenland Ice Core Project (NGRIP), and DYE-3 (42); (*ii*) 12,890 ± 260 b2k (13,150–12,630 b2k), from the Greenland Ice Sheet Program (GISP2) (43); (*iii*) 12,887 ± 260 b2k (13,147–12,627 b2k), for a peak in impact-related platinum, coeval with the onset of Younger Dryas cooling with the same uncertainty as the GISP2 core (18); (*iv*) 12,820 ± 30 Cal B.P. (12,850–12,790 Cal B.P.), from a count of annual varves in an ocean sediment core from the Cariaco Basin, Venezuela (44, 45); (*v*) 12,812 ± 49 Cal B.P. (12,861–12,763 Cal B.P.), from counting tree rings in the German pine record (46); (*vi*) 12,823 ± 60 Cal B.P. (12,883–12,763 Cal B.P.), based on oxygen isotope changes (δ^{18}O)

in speleothems from Hulu Cave, China (47); and (*vii*) 12,680 ± 127 varve years (before 1950 AD; 12,807–12,553 varve years; avg. error, 1%), a varve count for cores from Meerfelder Maar, Germany (48). The first six records above show striking similarities in both mean values and age ranges. Even though the mean ages of Meerfelder Maar and other varve records appear ~200 y younger, all of the age estimates investigated overlap the previously published YDB age range of 12,950–12,650 Cal B.P. This leaves open the possibility that the Younger Dryas onset and the YDB impact event are synchronous.

YDB Datum Layer. In a number of sedimentary sections, individual types of YDB-like proxies have been observed intermittently in relatively low abundances outside of the YDB layer. However, only the YDB layer exhibits distinct abundance peaks in multiple impact-related proxies and, as such, forms a distinct, widely distributed event horizon or datum layer, similar, for example, to a geochemically distinctive volcanic tephra layer and the iridium-rich K–Pg impact layer. Existing stratigraphic information suggests that the YDB layer reflects the occurrence of a singular cosmic impact by a fragmented comet that resulted in widely distributed multiple impacts. The YDB datum concept as a singular event can be further tested through ultra-high-resolution chronostratigraphic investigations. This proposed datum layer should be synchronous over broad areas.

Synchroneity. We conducted a Bayesian test of synchroneity to explore whether the probability distributions overlap for all 23 YDB and 7 Younger Dryas onset dates and, therefore, the 30 sites could be contemporaneous. In accordance with the protocol for testing synchroneity, as described in Parnell et al. (49) and Bronk Ramsey (23), we used OxCal's Sequence and Difference codes to determine the duration of the most likely common age interval for the 30 records (Fig. 9). In this test, if the computed interval at 95% CI allows for a full overlap, i.e., includes zero years, then synchroneity is possible and is not rejected. On the other hand, if the estimated interval at 95% CI includes only nonzero values, then it is probable that the dated events occurred over a span of years, and synchroneity can be rejected. For the 30 sites, OxCal computed a minimum interval of zero years at 68% CI (range: 0–60 y). At 95% CI, the difference among the 30 sites ranges from 0 y to 130 y, and therefore, synchroneity is statistically possible and is not rejected.

Using the Difference code, we also calculated the modeled age span of the potential YDB overlap for the 30 sites. To do so, we used the Date code in OxCal with the Start and End Boundary ages to compute an age interval for the YDB event of 12,810–12,760 Cal B.P. (12,785 ± 25 Cal B.P.) at 68% CI and 12,835–12,735 Cal B.P. (12,785 ± 50 Cal. B.P.) at 95% CI. These ranges fall within the previously published YDB age range of 12,950–12,650 Cal B.P. For details, see *SI Appendix,* Table S28; for coding, see *SI Appendix, Coding.*

Additional support for synchroneity comes from the GISP2 ice core, in which a significant, well-defined, ~18-y-long platinum peak was found in an ice interval spanning 279 y from 13,060–12,781 b2k (18). This single, short-duration platinum peak supports the occurrence of just one, rather than multiple events during that 279-y interval.

In summary, these statistical tests produced an overlapping unmodeled range of 12,840–12,805 Cal B.P. at 95% CI and an overlapping Bayesian-modeled range of 12,835–12,735 Cal B.P.

Therefore, the 23 YDB age estimates appear isochronous within the limits of chronological resolution (~100 y) and could have been deposited during a single event (*SI Appendix,* Tables S26 and S28). These findings refute the claim of Meltzer et al. (10) that YDB ages are asynchronous. Furthermore, the ages of the YDB at 23 sites are statistically contemporaneous with the independently determined onset of the Younger Dryas climate episode, suggesting a causal link between the two (*SI Appendix,* Tables S26 and S28).

Conclusions

Our results support six conclusions: (*i*) Bayesian analyses of 354 dates at 23 sites in 12 countries across four continents demonstrate that modeled YDB ages are consistent with the previously published range of 12,950–12,650 Cal B.P. (9, 11–13), contradicting claims that previous YDB age models are inaccurate (10, 14–16). (*ii*) Bayesian analyses indicate that YDB dates could be synchronous within the limits of uncertainties (~100 y), contradicting claims that YDB dates are diachronous. (*iii*) Comparison with calibrated, unmodeled ages shows that Bayesian modeling does not significantly alter the calculated span of the YDB event. (*iv*) The ages of the 23 sites are coeval with the Younger Dryas onset in six records and with the age of deposition of extraterrestrial platinum in the GISP2 ice core at the Younger Dryas onset. This temporal relationship supports a causal connection between the impact event and the Younger Dryas. (*v*) These analyses produced a more refined modeled age for the YDB event of 12,835–12,735 Cal B.P. at 95% CI. Although Bayesian analysis alone cannot determine unequivocally that the YDB is synchronous at these 23 sites, a single event is the most plausible conclusion, given the widespread presence of peaks in impact-related spherules, melt glass, nanodiamonds, and other markers that all fall within a narrow temporal window of ~100 y.

Methods

Sites for sampling were chosen because of accessibility and because Younger Dryas-aged strata already had been identified stratigraphically by independent workers (23 sites) and/or independently dated (18 of 23 sites). Radiocarbon dates (*n* = 354) were compiled from independent publications for 18 sites and from previous YDIH-group publications for the remaining 5 sites. We used all available dates, except in most cases where median dates were >15,000 Cal B.P. or <10,000 Cal B.P. in age; dates extending outside those limits were sometimes used when a site had only a few intermediate dates. For sites with widely scattered dates (Blackwater Draw and Murray Springs), we used only those dates within less than ~60 m of the sampled section, on the assumption that those dates would provide the most accurate age model. Testing indicated that excluding such dates had no effect on the age–depth model between 13,100 Cal B.P. and 12,500 Cal B.P. We calibrated all dates using the IntCal13 dataset within OxCal v4.2.4 r:5 (23) and then calculated age models using Bayesian analyses in OxCal, based on the Markov chain Monte Carlo algorithm. We used standard codes and commands in OxCal, including P_Sequence, Sequence, and Phase. The Outlier code was also used because charcoal derives from vegetation that is, by necessity, older than the fire that carbonized it. OxCal's Difference code was used to explore potential synchroneity (for more details, see *SI Appendix, Methods*).

1. Firestone RB, et al. (2007) Evidence for an extraterrestrial impact 12,900 years ago that contributed to the megafaunal extinctions and the Younger Dryas cooling. *Proc Natl Acad Sci USA* 104(41):16016–16021.

2. Kennett DJ, et al. (2008) Wildfire and abrupt ecosystem disruption on California's Northern Channel Islands at the Allerød–Younger Dryas boundary (13.0–12.9 ka). *Quat Sci Rev* 27(27-28):2530–2545.

3. Anderson DG, Goodyear AC, Kennett J, West A (2011) Multiple lines of evidence for possible human population decline/settlement reorganization during the early Younger Dryas. *Quat Int* 242(2):570–583.

4. Jones TL, Kennett DJ (2012) A land impacted? The Younger Dryas Boundary event in California. *Contemporary Issues in California Archaeology*, eds Jones TL, Perry JE (Left Coast Press, Walnut Creek, CA), pp 37–48.

5. Moore AMT, Kennett DJ (2013) Cosmic impact, the Younger Dryas, Abu Hureyra, and the inception of agriculture in Western Asia. *Eurasian Prehist* 10(1-2):57–66.

6. Kennett DJ, Culleton BJ, Dexter J, Mensing SA, Thomas DH (2014) High-precision AMS ^{14}C chronology for Gatecliff Shelter, Nevada. *J Arch Sci* 52:621–632.

7. Schiffer MB (1986) Radiocarbon dating and the "old wood" problem: The case of the Hohokam chronology. *J Archaeol Sci* 13(1):13–30.

8. Telford RJ, Heegaard E, Birks HJB (2004) All age–depth models are wrong: But how badly? *Quat Sci Rev* 23(1-2):1–5.

9. Kinzie CR, et al. (2014) Nanodiamond-rich layer across three continents consistent with major cosmic impact at 12,800 cal BP. *J Geol* 122(5):475–506.

10. Meltzer DJ, Holliday VT, Cannon MD, Miller DS (2014) Chronological evidence fails to support claim of an isochronous widespread layer of cosmic impact indicators dated to 12,800 years ago. *Proc Natl Acad Sci USA* 111(21):E2162–E2171.

11. Israde-Alcántara I, et al. (2012) Evidence from central Mexico supporting the Younger Dryas extraterrestrial impact hypothesis. *Proc Natl Acad Sci USA* 109(13):E738–E747.

12. Bunch TE, et al. (2012) Very high-temperature impact melt products as evidence for cosmic airbursts and impacts 12,900 years ago. *Proc Natl Acad Sci USA* 109(28):E1903–E1912.

13. Wittke JH, et al. (2013) Evidence for deposition of 10 million tonnes of impact spherules across four continents 12,800 y ago. *Proc Natl Acad Sci USA* 110(23):E2088–E2097.

14. Boslough MB, et al. (2012) Arguments and evidence against a Younger Dryas impact event. *Climates, Landscapes, and Civilizations*, Geophysical Monograph Series, eds Giosan L, Fuller DQ, Nicoll K, Flad RK, Clift PD (Am Geophys Union, Washington, DC), Vol 198, pp 13–26.

15. van Hoesel A, et al. (2012) Nanodiamonds and wildfire evidence in the Usselo horizon postdate the Allerod–Younger Dryas boundary. *Proc Natl Acad Sci USA* 109(20):7648–7653.

16. van Hoesel A, et al. (2014) The Younger Dryas impact hypothesis: A critical review. *Quat Sci Rev* 83(1):95–114.

17. Blaauw M, Holliday VT, Gill JL, Nicoll K (2012) Age models and the Younger Dryas impact hypothesis. *Proc Natl Acad Sci USA* 109(34):E2240, author reply E2245–E2247.

18. Petaev MI, Huang S, Jacobsen SB, Zindler A (2013) Large Pt anomaly in the Greenland ice core points to a cataclysm at the onset of Younger Dryas. *Proc Natl Acad Sci USA* 110(32):12917–12920.

19. Millard AR (2014) Conventions for reporting radiocarbon determinations. *Radiocarbon* 52(2):555–559.

20. Blaauw M (2010) Methods and code for 'classical' age-modelling of radiocarbon sequences. *Quat Geochronol* 5(5):512–518.

21. Michczynski A (2007) Is it possible to find a good point estimate of a calibrated radiocarbon date? *Radiocarbon* 49(2):393–401.

22. Erlandson JM, Braje TJ, Graham MH (2008) How Old is MVII? Seaweeds, shorelines, and the pre-Clovis chronology at Monte Verde, Chile. *J Island Coast Archaeol* 3:277–281.

23. Bronk Ramsey C (2009) Bayesian analysis of radiocarbon dates. *Radiocarbon* 51(1):337–360.

24. Bronk Ramsey C, Lee S (2013) Recent and planned developments of the program OxCal. *Radiocarbon* 55(2-3):720–730.

25. Blaauw M, Christen JA (2011) Flexible paleoclimate age-depth models using an autoregressive gamma process. *Bayesian Anal* 6(3):457–474.

26. Bronk Ramsey C (1998) Probability and dating. *Radiocarbon* 40(1):461–474.

27. Buck CE, Christen JA, James GN (1999) BCal: An on-line Bayesian radiocarbon calibration tool. *Internet Archaeol* 7:dx.doi.org/10.11141/ia.7.1.

28. Haslett J, Parnell A (2008) A simple monotone process with application to radiocarbon-dated depth chronologies. *J R Stat Soc Ser C* 57(4):399–418.

29. Moore AMT, Hillman GC, Legge AJ (2000) *Village on the Euphrates* (Oxford Univ Press, New York).

30. Bement LC, et al. (2014) Quantifying the distribution of nanodiamonds in pre-Younger Dryas to recent age deposits along Bull Creek, Oklahoma panhandle, USA. *Proc Natl Acad Sci USA* 111(5):1726–1731.

31. Erlandson J, et al. (1996) An archaeological and paleontological chronology for Daisy Cave (CA-SMI-261), San Miguel Island, California. *Radiocarbon* 38(2):355–373.

32. Haynes CV, Jr (1998) Arizona's famous Clovis sites could be displayed for public. *Mammoth Trumpet* 13(2):2–6, 20.

33. Haynes CV, Jr (2008) Younger Dryas "black mats" and the Rancholabrean termination in North America. *Proc Natl Acad Sci USA* 105(18):6520–6525.

34. Fayek M, Anovitz LM, Allard LF, Hull S (2012) Framboidal iron oxide: Chondrite-like material from the black mat, Murray Springs, Arizona. *Earth Planet Sci Lett* 319:251–258.

35. Waters MR, Stafford TW, Jr (2007) Redefining the age of Clovis: Implications for the peopling of the Americas. *Science* 315(5815):1122–1126.

36. Firestone RB (2009) The case for the Younger Dryas extraterrestrial impact event: Mammoth, megafauna, and Clovis extinction, 12,900 years ago. *J Cosmol* 2:256–285.

37. LeCompte MA, et al. (2012) Independent evaluation of conflicting microsphere results from different investigations of the Younger Dryas impact hypothesis. *Proc Natl Acad Sci USA* 109:E2960–E2969.

38. Haynes CV, Jr, et al. (1999) A Clovis well at the type site 11,500 B.C.: The oldest prehistoric well in America. *Geoarchaeol* 14(5):455–470.

39. Wu Y, Sharma M, LeCompte MA, Demitroff MN, Landis JD (2013) Origin and provenance of spherules and magnetic grains at the Younger Dryas boundary. *Proc Natl Acad Sci USA* 110(38):E3557–E3566.

40. Mahaney WC, et al. (2010) Evidence from the northwestern Venezuelan Andes for extraterrestrial impact: The black mat enigma. *Geomorphology* 116(1-2):48–57.

41. Steffensen JP, et al. (2008) High-resolution Greenland ice core data show abrupt climate change happens in few years. *Science* 321(5889):680–684.

42. Rasmussen SO, et al. (2006) A new Greenland ice core chronology for the last glacial termination. *J Geophys Res* 111(D6):D06102.

43. Meese DA, et al. (1997) The Greenland Ice Sheet Project 2 depth-age scale: Methods and results. *J Geophys Res* 102(C12):26411–26423.

44. Lea DW, Pak DK, Peterson LC, Hughen KA (2003) Synchroneity of tropical and high-latitude Atlantic temperatures over the last glacial termination. *Science* 301(5638):1361–1364.

45. Haug GH, Hughen KA, Sigman DM, Peterson LC, Röhl U (2001) Southward migration of the intertropical convergence zone through the Holocene. *Science* 293(5533):1304–1308.

46. Kromer B, et al. (2004) Late glacial ^{14}C ages from a floating, 1382-ring pine chronology. *Radiocarbon* 46(3):1203–1209.

47. Wang YJ, et al. (2001) A high-resolution absolute-dated late Pleistocene Monsoon record from Hulu Cave, China. *Science* 294(5550):2345–2348.

48. Brauer A, Endres C, Negendank JF (1999) Lateglacial calendar year chronology based on annually laminated sediments from Lake Meerfelder Maar, Germany. *Quat Int* 61(1):17–25.

49. Parnell AC, et al. (2008) A flexible approach to assessing synchroneity of past events using Bayesian reconstructions of sedimentation history. *Quat Sci Rev* 27(19-20):1872–1885.

Bayesian chronological analyses consistent with synchronous age of 12,835-12,735 Cal B.P. for Younger Dryas Boundary on four continents

SUPPORTING INFORMATION

DATING INFORMATION

Scientists typically assume that radiocarbon dates with high precision necessarily have high accuracy, but that assumption is frequently incorrect, as demonstrated by Telford et al. (1, 2) for two lakes, one in Germany and the other in the U.S.A. Those authors compared two different age-depth models, one based on radiocarbon dating and the other on high-resolution counting of varves (annual lake sediment layers). They found that even though the radiocarbon dates had measurement precisions of 40 years or less, some ages had inaccuracies of ±400 years, when compared to the more accurate varve dates. Those authors' title, "*All age–depth models are wrong: but how badly?*" reflects their conclusions.

Radiocarbon limitations. Age models may be incorrect for many reasons, and the most important one is that the past radiocarbon content of Earth's atmosphere has not remained stable, but rather has experienced substantial oscillations. During the latest Quaternary, these oscillations resulted from several large-scale processes, including changes in ocean turnover and the related transfer of ^{14}C-depleted carbon from deep ocean reservoirs to near-surface ocean waters and into the atmosphere (3). Changes in radiocarbon content also have resulted from fluctuations in cosmic radiation due to solar activity, near-Earth supernovae, and other cosmic phenomena (4) and from fluctuations in Earth's magnetic field (3). The YDB impact event also may have affected atmospheric radiocarbon concentrations through extensive biomass burning that released abundant ^{14}C into the atmosphere and by the influx of extraterrestrial ^{14}C contained in cometary material (5).

Radiocarbon dating has limitations that make it difficult to date a brief event, such as the YDB impact. Those limitations include the following:

- The age of charcoal or the carbon in a fossil is determined by the degree to which ^{14}C has decayed (the rate equals ≈0.012% per year or 0.12 per mil). The half-life of ^{14}C has an uncertainty of ≈±0.7% leading to a systemic error of 90 years at 13,000 Cal B.P.
- Near the time of the YDB event, the stated precision of the IntCal calibration is ≈1% or 10 per mil, which corresponds to a systemic uncertainty of 83 years. That is a minimum value, and all other uncertainties for any Accelerator Mass Spectrometry (AMS) ^{14}C measurement should be compounded with the calibration error and would at least double it.

- Some radiocarbon laboratories round their dates to the nearest 5, 10, or 100 years, meaning that dates can vary by up to ≈0.4% at 13,000 Cal B.P., thus adding more uncertainty to the true age.
- Almost all radiocarbon dates are corrected for fractionation, using the δ^{13}C value as a surrogate, which can yield a correction of up to ≈200 years. However, ^{13}C/^{12}C ratios vary significantly among plants and animals, adding additional uncertainty to corrections for fractionation, if not directly measured.
- There is additional uncertainty in marine radiocarbon dates, which typically are 400 ^{14}C years or much older than terrestrial dates at 12,800 Cal B.P., but vary by geographic location. This difference means that for a short-duration event, such as the proposed YDB impact, the apparent ages from an ocean sediment record may be much older than dates on nearby terrestrial samples.
- Modern dates from the Southern Hemisphere can be ≈30 ^{14}C years older than those from the Northern Hemisphere due to incomplete atmospheric mixing. Hence, dates will be different for an identical event in both hemispheres.
- More uncertainty can result when groundwater dissolves limestone, making samples appear up to thousands of years too old, with variations as large as 2000 ^{14}C years in a single river (6). Secondary carbonate precipitation (hard water effect) in fluvial, lacustrine, and marine deposits can deplete ^{14}C abundance, resulting in age differences of up to 4,000 ^{14}C years (7).
- After deposition of a carbon sample, contamination with older or younger organic carbon can produce dating errors of hundreds, if not thousands of years. For example, high terrestrial runoff can transport old charcoal-rich soil into a lake, thus increasing the apparent age of the deposit. This can be especially problematic when dates are acquired from bulk sedimentary carbon (8).
- Another complication can result from the old wood effect. For example, at Arlington Canyon, California, trees lived for up to ≈1300 years, making it more difficult to accurately date any fire in which those old trees burned (9).
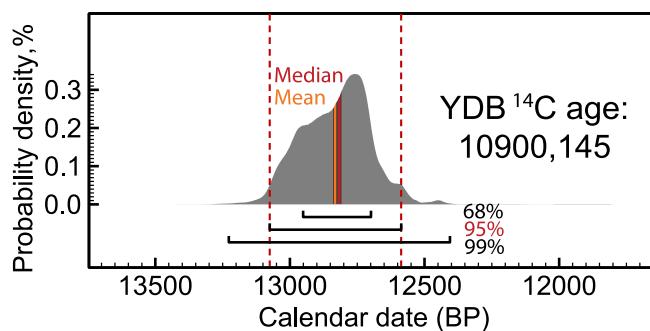
Fig. S1. YDB age range. Probability distribution plot (gray) for 10,900 ± 145 ^{14}C BP using IntCal13. Solid red vertical line represents median age; solid orange vertical line is the mean. Black horizontal bars are probabilities of 68%, 95%, and 99%; red vertical dashed lines represent the 95% range. The y-axis shows that the median and mean years have a very low likelihood of representing the true calibrated radiocarbon date (probability density equals <0.3%).

Radiocarbon calibration is a complex process, with the result that calibration curves are regularly revised because of ever-increasing knowledge. For example, there have been four IntCal calibration curve revisions released over the fifteen-year span from 1998 to 2013 (10). During that time, the calibrated age for 10,900 ± 145 ^{14}C years has changed four times, yielding results that differ from 12,929 ± 180 Cal B.P. in IntCal 98 to 12,822 ± 147 Cal B.P. in IntCal 09, a difference of

107 mean years. In other words, the identical radiocarbon date produced four different age ranges. For this reason, use of the same calibration curve is essential when making comparisons between dates.

The amount of radiocarbon in the atmosphere and oceans has been highly variable over time, producing distinctive "plateaus" (11, 12), as well as significant short-term oscillations. An example of ^{14}C calibration complications is shown in **Fig. S2**, where a single radiocarbon date calibrated in OxCal may have three or four separate ages within each probability distribution. Each date is not equally probable, but all are possible, adding considerable uncertainty for determining the most likely age of any discrete event. Undoubtedly, calibration curves will continue to evolve with the result that any current calibrated date in calendar years is an approximation subject to change. Because of calibration issues, individual median dates should not be used without reporting the statistical uncertainties (13). In addition, it is better to model multiple dates with Bayesian analysis, because the results from multiple dates are more robust and accurate than those from a single date.

Optically stimulated luminescence (OSL) dating, another approach, is typically performed on quartz grains and is commonly used where there is a dearth of material for radiocarbon dating, such as at most of the YDB sites in eastern North America (14). OSL dates usually have large systematic errors (>500 years) that can result, for example, from incomplete bleaching due to insufficient exposure to

sunlight and from variable exposure to sedimentary radioactivity. Even though these cumulative issues can produce millennia-scale uncertainties, OSL dating can be invaluable when radiocarbon dating is not possible.

Chronological hygiene. For evaluating a series of ^{14}C dates, minimizing the above-mentioned dating problems may require use of established techniques of chronological hygiene (15). These approaches include *(i)* performing Bayesian analysis to exclude outliers (dates that are stratigraphically out of order, meaning they are too old or too young); *(ii)* favoring younger and higher precision dates as most reliable; *(iii)* preferring dates from short-lived samples (twigs, seeds, etc.); *(iv)* investigating the old wood issue by performing taxonomic identification; and *(v)* using individual pieces of charcoal rather than combining numerous charcoal fragments with different possible ages.

Dating summary. Multiple cumulative problems mean that the accuracy and precision of radiocarbon and OSL dates are limited, with the result that calibrated radiocarbon dates near 12,800 Cal B.P. cannot have the usually claimed precision of a few decades. These limitations do not mean that such dating is unreliable, but rather that high precision and high accuracy should not be assumed. Thus, radiocarbon and OSL dating should not be used in isolation, and instead, they should be integrated with relevant stratigraphic information (lithologic, climatic, paleontological, and archaeological), as can be done using Bayesian analysis (16).
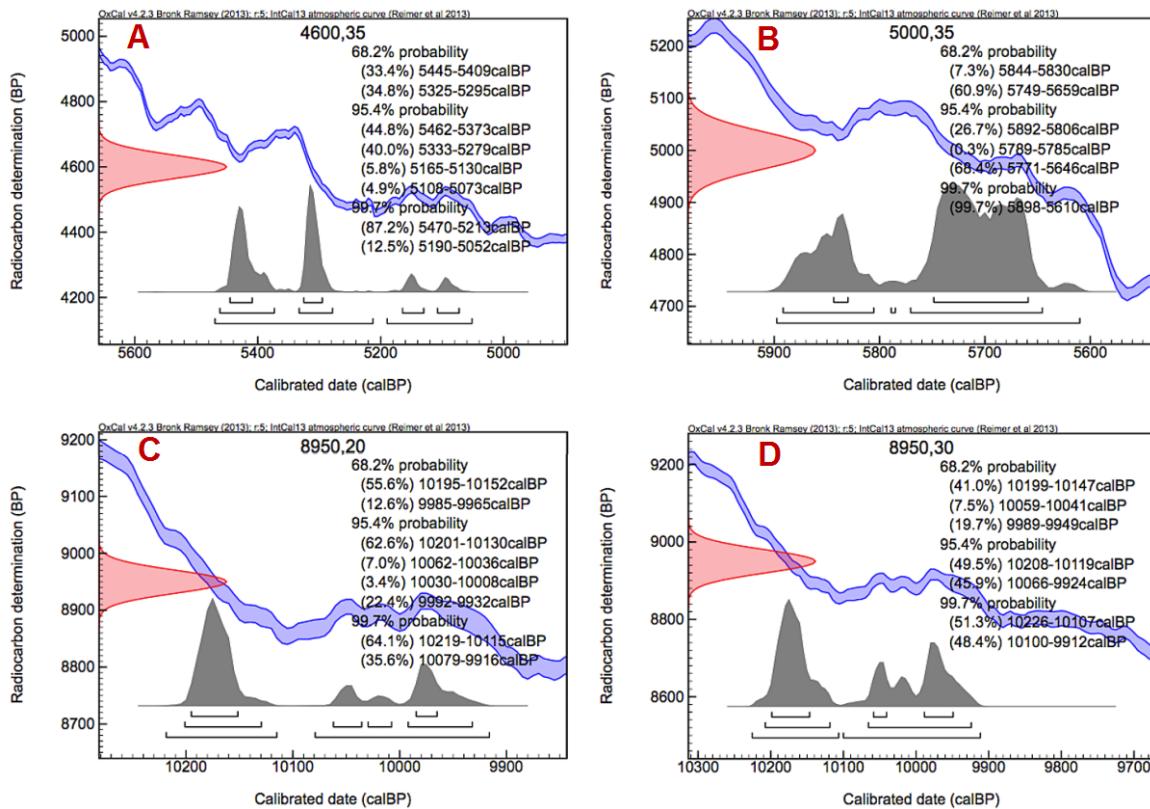
Fig. S2. Uncertainties in calibrating radiocarbon dates. *Panels A and B* show a single ^{14}C age that calibrates, not as one date, but as multiple calendar ages. Because the probabilities vary for each date, it is not possible to determine conclusively which one of the multiple calibrated dates is correct. For *panels C and D*, the same uncalibrated date (8950 ^{14}C BP) has uncertainties that change from 20 years (panel C) to 30 years (panel D). The resulting calibrated ages are highly variable, demonstrating that a small difference in uncertainty of only 10 years can have a significant effect. These examples clearly demonstrate the error in using median dates without reporting uncertainties (13).

Prior information and assumptions in OxCal

Bayesian analysis allows use of prior information and assumptions, and those data can make the age-depth model more robust. For example:

- OxCal assumes that all ages (modeled or real) should be younger with decreasing depth (law of superposition), but, in reality dating reversals are common. When two dates are out of chronologic sequence, OxCal determines which date has the highest probability of fitting the model, and the anomalous date is remodeled younger/older or rejected as an outlier. The result is that final modeled ages are in chronologic order, even if the original dates are not.
- To counter the old wood effect, OxCal uses Outlier coding that assumes most, if not all charcoal dates are older than the fire being dated. Next, a fixed percentage of those dates are considered to be outliers, i.e., they came from either older or younger trees that burned during the same fire.
- Similarly, some sites may be subject to a "young wood effect," whereby, younger charcoal moves downward,

making the stratum appear too young. OxCal's Outlier code can be set to adjust such dates.

- OxCal allows for the insertion of code for what are called "Boundaries." Typically, these designations are used with dates in stratigraphic order to represent, for example, a significant change in sediment characteristics, such as from clay to sand, from thick to thin strata, and/or from coarse to fine sediment. Based on changes in palynology, a boundary also may represent climate change, e.g., the onset of the Younger Dryas episode.
- OxCal allows for the designation of groups called "Phases," based on common distinguishing characteristics. Typically, Phases include dates in chronological order with no depth information. For example, a group of dates from multiple archaeological sites may contain several phases, each of which relates to a specific style of pottery. A phase also may be identified based on the presence or absence of extinct megafaunal remains or a specific style of projectile point, e.g., Clovis or Folsom.

SITE INFORMATION

Table S1. Site details: name, location, latitude-longitude, list of proxies that peak in the YDB layer at each site, and main references. "CS" represents carbon spherules; "GLC" = glass-like carbon; "PAHs" = polycyclic aromatic hydrocarbons.

Site	Loc	Lat-Long															Ref
Abu Hureyra	SYR	35.8667000°N, 38.400000°E	●	●	●	●	-	-	●	●	●	-	-	-	●	-	17
Arlington Cyn	CA, US	33.988587°N, 120.158047°W	-	●	-	●	●	●	-	●	●	●	-	-	-	-	9
Aalsterhut	NED	≈51.427254°N, ≈5.585360°E	●	-	-	-	●	●	●	●	●	-	-	-	-	-	18
Big Eddy	MO, US	37.736470°N, 93.786128°W	●	●	-	-	-	-	-	-	-	-	-	-	-	-	19
Bull Creek	OK, US	≈36.64000°N, ≈100.85000°W	●	-	-	●	-	-	-	-	●	-	-	-	-	-	9
Daisy Cave	CA, US	34.042070°N, 120.320090°W	●	●	-	-	-	●	●	●	-	-	●	●	-	-	20
Lake Hind	CAN	49.440000°N, 100.697700°W	●	-	-	●	-	●	●	●	●	-	-	-	●	●	4
Lingen	GER	52.5087510°N, 7.3138820°E	-	●	-	-	●	●	●	●	●	-	-	-	-	-	19
Sheriden Cave	OH, US	40.965055°N, 83.426038°W	●	●	-	-	●	●	-	●	●	-	-	-	-	-	21-29
Barber Creek	NC, US	35.6000592°N, 77.303636°W	●	●	-	-	-	-	-	-	-	-	-	-	-	-	19
Blackwater Draw	NM, US	34.275687°N, 103.326101°W	●	●	-	-	-	-	●	-	-	●	●	●	●	●	19
Indian Creek	MT, US	46.314439°N, 111.630274°W	●	-	-	-	-	●	-	-	●	-	-	-	-	-	20
Lindenmeier	CO, US	40.976424°N, 105.104108°W	●	-	-	●	-	-	-	-	●	-	-	-	-	-	20
Murray Spgs	AZ, US	31.570912°N, 110.177996°W	●	●	●	-	-	●	●	●	●	●	●	●	●	●	4
Santa Maira	SPN	38.7302850°N, 0.2150870°W	●	-	-	-	●	●	●	-	●	-	-	-	-	-	20
Talega	CA, US	33.470292°N, 117.600471°W	●	●	-	-	-	-	-	●	-	-	-	-	-	-	19
Topper	SC, US	33.005763°N, 81.489266°W	●	●	-	-	-	-	-	-	-	-	-	●	●	●	19
Blackville	SC, US	33.361545°N, 81.304348°W	-	●	●	-	-	-	-	-	-	-	-	●	●	●	17
Lake Cuitzeo	MEX	19.936516°N, 101.155676°W	●	●	-	-	●	-	●	-	-	-	-	-	-	-	37
Lommel	BEL	51.2362310°N, 5.2546860°E	●	●	-	-	●	●	●	●	-	-	-	-	-	●	19
Melrose	PA, US	41.925410°N, 75.510436°W	-	●	●	-	●	●	●	●	-	-	-	-	-	●	17
Mucunuque (MUM7b)	VEN	8.7757910°N, 70.8181220°W	●	●	●	-	-	●	-	●	-	-	-	-	-	-	30-36
Ommen	NED	52.5269500°N, 6.3635170°E	-	●	-	-	●	●	●	●	-	-	-	-	-	-	19
NOT USED FOR AGE MODELS			-	-	-	-	-	-	-	-	-	-	-	-	-	-	
Chobot	CAN	52.956004°N, 114.734872°W	-	●	-	●	●	●	●	●	-	-	-	-	-	-	19
Gainey	MI, US	42.885973°N, 83.614324°W	●	●	-	-	-	●	●	●	-	-	-	-	●	-	19
Kangerlussuaq	GRN	67.156400°N, 50.023300°W	-	●	-	●	-	-	-	-	-	-	-	-	-	-	38
Kimbel Bay	NC, US	34.981811°N, 78.776820°W	-	●	-	-	-	-	-	-	-	-	-	-	-	●	19
Morley	CAN	51.145737°N, 114.866317°W	-	●	-	-	-	-	-	-	-	-	-	-	●	-	4
Mt.Viso	FRA/ITA	≈44.698750°N, ≈7.0345750°E	-	●	-	-	-	●	●	-	-	-	-	-	●	-	36, 39
Newtonville	NJ, US	39.569579°N, 74.910859°W	●	●	●	●	-	-	-	●	●	-	-	-	-	●	40
Paw Paw Cove	MD, US	38.697466°N, 76.342255°W	●	●	-	-	-	-	-	-	-	-	-	-	-	-	40
Watcombe Bottom	UK	50.593900°N, 1.230800°W	●	●	-	-	●	●	-	●	●	-	-	-	-	-	20
TOTALS			23	27	6	11	11	20	17	20	23	5	3	3	10	9	
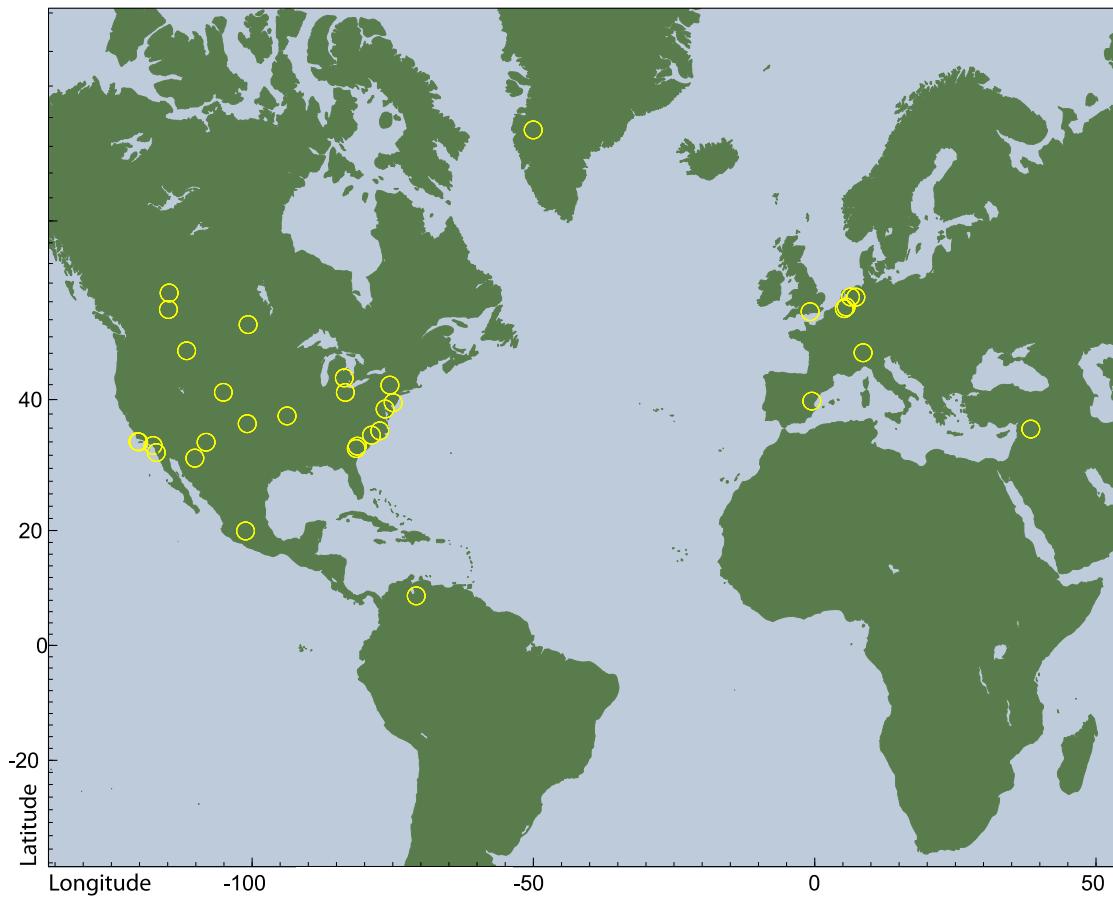
Fig. S3. Locations for 32 YDB sites on four continents. For latitude and longitude, see **Table S1**.

Table S2. YDB studies by proponents, independent workers, and critics. Each proxy shows references by number.

PROXY	PROPONENTS	INDEPENDENT WORKERS	CRITICS
Cosmic impact spherules	4, 9, 19, 37, 41, 42	21-29, 30-36, 39, 40, 46, 47, 56	58, 59, 60, 61
Meltglass	17, 19	30-36, 47, 56	--
Carbon sperules, glass-like carbon, aciniform carbon, PAHs, fullerenes	4, 9, 37, 41, 42	21-29, 30-36, 48	18, 59, 61, 62, 63
Nanodiamonds	4, 20, 37, 38, 41, 42, 44, 45	21-29, 48, 49, 50	18, 59, 61, 63, 64
Iridium	4, 41, 42	46, 51, 52	59, 60, 61, 65
Platinum	--	53	--
Osmium	--	51, 54, 55, 56	65
Nickel, cobalt, chromium, thorium, ^{14}C, ^{10}Be, ^{26}Al, REEs	4, 17, 19, 41, 42, 43	5, 51, 57	--

5

FIGURES AND TABLES for YDB sites

Most sites were chosen for YDB investigation because independent chronostratigraphic investigations already existed. Occasionally, we added one or more ^{14}C dates for a site. In some cases, the original workers rejected dates for various reasons, but for completeness, we have modeled all available dates.

For all images of age models below, horizontal red dashed lines indicate the upper and lower boundaries of the YDB sample. Vertical red dashed lines denote the previously published YDB age range at 68% (12,950 to 12,650 Cal B.P.). Laboratory numbers matching the accompanying tables are listed along the left side of each image, where those falling within the YDB interval are shown in green. Dates in blue were rejected by OxCal as outliers, i.e., either too old or too young for the model. Unmodeled probability distribution curves are in light gray, and OxCal's modeled and calibrated probability distributions are in dark gray. When present for age-depth models, the lighter blue curve represents the full-depth probability of the age-depth model at 95% and the darker blue represents 68%. Boxed areas that include the blue horizontal bar represent separate Phases, and the probability distributions between them represent the likely ages of transition. Earlier workers identified the stratigraphic intervals for most sites (see source papers in **Table S2**). All phases are in stratigraphic order with dates in chronological order within each phase. Notations are the same for all similar figures below. OxCal's coding for each site is in **SI Appendix—Code.**

HIGH-QUALITY CHRONOLOGIES

Abu Hureyra, Syria

Except for the age model and data table below, the following information was extracted from Bunch et al. (17) and Wittke et al. (19). See main manuscript and **Tables S1-S2** for other site information. This is an excavated archaeological site ("tell") located on a terrace near the Euphrates River on well-developed, limey, silty, unconsolidated sand, atop massive limestone deposits (66). Several 12,800-year-old pit-houses at Abu Hureyra and their immediate environs were associated with a dark, 3-cm-thick, charcoal-rich layer (centered at 420 cmbs (centimeters below surface) or 284.6 masl (meters above sea level), indicating a major burning episode. The original excavators previously attributed this layer to residue from cooking fires (66), but now attribute it to biomass burning at the time of the YDB impact event (17). The proxy-rich YDB layer contained abundance peaks in charcoal, nanodiamonds, carbon spherules, impact-related spherules (595/kg) and melt-glass (15.8 g/kg; the highest of any YDB site investigated) (17, 19, 20, 67).

The palynological and macrobotanical record demonstrates that the YDB layer coincides with major climatic change, interpreted to represent the onset of the Younger Dryas episode (66, 68). At that time, the regional environment of Abu Hureyra abruptly changed from moist woodland-steppes to arid, mostly treeless steppes. This change is reflected in the sudden decline in abundance of charred seed remains of several major food groups. First, there was a decline by ≈50% in seeds of food plants, such as wild pears and cherries, found in an oak-dominated park-woodland that disappeared from the Abu Hureyra area at the Younger Dryas onset. Second, there was a decline of ≈70% in seeds of some legumes. Third, there was a decline of ≈60% in grains of wild ryes and wheat (68). Altogether, changes in more than 150 species of plants reflect the major effects of this abrupt climatic change from warmer, moister conditions, equivalent to the Allerød oscillation in Europe, to cooler, dryer conditions at the onset of the Younger Dryas at ≈12,800 years ago. This climatic change coincides with deposition of impact-related proxies in the YDB layer at Abu Hureyra.
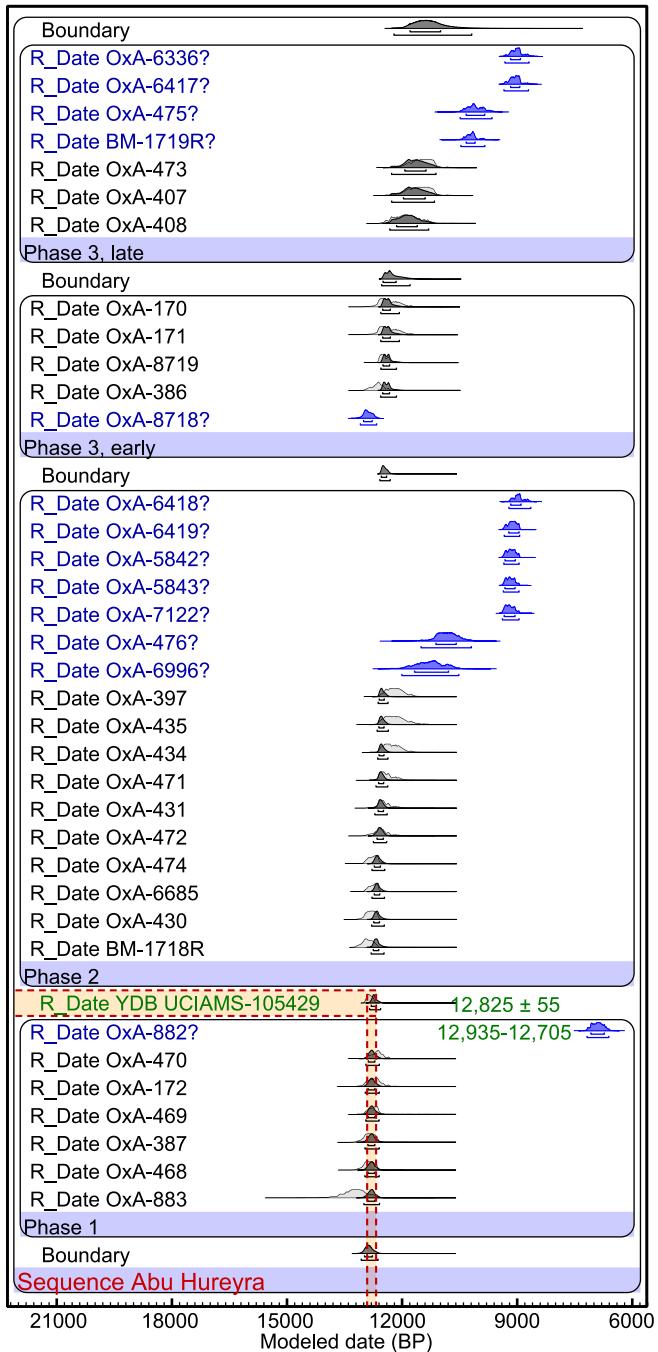
Fig. S4. Abu Hureyra age-sequence model. For this and chronological figures below, the vertical dashed lines represent the previously published YDB range of 12,950 to 12,650 Cal B.P. (19, 20). Horizontal red dashed lines represent the bounds of the proxy-rich sample. Laboratory numbers of dates are along the left side with dates falling within the YDB interval shown in green text. "R_Date" represents ^{14}C dates and "C_Date," when present, represents OSL, varve, and ice layer dates. OxCal's individual unmodeled probability distribution curves are shown in light gray, and modeled probability distributions in dark gray. This figure and all similar models have multiple boxed areas that represent separate chronostratigraphic Phases or Sequences, where the probability distributions of the boundaries between phases represent the likely ages of the transition. These phases mainly were identified by earlier site investigators, using prior, temporally diagnostic information, including stratigraphy, archaeology, palynology, and/or climatology. All Phases are in stratigraphic order, and dates within each Phase typically are in chronological order. Notations are the same for all similar figures below.

Table S3. Abu Hureyra: modeled and unmodeled Bayesian ages for this site, as for all tables below. The first few columns list laboratory numbers, uncalibrated ^{14}C dates (with OSL dates, when used), labeled as "μ," statistical uncertainties (errors), labeled as "σ," with depths, where available. The term "R_Date" refers to ^{14}C dates, and "C_Date" refers to OSL, varve, or ice layer dates. The next group of columns shows unmodeled calibrated ages at 95% and 68% CI, followed by a group of columns for modeled calibrated ages. Agreement indices are shown for individual dates, with A_{model} and $A_{overall}$ percentages, where

7

≥60% agreement is equivalent to ≥95% CI. Last, the type of material dated is listed, when available. The modeled YDB age is highlighted in green. Dates rejected by OxCal are in blue. Rarely, dates in red at the bottom of the table were excluded for the reasons stated.

For Abu Hureyra, all dates are from Moore et al. (66). Wittke et al. (19) listed these dates in approximate stratigraphic order within the 7×7-meter trench. However, some of the dates used in the model are from sediment separated by up to ≈10 m within the trench, and so, their exact stratigraphic relationships are not always clear. For greater clarity in this contribution, we placed the dates in chronological order within each Phase. In spite of the relationship between other dates, the proxy-rich YDB layer is accurately dated to 12,825 ± 55, because a radiocarbon date (UCIAMS-105429) was acquired from charcoal taken directly from that layer. This is the same age as reported in Kinzie et al. (20) and overlaps the date of 12,815 ± 160 (OxA-172; IntCal09) originally presented by Wittke et al. (19) for an adjacent sample.

Laboratory #	μ	σ	UNMODELED 95.4% range		μ	σ	Modelled (BP) 95.4% range		μ	σ	Amodel=83.7 Aoverall=81.4	
Boundary							12345	10355	11360	520		
R_Date OxA-6336	8140	90	9405	8770	9095	145	9405	8770	9095	150	0.6	Grain (domestic einkorn)
R_Date OxA-6417	8170	90	9430	8785	9140	135	9430	8785	9140	135	0.7	Grain (domestic w heat)
R_Date OxA-475	9060	140	10570	9740	10185	215	10570	9740	10185	215	3.4	Charred gazelle bone
R_Date BM-1719R	9100	100	10555	9925	10280	140	10555	9925	10280	140	3.8	Charcoal
R_Date OxA-473	10000	170	12370	11090	11585	285	12375	11225	11750	275	87.1	Charred sheep bone
R_Date OxA-407	10050	180	12385	11175	11660	305	12370	11260	11790	275	93.7	Charred wild sheep bone
R_Date OxA-408	10250	160	12535	11355	11965	305	12415	11410	11950	260	108.6	Humic fraction of OxA-407
Phase 3, late												
Boundary							12635	11915	12345	200		
R_Date OxA-170	10600	200	12890	11815	12415	265	12655	12190	12465	125	128.4	Grain (wild einkorn)
R_Date OxA-171	10600	200	12890	11815	12415	265	12655	12190	12465	125	128.4	Grain (wild einkorn)
R_Date OxA-8719	10610	100	12730	12170	12535	130	12655	12250	12490	95	101.1	Grain (domestic rye)
R_Date OxA-386	10800	160	13075	12385	12710	175	12660	12250	12495	100	66.8	Grain (wild einkorn)
R_Date OxA-8718	11140	100	13180	12750	12980	110	13180	12750	12980	110		Grain (domestic rye)
Phase 3, early												
Boundary							12675	12430	12560	65		
R_Date OxA-6418	8115	80	9300	8725	9050	140	9300	8725	9050	140		Grain ((domestic barley)
R_Date OxA-6419	8230	80	9420	9015	9210	115	9420	9015	9210	115		Grain (domestic emmer)
R_Date OxA-5842	8260	75	9435	9030	9245	110	9435	9030	9245	110		Grain (splt/br.w heat)
R_Date OxA-5843	8275	65	9445	9030	9265	105	9445	9030	9265	105		Grain (domestic rye)
R_Date OxA-7122	8290	75	9470	9030	9275	110	9470	9030	9275	110		Grain (domestic einkorn)
R_Date OxA-476	9600	200	11600	10280	10925	285	11595	10275	10925	285		Fulvic fraction of OxA-434
R_Date OxA-6996	9860	220	12095	10605	11370	375	12100	10605	11370	375	0.1	Grain (domestic rye)
R_Date OxA-397	10420	140	12675	11810	12260	230	12725	12485	12615	60	48.4	Grain (wild einkorn)
R_Date OxA-435	10450	180	12720	11650	12255	275	12750	12480	12630	65	72.9	Humic fraction of OxA-434
R_Date OxA-434	10490	150	12715	11835	12335	220	12735	12485	12625	65	79.8	Charred gazelle bone
R_Date OxA-471	10620	150	12770	12060	12485	190	12780	12500	12645	65	122.6	Humic, repeat of OxA-407
R_Date OxA-431	10680	150	12850	12100	12555	180	12805	12510	12660	70	128.1	Humic fraction of OxA-430
R_Date OxA-472	10750	170	13035	12155	12635	200	12840	12525	12680	75	135.4	Humic fraction of OxA-473
R_Date OxA-474	10930	150	13095	12600	12850	130	12875	12580	12735	70	110.6	Humic fraction, sheep bone
R_Date OxA-6685	10930	120	13065	12675	12845	105	12880	12600	12745	65	113.6	Grain (domestic rye)
R_Date OxA-430	11020	150	13155	12685	12905	125	12890	12600	12750	70	97.5	Charred gazelle bone
R_Date BM-1718R	11140	140	13250	12730	12990	135	12900	12615	12765	70	73.2	Charcoal
Phase 2												
R_Date UCIAMS-105429	11070	40	13060	12805	12935	70	12935	12705	12825	55	80.7	Charcoal
R_Date OxA-882	6100	120	7260	6675	6980	150	7260	6680	6980	150		Grain (wild einkorn)
R_Date OxA-470	10820	160	13070	12415	12735	170	13030	12730	12885	75	79.8	Humic fraction of OxA-468
R_Date OxA-172	10900	200	13205	12400	12810	195	13045	12730	12890	80	116.9	Grain (wild einkorn)
R_Date OxA-469	10920	140	13085	12620	12840	120	13035	12735	12890	75	100.9	Humic fraction of OxA-468
R_Date OxA-387	11070	160	13225	12695	12940	140	13055	12735	12895	80	117.7	Charred *Bos* bone
R_Date OxA-468	11090	150	13215	12705	12950	135	13060	12735	12895	80	116.2	*Bos* bone, repeat OxA-387
R_Date OxA-883	11450	300	13935	12720	13315	305	13080	12730	12905	85	65	Grain (wild einkorn)
Phase 1												
Boundary							13155	12765	12970	95		
Sequence Abu Hureyra												

Arlington Canyon, California

Except for the age model and data table below, the following information was extracted from a detailed description in Kennett et al. (9) and Wittke et al. (19). See main manuscript **Table 1** and **Tables S1-S2** for other site information. At this site, the sampled section is exposed in a stream cut on the northwest part of Santa Rosa Island, California. At the base of the section, extending below creek level, a 44-cm-thick, organic-rich, dark blue-gray, silty mud layer rests directly on a gravel deposit at 5.03 meters below surface (mbs). This layer is capped by a coarse, cobble-rich deposit (≈60 cm thick) and in turn by a second less dark layer (20 cm thick) of gray to black laminated sandy silt. Alluvial sands and gravels represent the remainder of the overlying sequence. Ten nearly continuous samples, varying from 2 to 6 cm thick, were from the 44-cm lower dark layer between 459

and 503 cm below surface (cmbs). Four more samples were from the upper dark layer, spanning a total of 111 cm (9). This entire section contained impact-related proxies (magnetic spherules, carbon spherules, elongated spherules, nanodiamonds, charcoal, and aciniform carbon), although the lower section contained most of the peaks. Therefore, the bottom probably best represents the YDB layer, even though the ages of the upper and lower sections are nearly indistinguishable. This similarity in age of all parts of this section supports rapid deposition over a short time span (9).

The YDB layer at Arlington Canyon is coeval with the Younger Dryas onset in the Santa Barbara Basin and corresponds to a major transition from conifer-dominated forests to modern chaparral-oak woodlands on the island (9). The pollen record indicates the island was partly forested by several species of long-lived conifers, including Douglas fir (*Pseudotsuga menziesii,* max lifespan: >1,300 years), Torrey pine (*Pinus torreyana*, max: >450 years), and Monterey cypress (*Cupressus macrocarpa*, max: >250 years) (9, 20). Radiocarbon dating of wood for Arlington Canyon is subject to a significant old wood effect from these long-lived trees and was accounted for in the age-depth model of this paper, as was done by Kennett et al. (9), but not by van Hoesel et al.

(18) or Meltzer et al. (13). We investigated the old wood effect using the Charcoal Outlier coding in OxCal, which accepted all 12 dates from the proxy-rich YDB section as being part of the same model. This means that all carbon material could have been produced during one YDB wildfire episode or some could have been redeposited over a short interval.

In addition, the YDB correlates with the extinction of the island's pygmy mammoths, which, in turn, is closely coincident with megafaunal extinctions on the continent. The YDB also marks the likely abandonment of the island by humans for ≈800 years (9), corresponding to a proposed human population decline across the Northern Hemisphere.

Meltzer et al. (pg. 7 of (13)) stated that for the YDB layer, "*it is also reasonable to expect that the layers above and below it should not be the same age. If they are, then they should have impact indicators as well.*" In reaching that conclusion, those authors overlooked the conclusions of Kennett et al. (9, 45) that the proxy-rich layer at Arlington Canyon was deposited within a few decades or less, so that YDB impact proxies were reworked and distributed throughout a 111-cm profile. A span of a few decades cannot be accurately dated using radiocarbon dates with uncertainties of a few decades, although Bayesian analyses can assist.

Table S4. Arlington Canyon, California. Dates are from Kennett et al. (9). No ^{14}C dates are available from below the rapidly accumulated YDB layer because the water table was encountered at that depth. The ages highlighted in yellow were used to define the YDB layer, and then used as Priors to determine the age of the YDB layer, as noted in **SI—Methods**, below, and in **SI—Code**. Age-depth plot is **Fig. 1** in the main manuscript. Median depths are shown for samples; details in Kennett et al. (9).

Laboratory #	μ	σ	Depth (cm)	UNMODELED (BP) 95.4% range		μ	σ	Modelled (BP) 95.4% range		μ	σ	Amodel=66.2 Aoverall=65.4	
Boundary								12815	12330	12630	120		
R_Date UCIAMS-47235	11040	30	97.0	13020	12790	12905	60	12820	12440	12665	95	99.5	Charcoal
R_Date UCIAMS-47236	12095	40	181.0	14100	13785	13945	80	12820	12515	12690	75	97.4	Charcoal
R_Date UCIAMS-47237	10895	35	216.0	12815	12700	12755	30	12825	12570	12715	60	86	Charcoal
R_Date UCIAMS-47238	11105	30	268.5	13080	12850	12985	60	12870	12615	12745	60	91.8	Charcoal
Sequence Upper layer													
Boundary YDB_top								12905	12645	12770	65		
R_Date UCIAMS-47239	11105	30	394.0	13080	12850	12985	60	12910	12655	12775	60	93.5	Charcoal
R_Date UCIAMS-36308	11095	25	466.5	13070	12840	12975	60	12910	12660	12780	60	95.2	Wood
R_Date UCIAMS-42816	11095	25	404.5	13070	12840	12975	60	12915	12670	12785	60	95.5	Wood
R_Date UCIAMS-36307	11070	25	472.0	13045	12815	12935	60	12915	12675	12790	60	101.5	Wood
R_Date UCIAMS-36961	11440	90	482.5	13450	13105	13280	90	12920	12680	12795	60	97.1	Carbon elongate
R_Date UCIAMS-36960	11185	30	482.5	13115	13000	13060	30	12925	12685	12800	60	98.1	Carbon spherule
R_Date UCIAMS-36962	11110	35	482.5	13080	12840	12985	60	12925	12690	12805	60	95.9	Wood
R_Date UCIAMS-36959	11075	30	482.5	13055	12820	12940	65	12930	12695	12810	60	103.2	Glassy carbon
R_Date BETA-161032	10860	70	482.5	12915	12660	12760	60	12940	12695	12815	65	29.6	Charcoal
R_Date UCIAMS-36306	11375	25	488.0	13290	13135	13215	40	12945	12695	12820	65	97.5	Wood
R_Date UCIAMS-36305	11235	25	495.5	13145	13050	13095	25	12955	12700	12825	65	100.2	Wood
R_Date UCIAMS-36304	11020	25	500.5	13000	12780	12880	60	12960	12700	12830	70	96.4	Wood
Sequence YDB_layer													
Boundary YDB_base								12975	12700	12835	70		
Sequence Arlington Canyon													
YDB age from Priors													
Arlington_YDB_layer								12925	12695	12805	55		

Aalsterhut, Netherlands

Except for the age model and data table below, the following information was extracted with minor modifications from van Hoesel et al. (18, 63), who sampled the site for impact proxies. See main manuscript **Table 1** and **Tables S1-S2** for other site information. The Late Glacial-Holocene stratigraphy at Geldrop-Aalsterhut is similar to that of Lingen, Lommel, and Ommen. Eolian deposits, called Younger Coversands I, formed during the Older Dryas cold stadial, and later, during the Allerød climate oscillation, the Usselo layer formed above them. Now visible as a bleached sand layer, the

Usselo layer generally contains abundant charcoal particles at its upper boundary, indicating the position of the YDB layer. The stratum overlying the YDB and the Usselo, the Younger Coversands II, formed during the Younger Dryas due to increased eolian activity as vegetation cover diminished during the colder climate.

The age-sequence model in **Fig. S5** below is based on the reported stratigraphic profile (18), where a nanodiamond-rich layer is the base. Only the three dates from the proxy-rich layer were used in the age model.
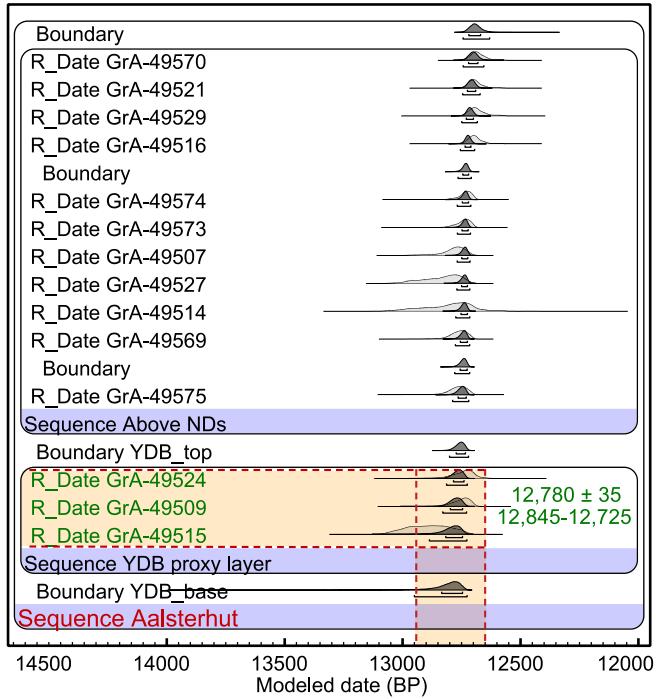
Fig. S5. Aalsterhut age-sequence model. Three dates are on charcoal from directly within the proxy-rich layer, containing nanodiamonds. Eleven dates come from above that layer. The YDB age is a weighted average of the bottom three modeled dates.

Table S5. Aalsterhut, Netherlands. Dates from van Hoesel et al. (18). The ages of the two boundaries highlighted in yellow were used to calculate the age of the YDB layer, highlighted in green.

Laboratory #	μ	σ	depth (cm)	UNMODELED 95.4% range		μ	σ	Modelled (BP) 95.4% range		μ	σ	Amodel=160.9 Aoverall=160.1	
Boundary								12745	12630	12690	25		
R_Date GrA-49570	10735	45	-4.50	12740	12595	12680	35	12745	12655	12700	20	119.9	charcoal
R_Date GrA-49521	10765	50	-4.50	12750	12625	12690	30	12750	12670	12710	15	126.7	charcoal
R_Date GrA-49529	10755	55	1.00	12745	12590	12685	35	12750	12680	12715	15	122.9	charcoal
R_Date GrA-49516	10765	50	1.00	12750	12625	12690	30	12755	12695	12725	15	109.2	charcoal
Boundary								12765	12705	12735	15		
R_Date GrA-49574	10845	45	1.00	12800	12685	12735	30	12770	12710	12735	15	131.3	charcoal
R_Date GrA-49573	10860	45	1.00	12810	12690	12740	30	12770	12710	12740	15	133.9	charcoal
R_Date GrA-49507	10920	50	1.00	12915	12700	12785	55	12770	12710	12740	15	99.7	charcoal
R_Date GrA-49527	10960	60	1.00	12990	12715	12835	75	12775	12715	12740	15	83.5	charcoal
R_Date GrA-49514	10880	110	3.00	13035	12635	12805	100	12775	12715	12740	15	153.4	charcoal
R_Date GrA-49569	10895	45	3.00	12840	12695	12765	40	12780	12715	12745	15	120	charcoal
Boundary								12780	12715	12745	15		
R_Date GrA-49575	10900	50	3.25	12875	12690	12770	45	12790	12715	12750	20	126	charcoal
Sequence Above NDs													
Boundary YDB_top								12805	12720	12760	20		
R_Date GrA-49524	10840	75	4.75	12910	12635	12750	60	12815	12725	12765	20	110	charcoal
R_Date GrA-49509	10865	55	4.75	12835	12680	12750	40	12830	12725	12775	25	93.6	charcoal
R_Date GrA-49515	11020	75	4.75	13050	12730	12890	85	12890	12725	12795	45	86.7	charcoal
Sequence ND-rich layer													
Boundary YDB_base								12950	12725	12815	70		
Sequence Aalsterhut													
YDB age from Priors													
Aalsterhut_YDB_layer								12845	12725	12780	35		

Big Eddy, Missouri

Except for the age model and data table below, the following information was extracted from Wittke et al. (19). See main manuscript **Table 1** and **Tables S1-S2** for other site information. This site lies in the floodplain of the Sac River in southwestern Missouri. At the site, frequent slackwater, overbank flooding produced a thick stratigraphic profile

dominated by alluvial, fine-grained, silty clay loam, occasionally intercalated with weakly developed soils. There is little difference between the YDB layer and surrounding alluvial sediment, although the deposits from 10 to 40 cm above the YDB appear slightly darker. Five 8-cm-thick continuous samples were taken at low resolution across a 40-cm interval from 311 to 351 cmbs, and the 8-cm-thick YDB sample at a depth of 327 to 335 cmbs displayed a peak of 100 spherules/kg.

Table S6. Big Eddy, Missouri. Dates used for age-depth model are from Hajic et al. (69) and Lopinot et al. (70, 71). The ages of the two boundaries highlighted in yellow were used to calculate the age of the YDB layer, highlighted in green. Age-depth plot is **Fig. 2** of the main manuscript.

Laboratory #	μ	σ	Depth (cm)	UNMODELED (BP) 95.4% range		μ	σ	Modelled (BP) 95.4% range		μ	σ	Amodel=101.7 Aoverall=101.5	
Boundary								11465	10920	11235	135		
R_Date AA-35462	9835	70	283.0	11600	11105	11270	95	11465	10920	11235	135	107.8	Charcoal
R_Date AA-72611	9751	64	285.0	11275	10805	11145	105	11470	10970	11255	125	114.2	Charcoal
R_Date AA-72609	9924	50	286.0	11605	11225	11360	100	11540	10970	11285	130	106.2	Charcoal
R_Date AA-72610	10440	160	294.0	12705	11770	12270	245	12275	11255	11840	280	92.1	Charcoal
R_Date AA-26653	10185	75	298.0	12150	11405	11855	165	12315	11365	11930	235	97.1	Charcoal
R_Date AA-75719	10506	53	303.0	12640	12155	12455	105	12520	11785	12160	185	93.2	Charcoal
R_Date AA-27487	10400	75	306.0	12540	12020	12270	140	12525	11885	12215	160	104.3	Charcoal
R_Date AA-27480	10340	100	308.0	12540	11810	12175	190	12545	11925	12245	155	109.4	Charcoal
R_Date AA-29022	10430	70	313.0	12555	12065	12310	135	12645	12035	12340	155	103.2	Charcoal
R_Date AA-75720	10896	54	315.0	12890	12690	12770	50	12735	12090	12410	165	102.9	Charcoal
R_Date AA-72607	9960	920	317.0	14070	9140	11625	1230	12755	12120	12440	165	105.1	Charcoal
R_Date AA-27488	10470	80	321.0	12620	12080	12365	145	12790	12195	12510	155	103.6	Charcoal
R_Date AA-27485	11280	75	322.0	13295	13025	13150	70	12895	12340	12640	145	100.4	Charcoal
R_Date AA-72612	10959	54	322.0	12980	12715	12825	70	12905	12390	12675	130	105.1	Charcoal
R_Date Beta-230984	10940	60	322.0	12975	12705	12815	70	12910	12415	12690	125	105.6	Charcoal
R_Date AA-27481	11160	75	326.0	13155	12805	13005	90	12925	12480	12725	115	94.2	Charcoal
YDB layer top								12935	12495	12735	110		
R_Date AA-25778	10260	85	328.0	12400	11645	12020	190	12400	11645	12020	190	0	Charcoal
R_Date AA-27486	11900	80	331.0	13980	13545	13725	110	12945	12540	12755	100	103	Charcoal
R_Date AA-26654	10710	85	333.0	12755	12435	12640	65	12950	12555	12765	95	102.4	Charcoal
YDB layer base								13010	12560	12790	105		
R_Date AA-27482	11190	75	338.0	13205	12835	13045	90	13085	12590	12830	115	95.7	Charcoal
R_Date AA-72608	12450	300	347.0	15620	13750	14650	485	13155	12675	12900	120	80.4	Charcoal
R_Date AA-26655	10940	80	347.0	13005	12700	12835	85	13165	12685	12910	120	92.4	Charcoal
R_Date AA-34586	12320	130	358.0	15015	13945	14415	275	14150	12970	13680	305	100.3	Charcoal
R_Date AA-34587	11930	110	364.0	14065	13490	13780	140	14210	13245	13785	240	97.1	Charcoal
R_Date AA-72613	11960	270	373.0	14875	13270	13955	405	14440	13475	13960	230	109.1	Charcoal
R_Date AA-34588	12250	100	375.0	14715	13830	14245	225	14535	13545	14020	235	107.5	Charcoal
R_Date AA-34589	11375	80	383.0	13385	13075	13220	80	13385	13075	13220	80	0.2	Charcoal
R_Date AA-27483	11910	440	384.0	15315	12935	14040	625	15030	13705	14320	345	91.3	Charcoal
R_Date AA-34590	12590	85	386.0	15235	14405	14875	210	15115	13795	14450	355	91.2	Charcoal
R_Date AA-27484	12700	180	396.0	15680	14265	15025	360	15455	13895	14705	395	100.6	Charcoal
Boundary								15455	13895	14705	395		
P_Sequence Big Eddy													
YDB age from Priors													
Big_Eddy_YDB_layer								12935	12580	12770	85		

Bull Creek, Oklahoma

See main manuscript **Table 1** and **Tables S1-S2** for details on stratigraphy, sampling, and proxies observed.
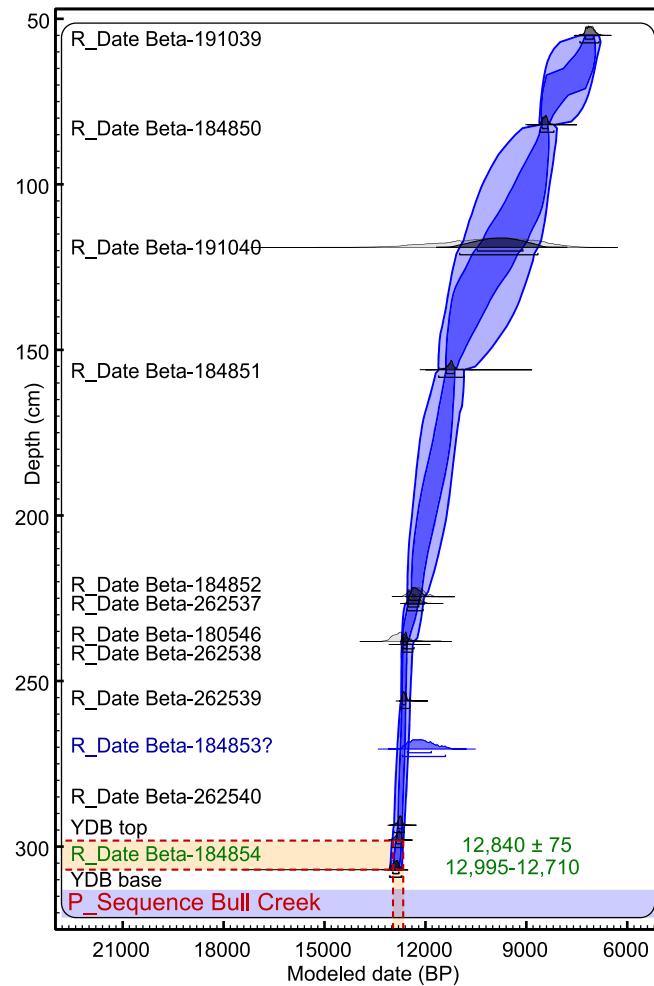
Fig. S6. Model for Bull Creek, Oklahoma. Biostratigraphic evidence indicates a significant expansion of grasslands (prairie) that occurred at the Younger Dryas onset, consistent with the Bayesian age of the YDB layer (50, 72). This style of age-depth model using probability curves was used because the deposition was judged to be reasonably continuous.

Table S7. Bull Creek, Oklahoma. Dates from Bement et al. (72) and Conley et al. (73). Yellow equals YDB top and base.

Laboratory #	μ	σ	Depth (cm)	UNMODELED (BP) 95.4% range		μ	σ	Modelled (BP) 95.4% range		μ	σ	Amodel=100.2 Aoverall=100.7	
Boundary								7405	6855	7110	125		
R_Date Beta-191039	6200	90	55	7315	6860	7095	115	7405	6855	7110	125	97.3	sed. organics
R_Date Beta-184850	7660	80	82	8600	8340	8465	70	8605	8175	8420	120	100.2	sed. organics
R_Date Beta-191040	8670	990	119	12720	7820	10125	1305	10980	8650	9810	615	126.1	sed. organics
R_Date Beta-184851	9850	90	156	11705	11095	11320	150	11605	10855	11240	170	106	sed. organics
R_Date Beta-184852	10400	120	224.5	12635	11825	12255	200	12540	12025	12290	140	115.2	sed. organics
R_Date Beta-262537	10410	70	226.5	12545	12045	12285	135	12550	12065	12315	135	100.4	sed. organics
R_Date Beta-180546	10850	210	238	13185	12170	12760	225	12705	12350	12565	95	93.9	sed. organics
R_Date Beta-262538	10750	70	239	12755	12565	12675	50	12710	12385	12580	90	74	sed. organics
R_Date Beta-262539	10640	70	256	12720	12425	12605	70	12725	12475	12620	70	107.7	sed. organics
R_Date Beta-184853	10350	210	270.5	12685	11400	12100	340	12685	11405	12100	340	3.9	sed. organics
R_Date Beta-262540	10870	70	293.5	12935	12675	12770	60	12935	12635	12765	70	91.7	sed. organics
YDB_top								12985	12660	12805	80		
R_Date Beta-184854	11070	60	298	13075	12780	12930	80	13045	12715	12875	85	98.9	sed. organics
YDB_base								13060	12710	12890	115		
P_Sequence Bull Creek													
YDB age from Priors													
Bull_Crk_YDB_layer								12995	12710	12840	75		

12

Daisy Cave, California

Except for the age model and data table below, the following information was extracted from Kinzie et al. (20). See main manuscript **Table 1** and **Tables S1-S2** for other site information. This cave/rockshelter complex is located on the northeast coast of San Miguel Island off the Southern California coast. Situated ≈15 km west of Arlington Springs, where human bones have been dated to ≈13,000 Cal B.P., Daisy Cave was occupied by Paleo-Indian people at ≈11,700 Cal B.P., and is one of several sites demonstrating that Paleo-Indians had boats capable of reaching the islands. Paleo-Indian artifacts dating to the latter part of the Younger Dryas episode (≈11,500 Cal B.P.) are found in correct chronostratigraphic position higher in the profile, as expected (74). Cut by erosion into a cliff overlooking the Pacific Ocean, the cave is currently ≈15 m above modern sea level, which was ≈60-70 m lower at 12,800 Cal B.P. Because the ocean floor drops off rapidly adjacent to the cave, the site has remained close to the coastline during the last 13,000 years.

Table S8. Daisy Cave, CA. Dates are from Erlandson et al. (74), <1 m away from the sampling trench. Dates on marine mollusca (red text) were not used because of the marine reservoir age offset. Age-depth plot is **Fig. 3** in the main manuscript.

Laboratory #	μ	σ	Depth (cm)	UNMODELED (BP) 95.4% range		μ	σ	Modelled (BP) 95.4% range		μ	σ	Amodel=99.6 Aoverall=99.6	
Boundary								3755	-300	2360	1250		
R_Date A1: CAMS-8864	3220	70	n/a	3615	3250	3450	80	3880	3240	3515	150	100.3	Charred twig
R_Date A3: CAMS-9095	3110	60	n/a	3450	3170	3310	75	3780	3140	3385	150	100.2	Charred twig
R_Date C: CAMS-8862	6000	70	5.1	7145	6665	6850	95	7285	6645	6905	160	100	Charred twig
R_Date E1: CAMS-8866	7810	60	16.0	8855	8425	8605	95	9045	8420	8665	155	100	Charred twig
R_Date E4: CAMS-8865	8040	60	28.4	9115	8650	8900	110	9330	8640	8955	170	99.8	Charred twig
R_Date F1: CAMS-8867	8600	60	33.9	9700	9480	9585	60	10015	9445	9640	135	99.7	Charred twig
R_Date F3: CAMS-8863	8810	80	47.3	10170	9600	9880	160	10330	9555	9935	205	100	Charred twig
R_Date G: CAMS-9094	10390	130	54.1	12645	11800	12230	220	12740	11660	12230	260	97.5	Charcoal
Phase Upper section													
Boundary YDB_age								13320	12050	12730	320		
R_Date I: CAMS-9096	11180	130	90.3	13285	12760	13025	135	13440	12740	13080	180	101.3	Charcoal
Phase Dark layer													
Boundary								13755	12860	13335	225		
R_Date J: CAMS-14369	11700	70	102.8	13725	13405	13535	80	13950	13340	13595	150	99.9	Charred twig
Phase Lower Section													
Boundary								15380	13420	14105	550		
Sequence Daisy Cave													
Skipped dates on shells													
R_Date Beta-15619	3430	90	N/A	--	--	--	--	--	--	--	--	--	--
R_Date Beta-49997	3510	80	N/A	--	--	--	--	--	--	--	--	--	--
R_Date Beta-15620	6380	110	5.1	--	--	--	--	--	--	--	--	--	--
R_Date Beta-52359	6500	80	5.1	--	--	--	--	--	--	--	--	--	--
R_Date Beta-15621	8460	100	16.0	--	--	--	--	--	--	--	--	--	--
R_Date Beta-15622	8730	120	28.4	--	--	--	--	--	--	--	--	--	--
R_Date Beta-15623	8900	120	33.9	--	--	--	--	--	--	--	--	--	--
R_Date Beta-49948	9360	90	47.3	--	--	--	--	--	--	--	--	--	--
R_Date Beta-52360	10600	70	54.1	--	--	--	--	--	--	--	--	--	--
R_Date Beta-14660	10700	90	54.1	--	--	--	--	--	--	--	--	--	--

Murray Springs, Arizona

Except for the age model and data table below, the following information was extracted with minor changes from Wittke et al. (19). See main manuscript **Table 1** and **Tables S1-S2** for other site information. The stratigraphy of this site has been described in much detail by Haynes and Huckell (75), including the identification of lithologic units, or strata (identified as Phases in **Fig. S7** and **Table S9**). Marl deposits (stratum E) are locally incised and filled with or overlain by sandy and gravelly stream-channel alluvium (stratum F1). Based on radiocarbon dating and the presence of Clovis artifacts associated with mammoth bones, Haynes and Huckell (75) concluded that stratum F1 is of Clovis age. Beginning at the onset of Younger Dryas cooling at ≈12,800 Cal B.P., a thin intermediate layer, stratum F2/D, was deposited atop stratum F1. This unit is frequently capped by the distinctive carbon-rich "black mat" (stratum F2) of Haynes (76), mostly of algal origin, but also containing charcoal. The black mat, in turn, is overlain in places by silt (stratum F3), resulting from alluvial deposition, including slopewash.

Ten 1-cm to 5-cm-thick discontinuous samples of bulk sediment were collected from a 46-cm-thick interval of sediment between 216 and 262 cmbs, and Vance Haynes, principal site investigator who assisted with sampling, identified these samples as belonging to strata E, F1, and F2. The YDB is a 1-cm-thick layer at 246 to 247 cm between stratum F1 and F2 (in stratum F2/D), which itself is discontinuous across the approximately 300×400-m excavation area. The YDB layer is marked by distinct abundance peaks in impact-related spherules, melt-glass, nanodiamonds, glass-like carbon, aciniform carbon, PAHs, fullerenes, and iridium (4, 19, 20, 44). Haynes et al. (46) independently confirmed the spherule abundance peak in the same stratum, but speculated about a non-impact origin, although offered no supporting evidence for that interpretation.

Haynes (76) observed that the black mat deposits were draped over the Clovis artifacts, articulated megafaunal skeletons, and Paleo-Indian campsites at Murray Springs, and therefore, had been deposited within "*a few weeks or months after the Clovis departure.*" Afterwards, the entire state of Arizona was abandoned for "*500 years or more after the Clovis folks had left*" (77). No *in situ* Clovis artifacts have been found above the YDB layer throughout the western U.S.A., consistent with a significant human population decline and/or reorganization across much of North America at ≈12,800 Cal B.P. (78).

Meltzer et al. (13) argued against compiling dates from correlated strata that are spread laterally across a site, such as at Murray Springs. Although we agree that such dates are not as robust as using those from the same stratigraphic profile, this practice nevertheless provides valuable data and is widely used in Bayesian analysis (79, 80, 81, 82). When such dates are used at the same site, a discrete and clearly identifiable stratum can be dated in one part of a site, and then, that date can be assigned to the same clearly identifiable stratum at other parts of the site, albeit with greater uncertainty. In this contribution, spatially scattered dates were used only at independently dated sites, where we adopted the stratigraphic correlations published by the site's independent investigators, who were most familiar with the local stratigraphy. Furthermore, for nearly all YDB sites with spatially separated dates, one or more YDB dates came directly from or within a few meters of the sampled YDB layer.
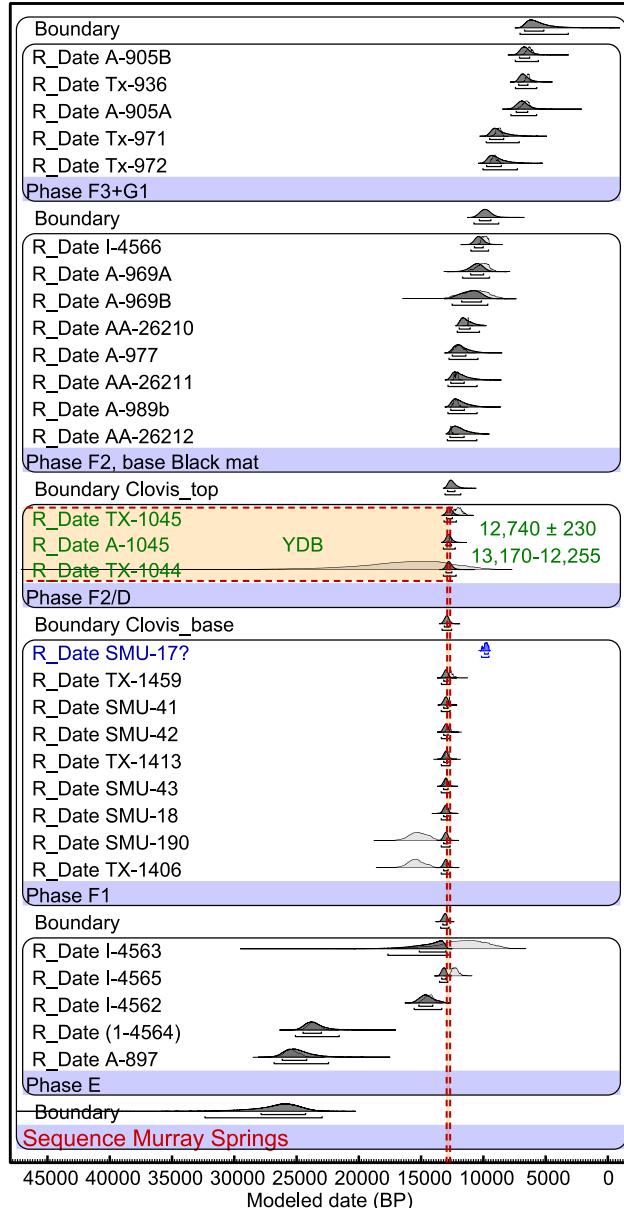

Fig. S7. Murray Springs, age-sequence model. The three dates highlighted in yellow (YDB) are on charcoal produced by Clovis campfires (76) that are contemporary with the YDB event. Strata are shown as Phases.

Table S9. Murray Springs, AZ. All dates are from independent site investigators (75). The strata sampled and the distances from the sampling site are shown in columns 4-5, based on Fig. 1.3 and Table A.1 in Haynes and Huckell (75). To establish a more robust age-sequence model, only those dates from within 40 m of the sampling site were used (column 5, below); one date (TX-1459) on a Clovis-age hearth is within ≈10 m of the sampling site. For date SMU-17, Haynes and Haas (83) reported that this was measured on charcoal, following contamination with wood preservative; OxCal rejected this sample as an outlier.

Laboratory #	μ	σ	Stratum & Distance (m)		UNMODELED (BP) 95.4% range		μ	σ	Modelled (BP) 95.4% range		μ	σ	Amodel=80.5 Aoverall=79.8
Boundary									7065	3180	5515	1095	
R_Date A-905B	5520	200	Profile N, G1a	15	6790	5900	6315	230	7440	5585	6585	475	100.1
R_Date Tx-936	5630	130	Area 1, G1a	30	6740	6180	6440	140	7425	5715	6670	445	99.8
R_Date A-905A	5750	250	Profile N, G1a	15	7170	6000	6600	290	7790	5725	6810	520	100.4
R_Date Tx-971	7920	150	Area 1, F3	30	9235	8410	8795	195	9780	7125	8690	700	100.7
R_Date Tx-972	8160	130	Area 1, F3	30	9465	8715	9105	195	10035	7270	8895	730	99.1
Phase F3+G1													
Boundary									10760	8770	9785	515	
R_Date I-4566	8830	170	Profile B, F2	10	10275	9515	9905	215	11010	9585	10320	360	98.6
R_Date A-969A	8900	400	Area 1, F2c	30	11180	9035	10075	535	11680	9510	10550	540	98.9
R_Date A-969B	9270	800	Area 1, F2c	30	12770	8640	10745	1075	12510	9650	11015	755	111.1
R_Date AA-26210	9823	46	Profile B, F2a4	10	11315	11175	11235	35	12105	10310	11340	475	99.4
R_Date A-977	10250	170	Area 1, F2b	30	12545	11345	11970	315	12765	10435	11750	610	100
R_Date AA-26211	10325	44	Profile B, F2	10	12390	11975	12170	120	12840	10505	11855	625	100.6
R_Date A-989b	10360	90	Area 1, F2a	30	12545	11830	12215	170	12855	10500	11855	625	98.4
R_Date AA-26212	10628	60	Profile B, F2a1	10	12715	12425	12600	65	12895	10525	11885	630	98
Phase F2, Black mat at base													
Boundary Clovis_top									13080	11810	12500	330	
R_Date TX-1045	10260	140	Area 4, F2/D	35	12530	11400	12000	280	13155	12165	12680	250	95.8
R_Date A-1045	10760	100	Area 4, F2/D	35	12850	12430	12675	85	13220	12260	12755	240	98.8
R_Date TX-1044	12600	2440	Area 4, F2/D	35	26535	9400	17010	4960	13210	12190	12725	255	108.3
Phase F2/D													
Boundary Clovis_base									13330	12550	12935	195	
R_Date SMU-17	8770	80	Area 1, F1	30	10155	9550	9820	160	10155	9550	9820	155	
R_Date TX-1459	10710	160	Profile B, F1	10	12980	12145	12595	190	13375	12670	13015	175	111.3
R_Date SMU-41	10840	70	Area 2, F1	30	12880	12640	12745	55	13380	12675	13020	175	101.3
R_Date SMU-42	10840	140	Area 2, F1	30	13065	12540	12770	135	13380	12670	13020	175	102.5
R_Date TX-1413	11080	180	Area 1, F1	30	13285	12690	12960	155	13380	12670	13020	175	101.8
R_Date SMU-43	11160	110	Area 2, F1	30	13240	12765	13005	120	13380	12670	13020	175	98.8
R_Date SMU-18	11190	180	Area 2, F1	30	13375	12720	13050	175	13380	12670	13020	175	100.2
R_Date SMU-190	12820	450	Area 1, F1	30	16565	13795	15220	715	13380	12670	13020	175	83
R_Date TX-1406	12940	390	Area 1, F1	30	16605	14095	15400	640	13380	12670	13020	175	78.5
Phase F1													
Boundary									13440	12755	13090	170	
R_Date I-4563	9780	1400	Profile A, E	40	15990	8175	11780	2005	17675	12830	14675	1440	51.6
R_Date I-4565	10430	160	Profile A, E	40	12700	11770	12255	250	13520	12855	13180	170	71.5
R_Date I-4562	12310	170	Profile A, E	40	15050	13815	14415	325	15565	13340	14530	560	99.9
R_Date I-4564	19620	380	Profile A, E	40	24545	22680	23645	465	25100	21580	23525	895	100.4
R_Date A-897	21200	500	Profile A, E	40	26565	24280	25445	565	26810	22430	24860	1135	96.9
Phase E													
Boundary									32365	22945	26890	2570	
Sequence Murray Springs													
YDB age from Priors													
Murray_Springs_YDB_layer									13170	12255	12740	230	

Sheriden Cave

Because of questions raised about the chronostratigraphic record of the site (13), we present here a detailed stratigraphic description of Sheriden Cave. This site is part of the Indian Trails Cave System, represented by six sinkhole entrances, including Sheriden Cave, Sheriden Pit, Cleveland Museum of Natural History Pit, the main entrance of Indian Trail Cavern, and two unnamed sinkholes. Sheriden Cave and the Indian Trails Cave System contain thick stratigraphic sequences of unconsolidated Quaternary sediments, for which six lithologic units have been identified based on changes in sediment color and particle size. Lithological descriptions of these units and their origins are based on observations from sedimentology, vertebrate paleontology, and archaeology (**Fig. S8**). Evidence exists for limited post-depositional soft sediment deformation, most likely related to freeze-thaw and solifluction processes during the Younger Dryas cooling episode, which sometimes stratigraphically displaced charcoal. Nevertheless, the radiocarbon dates indicate that the overall temporal sequence and stratigraphic integrity are intact. Interpretations of the sedimentary history below include a description of the nature of the units and their contacts (22-29).
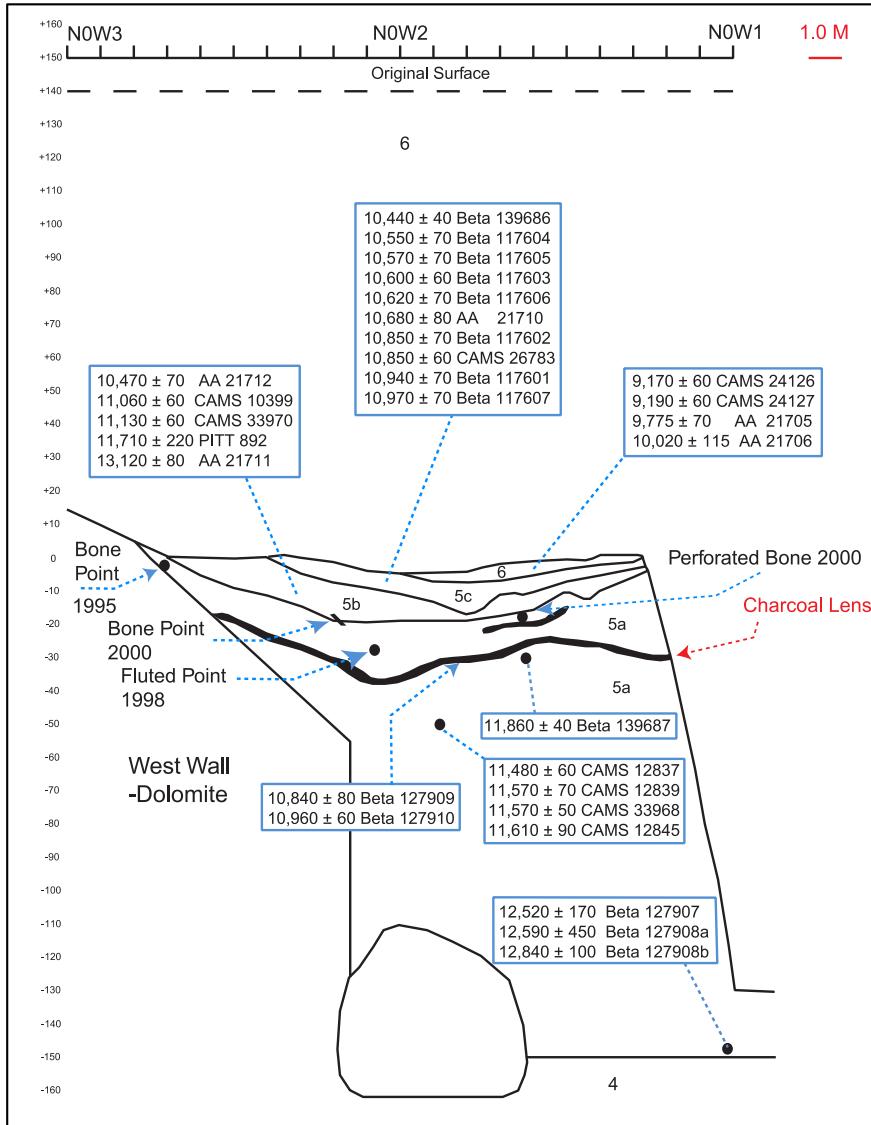
Fig. S8. Partial stratigraphic profile of Sheriden Cave. The YDB layer coincides with the charcoal lens (red arrow). The dates, shown in ^{14}C years BP, are laterally separated by up to ≈17 m. In the upper part of Phase 5a, there are three key dates: two are directly from the charcoal-rich layer containing impact proxies and one is directly from a Clovis bone projectile point, just above the charcoal layer. YDB proxies were found only in Phase 5a across an interval of <20 cm and not in any other stratigraphic level, except adjacent to the YDB at low concentrations (19, 20).

Lithology of Sheriden Cave.

Unit 1 is the oldest and deepest stratum. It is approximately 4 m thick and occurs between 12.5 and 16.5 m below the surface. Unit 1 is a light yellowish brown to dark grayish brown lake clay with higher silt and fine sands representing occasional episodes of turbidity transport (details for all units here and below from (21-29, 84).

Unit 2 is present in the Indian Trails Cave System, but absent in Sheriden Cave.

Unit 3 occurs in Sheriden Cave between 12 and 12.5 m below the surface. There is a transitional contact over 10 cm of a yellowish brown, medium-energy, or mixture of high and low energy, inwash with a high clay-silt-fine-sand ratio and sand-sized ceiling rain. The contact of Unit 3 with Unit 1 is a sharp highly oxidized reddish yellow film. The contact may represent a hiatus in deposition.

Unit 4 is between 10.5 and 12 m below the surface. Unit 4 is brownish gray, clast-supported angular Greenfield Dolomite pebble gravel with occasional glacial faceted and striated igneous and metamorphic pebble lithologies. No evidence exists of internal stratification, suggesting that Unit 4 is the result of cave roof collapse, sinkhole formation, and debris flow.

Unit 5 is up to 1.5 m in thickness and occurs between 9 and 10.5 m below the surface in the cave; the unit is fossil-rich and artifact-bearing. A lower sharp contact of Unit 5 with Unit 4 undulates laterally across 1-3-cm intervals because of post-depositional deformation, and the unit grades upwards over an interval of approximately 10 cm. The basal portion of Unit 5 is dark gray-and-white, matrix-supported, angular pebble gravel. Pebbles include dolomite, and occasional igneous or metamorphic erratics. The central portion of Unit 5 is thinly bedded gray or blue-gray silt, similar in lithology to the gray silt of Unit 6. Vertebrate fossils and fine pebble-size charcoal fragments are abundant. The sediments are weakly stratified, especially towards its top. Final deposition of this matrix-supported gravel might be related to freeze-thaw and solifluction processes during the Younger Dryas.

Subunit 5a, the upper portion of the unit, contains abundant and diverse late Pleistocene large and small vertebrate fossils and numerous pebble-sized carbonized plant remains. The subunit is also a dark gray-and-white, angular, matrix-supported pebble gravel, but in addition, it displays a sharply demarcated, few-cm-thick, dark charcoal layer containing Clovis artifacts; this is the YDB layer. Pebbles include several dolomite and occasional redeposited igneous and metamorphic erratics. The unit exhibits very weak, planar, internal stratification, and thus, is unlikely to be of debris flow origin. Furthermore, there is no clear upward or downward fining in clast size.

The contact of Units 5 and 6 is a reddish brown, discontinuous sheet of clayey silt, which may be a secondary feature resulting from chemical weathering. There is a sharp, but undulatory contact over a range of 1-3 cm in the central portion of the unit. This undulation is from the curvature of the originally planar silty gravel contact, due to post-depositional soft sediment deformation. There are several interbeds at the contact between Units 5 and 6, and thus, the coarse-grained lithology in Unit 5 does not abruptly change to the fine-grained lithology in Unit 6 across this contact.

Unit 6 is up to 2 m thick between 8 and 9 m below the surface. Early Holocene vertebrates and carbonized plant remains are abundant. The unit is laminated, suggesting episodic and frequent water-borne deposition, possibly sheet wash, with inputs of fine clastics. The source is likely to be eolian or re-worked eolian sediments, possibly loess. The contact with the lower portion of Unit 6 is transitional over approximately 20 cm. The basal contact portion of Unit 6 is an interbedded gray or blue-gray silt and pebbly gray silt and laminated sandy silt. It was deposited in a generally wetter environment than the upper portion of Unit 6. There is approximately 0.5 cm of thick gray silt beds interbedded with silty clay laminae or rhythmites. The thinly bedded gray silt is compatible with accumulation in a ponded, still-water setting,

and possibly with seasonal very-still-water times, possibly due to ice cover and frozen ground allowing the clay to settle out of suspension creating silty clay, varve-like couplets. There are some stringers of fine angular dolomitic pebbles in this deposit reflecting storm-driven influxes of water and sediment. In the basal 10 cm of Unit 6, a fine brown sand exhibits some cross stratification, indicative of deposition under temporarily flowing water. There is a transitional contact between the upper and lower portions of Unit 6 suggesting progressive dropping of the water table and a shift to storm-event driven deposition on a relatively dry surface from subaqueous, rhythmic deposition. The upper part of Unit 6 rises nearly to the bedrock roof and is composed mostly of brown sandy silt. The silt in this unit ultimately filled the cave sometime during the Holocene and remained above the water table.

Temporal Interpretations. Units 1, 2, and 3 represent ponded and inwash sediments that are late Pleistocene in age, greater than 50,000 years in age. Overlying radiocarbon ages suggest Unit 4 more likely represents an Older Dryas catastrophic debris flow event soon after the Last Glacial Maximum.

For Unit 5, radiocarbon ages, along with an abundant vertebrate fossil assemblage and Clovis artifacts, demonstrate that sediments began to accumulate during the Allerød climatic episode and continued until the early Younger Dryas. Unit 5a contains a charcoal-rich layer, coincident with the YDB that displays peaks in carbon spherules (148/kg), magnetic grains (2.5 g/kg), impact-related spherules (100/kg), nanodiamonds (400 ppb), and lonsdaleite-like nano-crystals. YDB proxies were not observed in Units 6, 4, 3, 2, and 1.

For Unit 6, radiocarbon ages and vertebrate fossil assemblages show that the unit represents early Holocene ponded sediments. It is possible, however, that the last cave filling may have occurred sometime between the early and middle Holocene.

Table S10. Sheriden Cave, OH. Dates from (21-29, 84, 85). Dates marked with "E" are dates on bones of extinct megafaunal, and "C" are dates on Clovis bone artifacts. The YDB age for Sheriden Cave is based on two radiocarbon dates from a single, thin, charcoal-rich layer that contains impact proxies (19, 20, 21-29). Using those two dates of 10,840 ± 80 and 10,960 ± 60 ^{14}C BP, we calculated a YDB average age of 12,840 ± 120 Cal B.P., which agrees with the published YDB age range. A Clovis bone projectile point, dating to 12,765 ± 30 Cal B.P. (10,915 ± 30 ^{14}C BP) was found 10 cm above the charcoal layer, along with a Clovis lithic point and another bone point (**Fig. S8**). Because the fire that produced the YDB charcoal lacked fuel inside the cave, the charcoal must have been redeposited from outside, possibly explaining the position of the two Clovis points above the impact-proxy layer. In any event, the dates on charcoal and the bone point are statistically identical. We used OxCal to produce an age-sequence model using the other thirty radiocarbon ages that have been obtained from Quaternary strata in Sheriden Cave (**Fig. 4** in main manuscript). Twenty-six of these radiocarbon ages are from the late Pleistocene stratum of Unit 5 and indicate an approximately continuous record of deposition from ≈16,000 to 12,000 Cal B.P.

Laboratory #	μ	σ	Depth (cm)	UNMODELED (BP) 95.4% range		μ	σ	Modelled (BP) 95.4% range		μ	σ	Amodel=94.9 Aoverall=95.4	
Boundary								10525	8785	9845	495		
R_Date CAMS-24126	9170	60	n/a	10500	10230	10350	75	10650	9910	10320	185	97.5	Wood charcoal
R_Date CAMS-24127	9190	60	n/a	10510	10235	10365	80	10660	9910	10330	190	98.2	Wood charcoal
R_Date AA-21705	9775	70	n/a	11355	10825	11175	105	11450	10405	11035	280	100	Wood charcoal
R_Date AA-21706	10020	115	n/a	11985	11235	11575	210	12095	10660	11420	355	100	Wood charcoal
Phase Unit 6													
Boundary								12645	12150	12435	135		
R_Date Beta-139686	10440	40	n/a	12530	12120	12330	115	12670	12300	12505	95	102	Reindeer collagen
R_Date Beta-117604	10550	70	n/a	12705	12185	12500	110	12685	12325	12525	90	110	Wood charcoal
R_Date Beta-117605	10570	70	n/a	12710	12240	12530	100	12690	12325	12525	90	107	Wood charcoal
R_Date Beta-117603	10600	60	n/a	12700	12420	12575	75	12695	12335	12530	90	101	Wood charcoal
R_Date Beta-117606	10620	70	n/a	12710	12420	12585	80	12695	12330	12530	90	100	Wood charcoal
R_Date AA-21710	10680	80	n/a	12735	12430	12625	70	12700	12335	12530	90	97.5	Wood charcoal
R_Date CAMS-26783-(E)	10850	60	n/a	12840	12745	12745	45	12705	12335	12535	90	103	Beaver collagen
R_Date Beta-117602	10850	70	n/a	12900	12650	12755	55	12705	12335	12535	90	104	Wood charcoal
R_Date Beta-117601	10940	70	n/a	12990	12705	12825	80	12705	12335	12535	90	107	Wood charcoal
R_Date Beta-117607	10970	70	n/a	13010	12710	12850	85	12705	12335	12535	90	105	Wood charcoal
Phase Unit 5C													
Boundary								12755	12460	12605	70		
R_Date AA-21712	10470	70	n/a	12585	12085	12370	140	12780	12505	12640	65	80.7	Wood Charcoal
R_Date CAMS-10349-(E)	11060	60	n/a	13070	12770	12920	80	12830	12520	12675	75	96.9	Peccary collagen
R_Date CAMS-33970	11130	60	n/a	13105	12820	12980	75	12830	12520	12675	75	90.9	Bone Collagen
R_Date PITT-0982	11710	220	n/a	14065	13115	13580	245	12830	12520	12675	75	89.1	Wood Charcoal
R_Date AA-21711	13120	80	n/a	16025	15405	15735	150	16025	15405	15735	150		Wood Charcoal
Phase Unit 5B													
Boundary YDB_top								12890	12565	12730	80		
R_Date UCI-38249-(C)	10915	30	n/a	12825	12705	12765	30	12975	12650	12815	80	100	Bone Clovis pt
R_Date Beta-127909	10840	80	n/a	12940	12630	12750	70	12985	12640	12810	85	99.3	Wood charcoal
R_Date Beta-127910	10960	60	n/a	12990	12715	12835	75	13040	12650	12835	95	103	Wood charcoal
Phase Unit 5A upper, charcoal layer													
Boundary YDB_base								13410	12720	12990	180		
R_Date CAMS-12837-(E)	11480	60	n/a	13455	13190	13325	65	13570	12970	13305	155	101	Bear collagen
R_Date CAMS-33968-(E)	11570	50	n/a	13490	13280	13400	55	13615	12995	13350	160	101	Bear collagen
R_Date CAMS-12839-(E)	11570	70	n/a	13550	13275	13400	70	13635	12995	13350	160	101	Bear collagen
R_Date CAMS-12845-(E)	11610	70	n/a	13485	13410	13450	20	13630	13040	13385	150	99.7	Bear collagen
R_Date Beta-139687-(E)	11860	40	n/a	13765	13570	13670	55	13865	13110	13530	200	99.9	Bear collagen
R_Date Beta-127907-(E)	12520	170	n/a	15290	14100	14710	325	15085	13145	14065	560	95.1	Stag-moose collagen
R_Date Beta-127908a-(E)	12590	450	n/a	16210	13585	14900	690	15210	13060	14010	600	93.8	Stag-moose collagen
R_Date Beta-127908b-(E)	12840	100	n/a	15710	15045	15345	170	15440	13160	14265	725	98	Stag-moose collagen
Phase Unit 5A, lower													
Boundary								15805	...	14555	790		
Sequence Sheriden Cave													
YDB age from Priors													
Sheriden_Cave_YDB_layer								13110	12625	12840	120		

Barber Creek, North Carolina

Except for the age model and data table below, the following information was extracted from Wittke et al. (19). See main manuscript **Table 1** and **Tables S1-S2** for other site information. This 4-meter-thick stratigraphic section is located at a high point, ≈6 masl, along a paleo-braidplain near the confluence of the Tar River and Barber Creek, North Carolina (86-92). Sediments from 100 to 300 cm below surface (cmbs) vary from coarse sand to fine with some small gravel that is predominantly alluvial in origin. These are overlain by ≈100 cm of medium to fine quartz sand mainly of eolian origin, representing sediments deposited as sand-sheets or dunes. An abrupt lithologic break and color change at ≈100 cmbs represents a change from alluvial to eolian sediment. Guided by OSL and radiocarbon dates and changes in sedimentation, three 2.5-cm-thick sediment samples were collected across a 7.5-cm interval from 95.0 to 102.5 cmbs. Analysis of these samples shows that the YDB occurs in the sample between 97.5 and 100 cmbs. The YDB layer is marked by a peak in impact-related spherules (1035/kg), with no spherules detected above and below that layer. The stratigraphic position of the YDB layer is consistent with earlier research indicating that the same layer corresponds to the onset of the Younger Dryas cooling episode (86-92).

Table S11. Barber Creek, North Carolina. Dates are in stratigraphic order within each Sequence, according to the site's investigators (91). The dated samples are from two trenches ≈10 m apart. Three OSL dates (UW1963, FS2797a, and FS2797b) were acquired from the same sample, using both multi-grain aliquots and single grains. Age-depth plot is **Fig. 5** in the main manuscript.

Laboratory #	Type	μ	σ	Depth (cm)	UNMODELED (BP) 95.4% range		μ	σ	Modelled (BP) 95.4% range		μ	σ	Amodel=64.6 Aoverall=61.3	
Boundary									11260	8375	9770	720		
R_Date Beta-188955	14C	8950	40	55.0	10225	9915	10075	95	11325	9260	10170	510	95.9	Charcoal
C_Date FS2476	OSL	9740	590	60.0	10860	8500	9680	590	11435	9550	10385	485	117.6	Quartz grn
R_Date Beta-166239	14C	8440	50	65.0	9535	9315	9460	50	11570	9760	10570	475	103.5	Charcoal
R_Date Beta-150188	14C	8940	70	75.0	10235	9785	10045	115	11880	10090	10900	465	98.4	Charcoal
R_Date Beta-166237	14C	9280	60	75.0	10650	10260	10455	95	12135	10345	11160	465	98.5	Charcoal
C_Date UW 1963	OSL	9100	700	77.0	10440	7640	9040	700	12350	10495	11350	480	36.4	Quartz grn
C_Date FS2797b =UW 1963	OSL	10390	620	77.0	11570	9090	10330	620	12710	10755	11675	505	109.1	Quartz grn
C_Date FS2797a =UW 1963	OSL	12800	710	77.0	14160	11325	12740	710	13140	11215	12105	490	65.2	Quartz grn
C_Date UW 1907	OSL	9200	700	80.0	10540	7740	9140	700	10545	7750	9140	700	12	Quartz grn
R_Date Beta-166238	14C	9860	60	95.0	11600	11175	11290	80	13380	11530	12370	485	94.6	Charcoal
Sequence Eolian														
C_Date YDB_age: UW 1908	OSL	12100	700	98.8	13440	10640	12040	700	13945	11865	12865	535	120.2	Quartz grn
R_Date Beta-188956	14C	10500	50	105.0	12615	12150	12445	100	14425	12445	13350	500	100.4	Charcoal
C_Date UW 1909	OSL	14500	1000	140.0	16440	12445	14440	1000	15645	12695	14070	760	83.5	Quartz grn
C_Date FS2511	OSL	16800	1900	315.0	20535	12950	16740	1900	16610	12865	14595	985	57.3	Quartz grn
Sequence Alluvial														
Boundary									17330	13025	14995	1165		
Sequence Barber Creek														

Blackwater Draw, New Mexico

Except for the age model and data table below, the following information was extracted from Wittke et al. (19). See main manuscript **Table 1** and **Tables S1-S2** for other site information. The stratigraphic section at this site, described by Haynes (76), is sandy alluvium, capped by lacustrine diatomite and silty muds. Unit C contains Clovis artifacts and mammoth bones, overlain by diatom-rich Unit D (76). The contact between Units D and C dates to the onset of Younger Dryas cooling (12,950 to 12,650 Cal B.P.) and represents the YDB layer.

From an exposure inside the South Bank Interpretive Center, fifteen discontinuous sediment samples (1 to 10 cm thick) were collected across a 1.67-m interval between 1237.8 and 1238.87 masl. A peak in impact-related spherules has been reported in a 1-cm-thick sample at the contact between Units D and C in three separate publications: Firestone et al. (4), Wittke et al. (19), and one by an independent group,

LeCompte et al. (40). Firestone et al. (4) reported finding 770 spherules/kg, whereas in a sample from the identical location, Surovell et al. (58) reported finding none. Subsequently, LeCompte et al. (40) reported concentrations of 1318/kg in a sample from the identical layer. The finding of 960 spherules per kg in Wittke et al. (19) is consistent with Firestone et al. (4) and LeCompte et al. (40) and contradicts the results of Surovell et al. (58), who did not follow the correct identification protocol (37, 40). Peaks in other proxies included glass-like carbon, charcoal, PAHs, fullerenes, nickel, and iridium.

We also examined sediment blocks collected ≈385 m north of the Interpretive Center. Called the "Folsom wedge" and "Clovis wedge," those blocks are associated with mammoth bones and Paleo-Indian projectile points, dating to 12,965 ± 65 Cal B.P. Confirming the wide extent of YDB proxies at the Blackwater Draw site, 90 spherules per kg were found in Clovis-age Level C with none above and below.
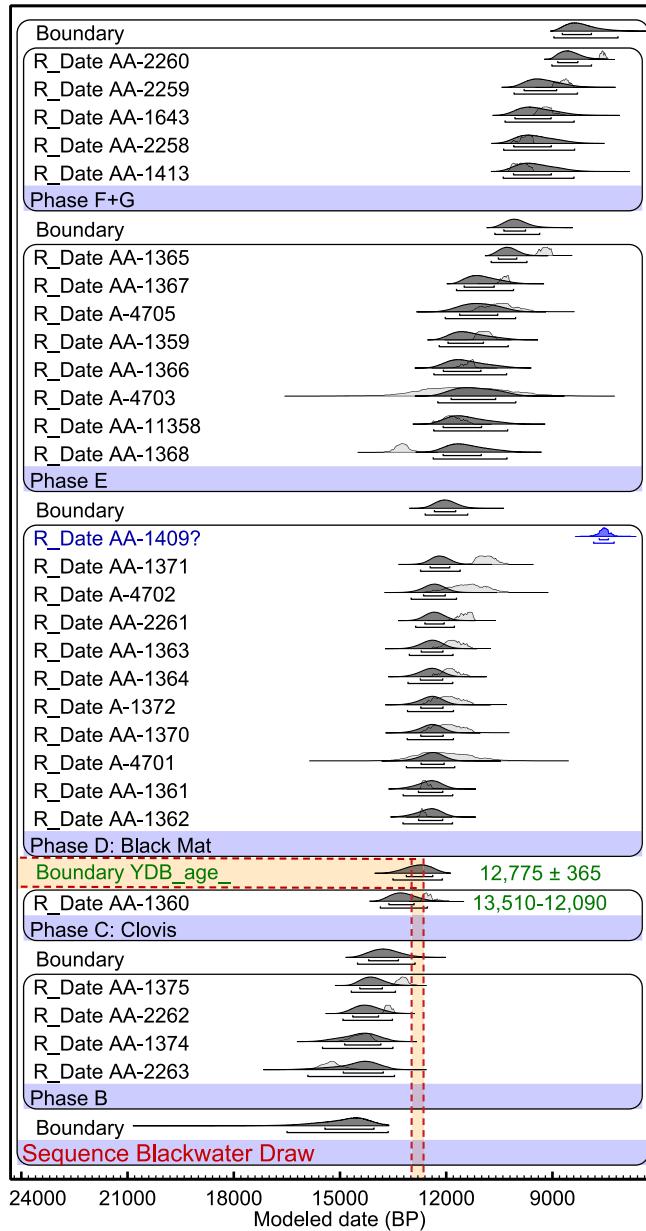
Fig. S9. Blackwater Draw age-sequence model. Phases (units) are in stratigraphic order, as determined by Haynes (93). Because the order of some stratigraphic layers is unclear, dates within Phases are plotted in chronologic order. The YDB proxies occur at the boundary between Phase C and D.

Table S12. Blackwater Draw, New Mexico. Dates are from profile A-A', as shown in Fig. 3 and Figs. 8G to 8K of Haynes (93). Stratum and distance from the YDB sampling site are shown in columns 4-5. The profile includes the South Bank Interpretive Center, where 4 dates are from sediment within 7 m of the proxy-rich YDB sample. To help produce a more constrained age-sequence model, only those dates from within 62 m of the sampling site were used (column 5, below). Although the proxy-rich "Folsom wedge" and "Clovis wedge" contained a peak in YDB proxies, a YDB date of 12,965 ± 65 Cal B.P. (11,095 ± 35 ^{14}C years BP; (94)) was not modeled because the wedges came from 385 m north of the Interpretive Center.

Laboratory #	μ	σ	Stratum & Distance (m)		UNMODELED (BP) 95.4% range			σ	Modelled (BP) 95.4% range			σ	Amodel=97 Aoverall=97.1
Boundary									8955	7035	8115	525	
R_Date AA-2260	6720	80	G/F	39	7690	7435	7580	65	9035	7820	8475	320	99.2
R_Date AA-2259	7850	110	G,G/F	39	8995	8440	8705	155	10085	8280	9240	470	100.6
R_Date AA-1643	8230	140	G1/F	37	9520	8775	9185	185	10350	8360	9420	520	98.1
R_Date AA-2258	8730	90	G1/F (bone)	37	10150	9535	9770	155	10390	8365	9450	530	104.5
R_Date AA-1413	8830	120	F/E	39	10195	9560	9900	180	10395	8380	9450	530	98.3
Phase F+G													
Boundary									10630	9370	10015	320	
R_Date AA-1365	8230	100	E4	51	9465	9000	9210	135	10735	9720	10230	260	93.8
R_Date AA-1367	9150	90	E5	51	10560	10180	10345	105	11710	10110	10965	420	99.9
R_Date A-4705	9260	320	E1	7	11250	9555	10495	450	12025	10030	11045	515	104.6
R_Date AA-1359	9590	120	E2, upper	39	11215	10585	10920	170	12190	10235	11300	510	99.7
R_Date AA-1366	9890	100	E4	51	11755	11140	11390	165	12350	10290	11410	535	104.7
R_Date A-4703	10000	910	E3	7	13610	9120	11470	1150	12230	10030	11160	585	104.3
R_Date AA-11358	10190	130	E2, upper	39	12390	11340	11855	270	12365	10275	11410	545	97.4
R_Date AA-1368	11400	190	E5	51	13585	12815	13245	185	12360	10270	11410	545	97.9
Phase E													
Boundary									12595	11385	12000	305	
R_Date AA-1409	6660	160	D2b	39	7840	7255	7540	140	7840	7255	7540	140	
R_Date AA-1371	9560	180	D2x2	62	11275	10295	10875	250	12720	11605	12160	280	74.3
R_Date A-4702	9870	320	D1A1	39	12515	10435	11405	510	12985	11695	12335	315	110
R_Date AA-2261	9950	100	D2	7	11815	11195	11470	175	12860	11760	12310	275	98.1
R_Date AA-1363	10160	120	D1gk)	53	12380	11305	11795	250	13035	11790	12400	310	102.5
R_Date AA-1364	10210	110	D1g	53	12385	11400	11895	240	13080	11805	12420	315	101.5
R_Date A-1372	10250	200	D/E	59	12560	11290	11955	345	13090	11780	12420	325	101.2
R_Date AA-1370	10260	230	D2z	60	12605	11260	11960	370	13100	11780	12415	325	101.4
R_Date A-4701	10470	580	D1e	53	13440	10570	12065	740	13120	11740	12405	340	110.9
R_Date AA-1361	10640	110	D1a3	39	12745	12170	12555	130	13220	11805	12475	350	93.8
R_Date AA-1362	10740	100	D1e	53	12815	12425	12655	85	13230	11810	12480	355	97.9
Phase D: Black Mat													
Boundary YDB_age									13510	12090	12775	365	
R_Date AA-1360	10580	100	C	49	12720	12150	12500	145	13865	12520	13210	345	101.6
Phase C: Clovis													
Boundary									14515	12860	13710	420	
R_Date AA-1375	11380	150	B1a	31	13550	12935	13230	145	14685	13405	14065	325	99.8
R_Date AA-2262*	11810	90	B1b2	7	13800	13445	13635	95	14930	13485	14235	365	100
R_Date AA-1374	12330	110	B2d	61	14940	13990	14415	245	15505	13480	14440	515	103
R_Date AA-2263	12790	160	B2d	61	15800	14535	15215	305	15940	13440	14535	630	91.8
Phase B													
Boundary									16635	13640	14980	815	
Sequence Blackwater Draw													

Indian Creek, Montana

Except for the age model and data table below, the following information was extracted with minor modifications from Baker et al. (48). See main manuscript **Table 1** and **Tables S1-S2** for other site information. Indian Creek, located ≈10 km west of Townsend, Montana, features a well-documented archeological excavation, described by Davis and Greiser (95) and Baker et al. (48). This stratigraphic section is approximately 600 meters downstream from the archeological excavation, where the Glacier Peak ash layer is well-exposed. These two locations were stratigraphically correlated by Baker et al. (48), using the two easily identified volcanic tephra layers, the earliest being from the Glacier Peak eruption. The YDB layer is marked by an abundance peak in nanodiamond-rich carbon spherules, with no impact proxies observed above or below. This layer is a mixture of local sand, gravel, and charcoal, also containing redeposited volcanic ash, interpreted to be a debris flow that post-dated the Glacier Peak eruption.
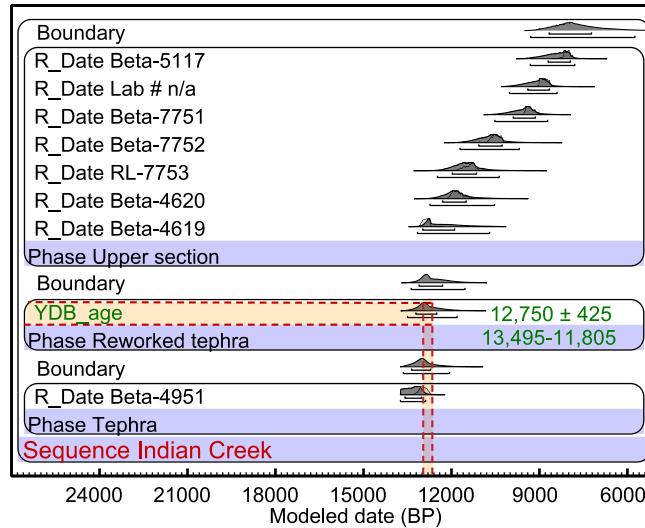
Fig. S10. Indian Creek age-depth model. YDB is mixed with reworked tephra.

Table S13. Indian Creek, MT. Dates are from Davis and Greiser (95).

Laboratory #			Depth	UNMODELED (BP)				Modelled (BP)				Amodel=98.8	
	μ	σ	(cm)	95.4% range		μ	σ	95.4% range		μ	σ	Aoverall=98.9	
Boundary								9300	5740	7690	975		
R_Date Beta-5117	7210	110	373	8310	7825	8045	115	9315	7790	8420	400	99	charcoal
R_Date Lab # n/a	7980	80	417	9025	8600	8835	120	10025	8395	9090	405	100.1	charcoal
R_Date Beta-7751	8340	100	479	9530	9035	9315	120	10520	8720	9545	420	100.1	charcoal
R_Date Beta-7752	9290	120	566	11065	10220	10500	170	11710	9680	10670	480	100.1	charcoal
R_Date RL-7753	9870	130	704	11935	10795	11380	230	12480	10370	11465	510	100.9	charcoal
R_Date Beta-4620	10160	80	770	12100	11400	11800	180	12735	10530	11780	525	98.7	charcoal
R_Date Beta-4619	10980	110	791	13060	12705	12875	100	13160	10695	12225	670	102	charcoal
Phase Upper section													
Boundary								13375	11535	12585	470		
YDB_age								13495	11805	12750	425		
Phase Reworked tephra													
Boundary								13640	12065	12915	400		
R_Date Beta-4951	11125	130	832	13220	12725	12975	130	13740	12875	13290	255	95.9	charcoal
Phase Tephra													
Sequence Indian Creek													

Lake Hind, Manitoba, Canada

Except for the age model and data table below, the following information was extracted from Running et al. (96) and Boyd et al. (97) with minor modifications. See main manuscript **Table 1** and **Tables S1-S2** for other site information. The sedimentary sequence at Lake Hind is from a cutbank above the Souris River that provides the most complete postglacial stratigraphic section in the Glacial Lake Hind Basin of southwestern Manitoba. The site's stratigraphy has been described in detail elsewhere by the above authors.

In summary, the 11-meter stratigraphic sequence consists of several lithologic units: *(i)* glaciolacustrine silts and clays close to river level, grading upwards with slightly increasing organics; *(ii)* then, a distinct peat layer; *(iii)* succeeded by fluvial marl and silts; *(iv)* dune sands; *(v)* fluvial deposits between eolian sand sheets; and *(vi)* relict parabolic dunes on the modern landscape. The YDB layer was identified by Firestone et al. (4) in the organic-rich upper part of the silt-clay unit, underlying the peat.
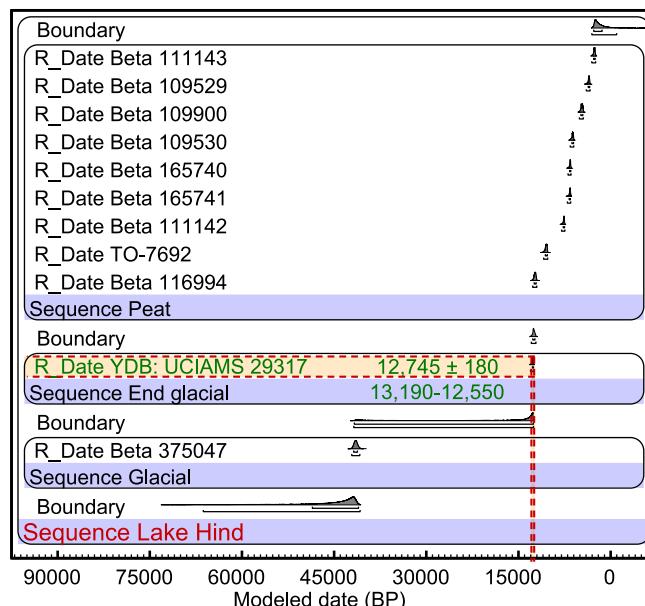
Fig. S11. Lake Hind age-sequence model. It is likely that UCIAMS 29317 is from the uppermost portion of the YDB layer, which extends further below it.

Table S14. Lake Hind, Manitoba, Canada. The youngest 9 dates are from Running et al. (96), and UCIAMS 29317 is from Firestone et al. (4). The radiocarbon dates, Beta-375047 and Beta-375046, are new from carbon-rich bulk sediment; the latter was too old to calibrate in IntCal13. The depth of 1097 cmbs for the YDB radiocarbon age is equivalent to 32 cm in Kinzie et al. (20), using a different starting reference depth.

Laboratory #	μ	σ	Depth (cm)	UNMODELED (BP) 95.4% range		μ	σ	Modelled (BP) 95.4% range		μ	σ	Amodel=97.9 Aoverall=98.1	
R_Date Beta 111143	2500	40	489	2745	2435	2590	85	3195	2420	2730	195	100.5	Bison skull collagen
R_Date Beta 109529	3250	70	547	3680	3345	3485	80	4095	3350	3615	190	99.9	Hearth soil (acid washes)
R_Date Beta 109900	4090	70	580	4825	4435	4625	115	5215	4430	4755	205	99.9	Bison bone collagen
R_Date Beta 109530	5350	50	632	6280	5995	6130	80	6715	5995	6260	185	99.8	Ungulate bone collagen
R_Date Beta 165740	5760	50	804	6715	6445	6580	60	7075	6440	6660	170	96.7	Charred foreset material
R_Date Beta 165741	5780	50	778	6670	6440	6560	60	7185	6500	6740	185	100.3	Charred foreset material
R_Date Beta 111142	6700	70	820	7675	7440	7565	60	8125	7445	7695	180	99.9	Wood
R_Date TO-7692	9250	90	1055	10660	10235	10435	115	11020	10245	10565	205	100	Seeds
R_Date Beta 116994	10420	70	1093	12550	12055	12300	135	12815	12015	12360	200	98.7	Seeds
Sequence Peat													
Boundary								13040	12145	12555	215		
R_Date YDB: UCIAMS 29317	10610	25	1097	12675	12545	12605	35	13190	12550	12745	180	99	Charcoal
Sequence End glacial													
Boundary								41830	12555	22465	10085		
R_Date Beta 375047	36830	310	1197	41975	40820	41420	285	42220	40825	41530	340	98.8	Microcharcoal
Sequence Glacial													
Boundary								66605	40860	48565	7955		
Sequence Lake Hind													
Date too old to calibrate													
Beta-375046	>43500												Microcharcoal

Except for the age model and data table below, the following information was extracted with minor modifications from Kinzie et al. (20). See main manuscript **Table 1** and **Tables S1-S2** for other site information. The stratigraphic sequence of this site is dominated by alluvial sediments and loess, as described by Wilmsen and Roberts (98). Fourteen samples were collected from the upper part of Stratum C to the lower part of Stratum D at 2-cm intervals, spanning a depth range of 80 to 113 cmbs. The YDB layer, located from 100 to 102 cm at the interface between Stratum C and D (the black mat), is marked by a peak in nanodiamonds. Stratum C, immediately beneath the YDB layer, is dominantly loess deposits with interbedded alluvial silt, sand, and gravel. The base of stratum D a dark gray, fine-grained, calcareous, humic, clayey silt with occasional gravel, similar to a marsh or bog deposit, and has been correlated with the black mat at Murray Springs and elsewhere (76).
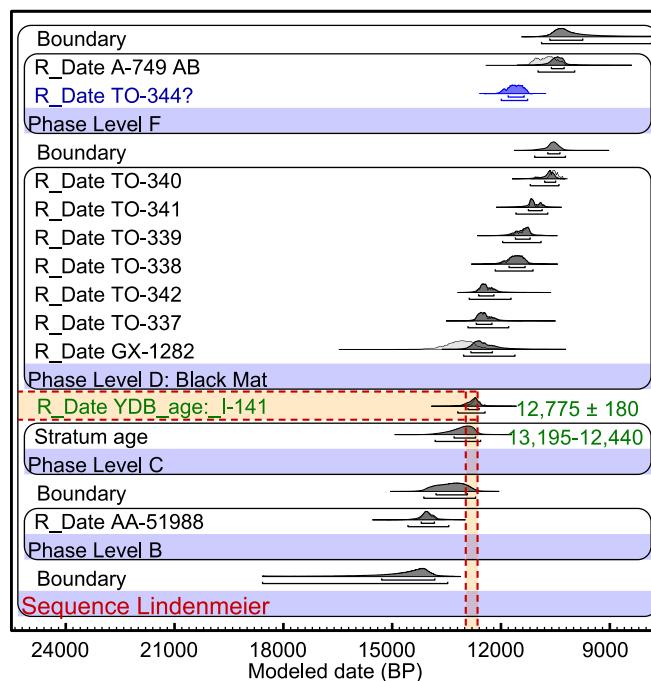
Fig. S12. Lindenmeier age-sequence model. Phases (strata) are in stratigraphic order, as determined by the site's principal investigators (98, 99), and dates within each Phase are in chronological order.

Table S15. Lindenmeier, CO. Dates are from Haynes et al. (99), who excluded one anomalous date that was accepted and remodeled by OxCal in this age model. The ^{14}C date on the YDB layer (I-141) is from numerous flakes of charcoal, collected from the interface between Phases C and D (98).

Laboratory #	μ	σ	Depth (cm)	UNMODELED (BP) 95.4% range		μ	σ	Modelled (BP) 95.4% range		μ	σ	Amodel=79.8 Aoverall=81.6	
Boundary								10885	7850	9965	660		
R_Date A-749 AB	9440	180	n/a	11185	10265	10740	255	10980	9965	10445	235	86.8	charcoal
R_Date TO-344	10060	100	n/a	11995	11265	11620	200	11995	11265	11620	200	0.1	charcoal
Phase Level F													
Boundary								11075	10220	10590	205		
R_Date TO-340	9330	70	n/a	10710	10295	10530	110	11195	10400	10720	200	91.6	charcoal
R_Date TO-341	9690	60	n/a	11235	10785	11055	130	11590	10705	11110	210	101.3	charcoal
R_Date TO-339	9880	100	n/a	11755	11130	11380	170	11955	10890	11410	240	99.9	charcoal
R_Date TO-338	10040	80	n/a	11950	11260	11575	175	12160	11115	11595	250	99.9	charcoal
R_Date TO-342	10500	80	n/a	12655	12115	12410	145	12880	11720	12370	275	99.9	charcoal
R_Date TO-337	10560	110	n/a	12710	12130	12465	160	12915	11785	12415	275	98.7	charcoal
R_Date GX-1282	11200	400	n/a	14030	12145	13110	445	13035	11615	12440	355	62.7	charcoal
Phase Level D: Black Mat													
R_Date YDB_age:_I-141	10780	135	n/a	13000	12420	12700	140	13195	12440	12775	180	102.9	charcoal
Stratum age								13820	12560	13085	320		
Phase Level C													
Boundary								14130	12700	13390	390		
R_Date AA-51988	12170	80	n/a	14295	13765	14050	135	14565	13435	14020	245	99.4	charcoal
Phase Level B													
Boundary								18575	13465	14970	1155		
Sequence Lindenmeier													

Lingen, Germany

Except for the age model and data table below, the following information was extracted from Wittke et al. (19). See main manuscript **Table 1** and **Tables S1-S2** for other site information. Because Lingen is stratigraphically similar to Lommel and Ommen, details for all three sites are discussed here. From approximately 14,400 to 13,000 years ago, dune-like eolian sediments blanketed extensive areas of northern Europe, extending from the UK to northern Russia and from Denmark to northern France. Called the Late-Pleistocene European Sand Belt, this region contains sediments known as coversands, comprised mostly of unconsolidated quartz sand, deposited during the Allerød warm period.

At ≈12,800 Cal B.P., conspicuous amounts of charcoal became intermixed with the upper few cm of the Usselo layer. At all three sites, this dark portion of the Usselo contains abundance peaks in a variable assemblage of impact-related spherules, charcoal, glass-like carbon, and/or nanodiamonds (4, 18, 49). The abundance of charcoal reflects widespread biomass burning precisely at the onset of Younger Dryas climate change at these three sites, at Aalsterhut, and at many other locations in the Netherlands, Great Britain, France, Germany, Denmark, and Poland (100, 101). Lingen, Lommel, Ommen, and Aalsterhut are up to 200 km apart, and the sites in Poland are 800 km away from those in Belgium, indicating extensive, coeval wildfires across a large part of northern Europe the time of the YDB impact event. Cultural artifacts are common in the region up until the Younger Dryas onset, marked by abundant charcoal, after which there is little evidence for human occupation across most of northwestern Europe for several centuries, suggesting a population decline related to the impact and/or climate change (78).

At Lingen, ten discontinuous samples of bulk sediment from 3 to 5 cm thick were collected across a 70-cm-thick interval between 7.5 and 77.5 cmbs. There was a peak of 30 impact-related spherules/kg at a depth of 43.5 to 47.5 cmbs in the 3-cm-thick, dark, charcoal-rich YDB layer at the top of the Usselo layer, coincident with the onset of Younger Dryas cooling.
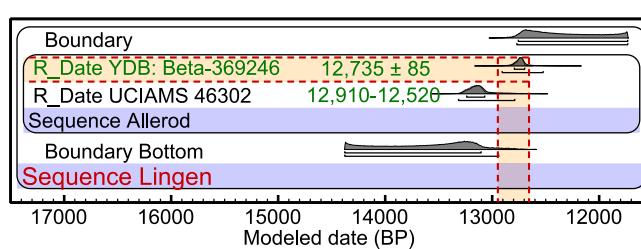
Fig. S13. Age-sequence model for Lingen, Germany.

Table S16. Lingen, Germany. The date UCIAMS 46302 is from Wittke et al. (19); Beta-369246 is from this paper, on charcoal taken directly from the proxy-rich YDB sample.

Laboratory #	μ	σ	Depth (cm)	UNMODELED (BP) 95.4% range		μ	σ	Modelled (BP) 95.4% range		μ	σ	Amodel=99.4 Aoverall=99.4	
Boundary								12770	11730	12330	320		
R_Date YDB: Beta-369246	10870	40	43.5	12805	12690	12745	30	12910	12520	12735	85	98.3	charcoal
R_Date UCIAMS 46302	11310	60	52.5	13280	13065	13170	55	13315	12785	13115	125	100.7	charcoal
Sequence Allerød													
Boundary Bottom								14380	12935	13605	425		
Sequence Lingen													

Lommel, Belgium

Except for the age model and data table below, the following information was extracted with minor modifications from Wittke et al. (19). See Lingen discussion above, along with main manuscript **Table 1** and **Tables S1-S2** for more information. Nine 2-cm to 5-cm-thick discontinuous samples of bulk sediment were from a 60-cm-thick sequence between 17.5 and 77.5 cmbs. A peak of 10 impact-related spherules/kg occurs in a 5-cm-thick layer at a depth of 48.5 to 52.5 cmbs at the top of the Usselo layer. Firestone et al. (4) reported similar concentrations of 16 spherules/kg from this same level, the YDB layer. In addition, Tian et al. (49) reported the presence of cubic nanodiamonds in the Lommel YDB layer, but not above or below.
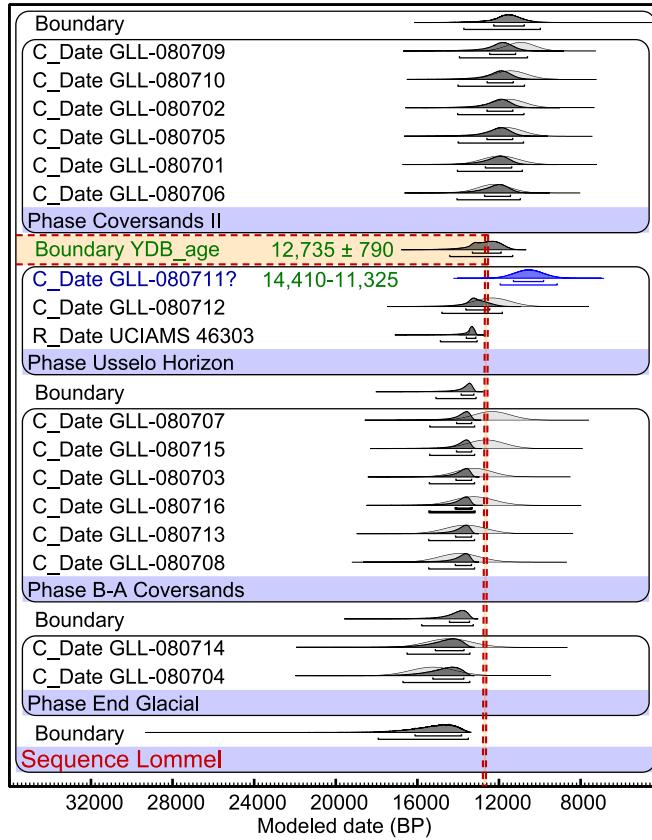
Fig. S14. Lommel age-sequence model. YDB corresponds to the charcoal layer.

Table S17. Lommel, Belgium. OSL dates ("C_Dates") are from Derese et al. (102), except for a single radiocarbon date ("R_Date") UCIAMS 46303 from Wittke et al. (19). One OSL date in blue was rejected as being too young.

| Laboratory #	Type	μ	σ	Depth (cm)	UNMODELED (BP) 95.4% range		μ	σ	Modelled (BP) 95.4% range		μ	σ	Amodel=139.3 Aoverall=137.8	
Boundary									13725	9970	11660	890		
C_Date GLL-080709	OSL	11000	700	n/a	12340	9540	10940	700	13940	10600	12040	810	85.2	quartz grains
C_Date GLL-080710	OSL	11500	800	n/a	13035	9840	11440	800	14010	10745	12145	795	116.8	quartz grains
C_Date GLL-080702	OSL	11600	800	n/a	13135	9940	11540	800	14025	10770	12165	795	119.7	quartz grains
C_Date GLL-080705	OSL	11700	800	n/a	13235	10040	11640	800	14005	10795	12180	790	121.7	quartz grains
C_Date GLL-080701	OSL	12000	900	n/a	13735	10140	11940	900	14040	10850	12230	790	124.3	quartz grains
C_Date GLL-080706	OSL	12300	800	n/a	13835	10640	12240	800	14060	10950	12280	775	113.1	quartz grains
Phase Coversands II														
Boundary YDB_age									14410	11325	12735	790		
C_Date GLL-080711	OSL	10600	700	n/a	11940	9140	10540	700	11940	9145	10540	700	1.1	quartz grains
C_Date GLL-080712	OSL	12400	900	n/a	14135	10540	12340	900	14800	11835	13210	715	113.6	quartz grains
R_Date UCIAMS 46303	14C	11480	100	n/a	13490	13100	13320	100	14870	13065	13595	525	94.4	charcoal
Phase Usselo Horizon														
Boundary									15090	13120	13775	570		
C_Date GLL-080707	OSL	12400	900	n/a	14135	10540	12340	900	15390	13190	13960	615	61.4	quartz grains
C_Date GLL-080715	OSL	12700	900	n/a	14435	10840	12640	900	15400	13190	13965	615	85.4	quartz grains
C_Date GLL-080703	OSL	13300	1000	n/a	15035	11440	13240	900	15410	13195	13985	625	125.9	quartz grains
C_Date GLL-080716	OSL	13300	900	n/a	15235	11240	13240	1000	15405	13195	13990	625	128.1	quartz grains
C_Date GLL-080713	OSL	13700	1000	n/a	15635	11640	13640	1000	15445	13195	14000	635	134.4	quartz grains
C_Date GLL-080708	OSL	14000	1000	n/a	15935	11940	13940	1000	15445	13195	14005	635	127.6	quartz grains
Phase B-A Coversands														
Boundary									15790	13260	14225	705		
C_Date GLL-080714	OSL	14500	1100	n/a	16635	12240	14440	1100	16505	13425	14730	845	123.6	quartz grains
C_Date GLL-080704	OSL	15300	1100	n/a	17435	13040	15240	1100	16705	13430	14820	900	95.9	quartz grains
Phase End Glacial														
Boundary									17920	13495	15390	1305		
Sequence Lommel														

26

Santa Maira, Spain

The stratigraphy and archaeology of this cave are described by Aura et al. (103). See main manuscript **Table 1** and **Tables S1-S2** for more information. The sampled sequence, dating to between ≈17,000 and 5,000 Cal B.P., is composed of sands, mud, and limestone gravel, interbedded with blocks of micritic limestone breccia and conglomerates, resulting from the episodic collapse of the cave roof and walls.

The radiocarbon dates used in this model came from sediment samples throughout the cave (<10-m apart), and the majority of them fall into two groups, one that predates the Younger Dryas cooling episode and one that dates to the Holocene (**Fig. S15** and **Table S18**). The distribution of radiocarbon dates, in combination with vertebrate and pollen biostratigraphy, suggests a reduction in sedimentation during the Younger Dryas climatic episode, forming only a thin, discontinuous deposit. A single radiocarbon date (Beta-75225), with a calibrated age range of 13,135 to 12,695 Cal B.P., indicates the presence of Younger Dryas sediments in the cave, and this date overlaps the previously published YDB age range. The YDB layer in the cave is marked by abundances in one sample of cosmic impact proxies that include carbon spherules (188/kg), nanodiamonds inside carbon spherules (38 ppb), charcoal (4.3 g/kg), and glass-like carbon (0.7 g/kg) (**Table S1**). In addition, the layer contained abundant framboidal spherules (3,668/kg), which are associated with the YDB layer at some other sites. No nanodiamonds, carbon spherules, glass-like carbon, or framboids were observed in a sample from immediately beneath the YDB layer.
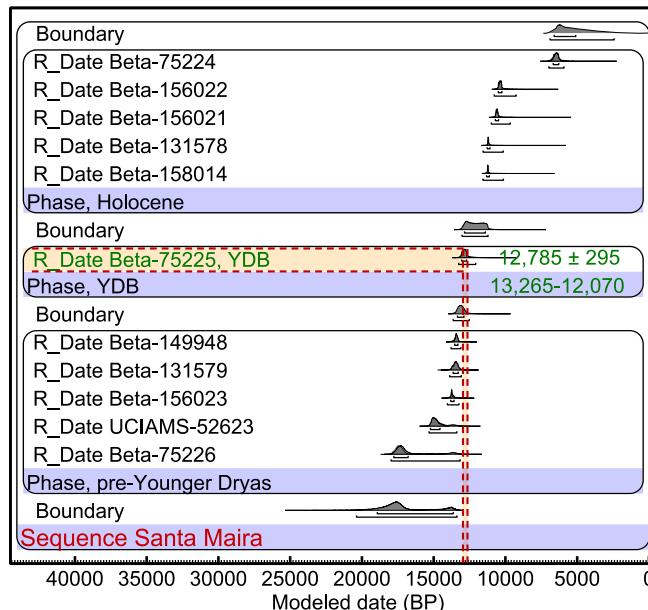

Fig. S15. Santa Maira age-sequence model. Phases are in stratigraphic order with dates in chronological order within each Phase, as determined by the site's investigators (103).

Table S18. Santa Maira, Spain. Cave dates are from Aura et al. (103).

Laboratory #	μ	σ	Depth (cm)	UNMODELED (BP) 95.4% range			μ	σ	Modelled (BP) 95.4% range			μ	σ	Amodel=98.6 Aoverall=98.5	
Boundary									6890	2425	5330	1325			
R_Date Beta-75224	5640	140	n/a	6785	6125	6455	150		6975	5915	6440	280		98.2	carbon aggregate
R_Date Beta-156022	9220	40	n/a	10505	10255	10380	70		10780	9255	10240	430		99.9	bone red deer
R_Date Beta-156021	9370	40	n/a	10705	10495	10600	55		10990	9660	10475	425		99.8	fruit/seed remains
R_Date Beta-131578	9760	40	n/a	11245	11130	11195	35		11560	10150	11025	580		99.7	carbon aggregate
R_Date Beta-158014	9820	40	n/a	11295	11180	11230	25		11575	10135	11100	400		99.7	oak wood
Phase, Holocene															
Boundary									13025	11210	12105	570			
R_Date YDB_age_Beta-75225	12615	99	n/a	13135	12695	12905	120		13265	12070	12785	295		101.6	charcoal
Phase, YDB															
Boundary									13645	12520	13080	275			
R_Date Beta-149948	11590	70	n/a	13560	13285	13415	70		13795	13105	13420	160		100.2	bone wild goat
R_Date Beta-131579	11620	150	n/a	13755	13155	13460	155		13885	13070	13465	200		101.9	carbon aggregate
R_Date Beta-156023	11920	40	n/a	13945	13565	13735	75		14050	13240	13685	185		99.7	bone wild goat
R_Date UCIAMS-52623	14310	190	n/a	15290	14390	14905	225		15320	13385	14670	515		98.6	carbon aggregate
R_Date Beta-75226	11020	140	n/a	17935	16900	17410	260		17970	13155	16570	1365		95.5	carbon aggregate
Phase, pre-Younger Dryas															
Boundary									20385	13370	17405	1865			
Sequence Santa Maira															

Talega, California

Except for the age model and data table below, the following information was extracted with minor modifications from Wittke et al. (19). See main manuscript **Table 1** and **Tables S1-S2** for other site information. The stratigraphy of this site has been described in detail by Bergin et al. (104). The stratigraphic section consists largely of alluvial/colluvial sand and silt with occasional peat layers, divided into 15 lithologic units. Trench and cores samples were collected from the surface to 21.5 mbs (meters below surface), distributed along an approximately 50-m-long retaining wall (Locus A in (104)). Stratum 10, between 7.2 to 9.7 mbs, is a soil of Younger Dryas age. Stratum 11, from approximately 9.7 to 12.8 mbs, is a Younger Dryas-age layer of alluvial sand with bands of dark peat, representing possibly marshy conditions that formed at the onset of the Younger Dryas cooling episode. Stratum 12, extending from approximately 12.8 to 15.2 mbs, is alluvial sand and silt, intercalated with black silty loam, deposited in a narrow channel that was cut and refilled rapidly.

Nine 30-cm-thick discontinuous samples of bulk sediment, collected from a 6.7-m-thick interval of sediment between 12.6 and 19.3 mbs (Strata 10-15) were examined for impact-related spherules, carbon spherules, and glass-like carbon. At the base of Stratum 12, a 30-cm-thick YDB layer (≈14.9 to 15.2 mbs) contained a major abundance peak in impact-related spherules (1930 /kg). This is one of the largest peaks yet detected and is at the greatest depth of all YDB sites examined to date (19). This proxy-rich layer dates to 12,860 + 150 Cal B.P., consistent with the age of the YDB elsewhere. This layer is underlain by Stratum 14 (15.2 to 18.4 mbs), comprised of colluvium, largely derived from the Monterey Formation, and this unit, in turn, is underlain by stream-laid Stratum 15. Significantly lower numbers of impact-related spherules were found above and below the YDB layer (19). The presence of these probably resulted from redeposition and/or vertical mixing during the rotary drilling.
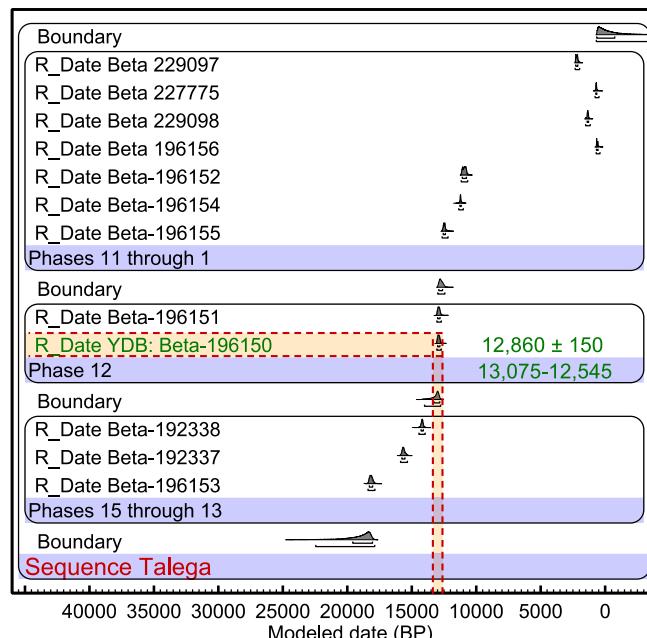

Fig. S16. Talega age-sequence model. Dates are in chronological order within identified stratigraphic Phases (groups of strata) include dates from multiple cores across the site.

Table S19. Talega, CA. Dates are from Bergin et al. (104) and were acquired from 28 boreholes and 5 excavation trenches adjacent to or distributed along a ≈50-m retaining wall.

Laboratory #	μ	σ	UNMODELED (BP) 95.4% range		μ	σ	Modelled (BP) 95.4% range		μ	σ	Amodel=101.2 Aoverall=101	
Boundary							11285	8680	10335	745		
R_Date Beta-196154	9830	50	11335	11170	11245	40	11395	10785	11170	175	98	charcoal
R_Date Beta-196155	10540	50	12665	12390	12505	80	12675	11600	12365	300	100.1	charcoal
Phase 11-10												
Boundary							13025	12120	12660	265		
R_Date Beta-196151	11060	60	13070	12770	12920	80	13075	12545	12855	150	103.4	charcoal
R_Date YDB: Beta-196150	11070	50	13065	12795	12930	75	13075	12545	12860	150	102.6	charcoal
Phase 12												
Boundary							14070	12695	13185	340		
R_Date Beta-192338	12310	10	14415	14090	14230	80	14495	13615	14140	220	99.6	charcoal
R_Date Beta-192337	13070	40	15875	15415	15665	110	15950	14900	15540	350	99.9	charcoal
R_Date Beta-196153	14980	70	18405	17975	18200	110	18490	16945	17975	690	99.4	charcoal
Phase 15-13												
Boundary							24780	17585	19530	1735		
Sequence Talega												

Topper, South Carolina

Except for the age model and data table below, the following information was extracted from Wittke et al. (19). See main manuscript **Table 1** and **Tables S1-S2** for other site information. The stratigraphy of this site is described in detail in Waters et al. (105). This site is located adjacent to the Savannah River that has cut into relatively unconsolidated clastic sediments of Tertiary age to form a terrace (105). Sediments are largely colluvial, quartz-rich sands, displaying several weakly defined stratigraphic units marked by iron staining. In the area sampled, abundant Clovis-age waste-flakes (debitage) occur at the contact between stratigraphic Unit 2b and overlying Unit 3b.

Seven 5-cm-thick discontinuous samples of bulk sediment were collected from a 180-cm-thick sequence between 0 and 180 cmbs. Six samples were analyzed for impact-related spherules revealing a peak of 110 spherules/kg in a 5-cm-thick YDB layer at the base of Unit 3b centered at a depth of 60 cmbs (57.5 to 62.5 cmbs). These results are comparable to abundances of YDB impact-related spherules reported by Firestone et al. (4) of 97 spherules/kg and LeCompte et al. (40) of 260 spherules/kg, all of which contradict Surovell et al. (58), who found no spherules (0/kg). Age-depth plot is **Fig. 6** in the main manuscript.

Table S20. Topper, SC. OSL dates are from Waters et al. (105); the radiocarbon date is from Wittke et al. (19).

Laboratory #	Type	μ	σ	UNMODELED (BP) 95.4% range		μ	σ	Modelled (BP) 95.4% range		μ	σ	Amodel=124.4 Aoverall=123.9	
Boundary								4930	600	3255	1285		
C_Date UIC1228	OSL	4300	300	4845	3640	4240	300	4980	3645	4310	335	96.8	quartz grains
C_Date UIC782	OSL	7300	800	8840	5645	7240	800	8830	5520	7180	830	100	quartz grains
C_Date UIC835	OSL	7600	900	9340	5745	7540	900	9325	5635	7480	925	100.1	quartz grains
C_Date UIC1229	OSL	8000	500	8940	6940	7940	500	8975	6795	7880	550	100	quartz grains
C_Date UIC836	OSL	8000	800	9540	6345	7940	800	9515	6225	7875	835	100	quartz grains
C_Date UIC1115	OSL	11000	800	12540	9345	10940	800	12155	9020	10600	800	100.9	quartz grains
Phase 3b upper													
Boundary								12975	10240	11885	795		
R_Date YDB: AA100294	¹⁴C	10958	65	12995	12710	12835	80	13085	12365	12785	185	100.4	charcoal
C_Date UIC1114	OSL	13000	900	14740	11145	12940	900	13845	11575	12740	525	122.4	quartz grains
C_Date UIC763	OSL	13200	1300	15740	10545	13140	1300	13970	11420	12735	590	125.7	quartz grains
Phase 3b base, Clovis													
Boundary								14795	12570	13430	580		
C_Date UIC837	OSL	14000	1200	16340	11545	13940	1200	15640	12815	14095	760	119.3	quartz grains
C_Date UIC764	OSL	14800	1500	17740	11745	14740	1500	16105	12795	14245	895	116.5	quartz grains
Phase Level 2b													
Boundary								18975	12815	15305	1990		
Sequence Topper													

Blackville, South Carolina

Except for the age model and data table below, the following information was extracted from Bunch et al. (17) and Wittke et al. (19). See main manuscript **Table 1** and **Tables S1-S2** for other site information. The lower part of the sequence (272-190 cmbs) is a massive, firm, red clay, separated unconformably at 190 cmbs by overlying coarser late Quaternary unconsolidated loamy to silty alluvium and eolian sediment (190 to surface).

Eleven of 18 continuous 15-cm-thick bulk sediment samples were examined for impact proxies. The YDB was clearly marked in the 15-cm-thick interval from 190-175 cmbs by peaks in impact-related spherules (525/kg), melt-glass (0.06 g/kg), carbon spherules, glass-like carbon, aciniform carbon, and iridium (**Table S1**). The high abundances of spherules extend ≈30 cm above the unconformity, indicating that the YDB layer is stratigraphically unrelated to it.
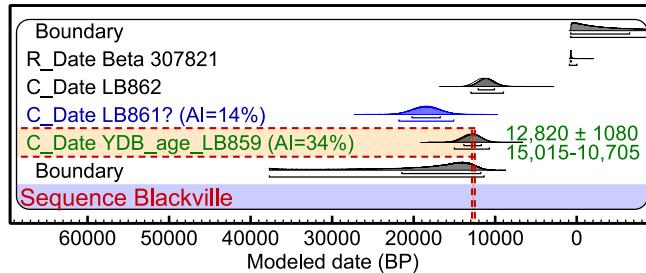

Fig. S17. Blackville age-sequence model. The two oldest OSL dates exhibit an age reversal. The older date (LB858, 12,960 ± 1190 Cal B.P.) has an Agreement Index (marked as "AI") value of 34%, and the younger date (in blue; LB861, 18,540 ± 1680 Cal B.P.) has a lower Agreement Index value of 14%. Consequently, OxCal rejected the younger date as being statistically less likely to be correct than the older date.

Table S21. Blackville, South Carolina. Dates reported in Bunch et al. (17) and this paper.

Laboratory #	Type	μ	σ	Depth (cm)	UNMODELED (BP) 95.4% range		μ	σ	Modelled (BP) 95.4% range		μ	σ	Amodel=105.4 Aoverall=104.7	
Boundary									760	-17885	-5040	5155		
R_Date Beta 307821	14C	830	30	20.0	790	685	740	35	900	-35	600	320	99.8	Charcoal
C_Date LB862	OSL	11500	1030	107.0	13495	9380	11440	1030	12970	8985	11010	995	103.3	Quartz grns
C_Date LB861	OSL	18540	1680	152.0	21835	15125	18480	1680	21810	15095	18480	1680		Quartz grns
C_Date YDB_age_LB859	OSL	12960	1190	183.0	15275	10520	12900	1190	15015	10705	12820	1080	106.3	Quartz grns
Boundary									37705	11360	19620	6950		
Sequence Blackville														
Date too old to measure														
Beta 207164	14C	>46600		210.0	>46600				>46600					Charcoal

Lake Cuitzeo, Mexico

Except for the age model and data table below, the following information was modified from Israde et al. (37) and Wittke et al. (19). See main manuscript **Table 1** and **Tables S1-S2** for other site information. From the second largest lake in Mexico, a 27-m-long lake core was recovered, consisting of interbedded lacustrine sands, silts, clays, epiclastites, and tephra layers. A conspicuous, dark, carbon-rich layer,

dominated by clay and silt, occurs between 250 and 282 cmbs and resembles the black mat at other YDB sites across North America. The YDB layer is marked by peaks of impact-related spherules (2055 /kg), nanodiamonds (493 ppb), and carbon spherules (684/kg) in a 5-cm layer between 277.5 to 282.5 cmbs (incorrectly reported previously as 280 to 275 cmbs in both (20 and 37).
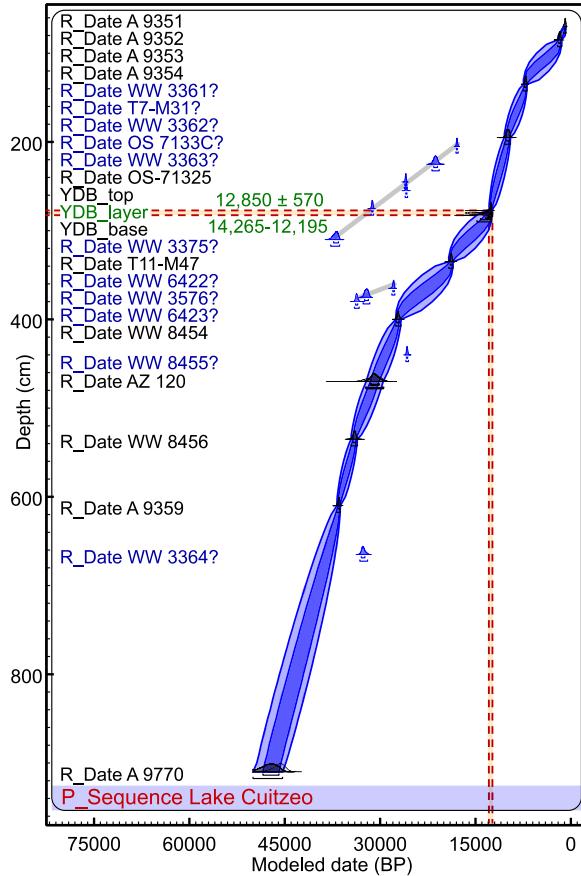
Fig. S18. Lake Cuitzeo age-depth model. Bayesian analysis rejected two unusual linear clusters of outliers, shown as blue age distributions connected by gray lines. These indicate the influx of older carbon from an unknown source.

Dating. The presence of several anomalously old dates in the lake Cuitzeo section has caused difficulties in producing a robust age-depth model. Therefore, we consider three possible models. *(i)* In the test shown in **Fig. S18** above, we included the new date on the black mat from the shoreline sequence and then, modeled an age for the YDB layer of 12,850 ± 570 Cal B.P. at 68% (see main paper). *(ii)* In the second test (not shown), we excluded the shoreline sequence date from the age-depth model, producing an age for the YDB layer of ≈15,300 ± 1100 Cal B.P., similar to the minimum age proposed by Blaauw et al. (106). *(iii)* For the third test (not shown), we included all anomalously old dates and excluded the conflicting younger dates, producing a much older modeled age for the YDB of 27,100 ± 400 Cal B.P., about 9,000 years prior to the last Glacial Maximum.

All three of these models are statistically possible, but the question is which model best fits other available stratigraphic evidence. Israde et al. (37, 107) produced a paleoclimatic record for the lake section, based on pollen, spores, and diatoms. These workers presented clear evidence of a warm paleoclimatic interval of >1000 years, interpreted as the Bølling–Allerød interstadial. This was followed by a distinctive cooling period, interpreted as the Younger Dryas cooling episode. This record is most consistent with model (*i*) above (**Fig. S18**) that dates the YDB

to 12,850 ± 570 Cal B.P. (68%). On the other hand, the Lake Cuitzeo record is inconsistent with the YDB dates in alternative model (*ii*), centered at 15,300 Cal B.P., and model (*iii*), centered at 27,100 Cal B.P. Both of those place the age of the impact-proxy-rich layer within the last glacial episode, which lacks evidence of any such warm intervals.

Furthermore, the paleoclimatic record in Lake Cuitzeo closely matches the succession of Bølling–Allerød warming, followed by Younger Dryas cooling that is well documented in sedimentary sections over a broad area of Central America and northern South America (see (37), for details). These sites include La Chonta Bog in Costa Rica (108), Lake La Yeguada in Panama (109), Lake Peten Itza in Guatemala (110, 111), and the Cariaco Basin marine core from offshore Venezuela (112, 113). Indeed, Bush et al. (109) identified a "time of crisis" that dates to ≈12,720 Cal B.P. (10,800 ^{14}C BP) at the onset of the Younger Dryas episode. Representing the most distinctive layer in this record, the crisis interval is marked by dramatic changes in pollen, diatoms, biotic turnover, clay mineralogy, sedimentary geochemistry, and charcoal influx. The changes occurring in this interval at Lake La Yeguada are similar to those at Lake Cuitzeo, suggesting that both records are contemporaneous. Thus, based on available regional evidence, the best-fitting model places the YDB age at 12,850 ± 570 Cal B.P., but with uncertainty.

31

Table S22. Lake Cuitzeo, Mexico. Dates are from Israde et al. (37), except for date OS-71325 from Kinzie et al. (20) that was acquired on stratigraphically correlated sediment on the lakeshore, adjacent to the lake sampling site. The lakeshore date is from previously acquired archival material, with insufficient sediment available for further investigation of YDB proxies.

Laboratory #	μ	σ	Depth (cm)	UNMODELED (BP) 95.4% range			μ	σ	Modelled (BP) 95.4% range			μ	σ	Amodel=91.8 Aoverall=91.7	
Boundary									995	630	835	85			
R_Date A 9351	930	55	70	940	730	845	55		995	630	835	85	100.6	sed. carbon
R_Date A 9352	1755	115	85	1930	1405	1680	135		1985	1300	1645	170	100.3	sed. carbon
R_Date A 9353	6165	70	135	7250	6890	7065	95		7300	6490	6970	310	99.4	sed. carbon
R_Date A 9354	8830	215	195	10490	9465	9920	260		10415	9175	9790	325	102.4	sed. carbon
R_Date WW 3361	14720	50	205	18080	17725	17910	85		18080	17725	17910	85		sed. carbon
R_Date T7-M31	17605	215	225	21860	20715	21295	295		21865	20720	21295	295		sed. carbon
R_Date WW 3362	21730	70	245	26115	25825	25970	75		26120	25825	25970	75		sed. carbon
R_Date OS 7133C	21600	100	255	26065	25690	25880	90		26065	25690	25880	90		sed. carbon
R_Date WW 3363	27360	130	275	31435	31030	31230	100		31435	31030	31230	100		sed. carbon
R_Date OS-71325	10550	35	277	12630	12415	12520	60		12720	12260	12500	155	99	sed. carbon
YDB_top									13275	12100	12580	310		
YDB_layer									14265	12195	12850	570		
YDB_base									14855	12265	13115	725		
R_Date WW 3375	32940	190	310	37785	36370	37030	375		37790	36370	37030	375		sed. carbon
R_Date T11-M47	15500	130	335	19030	18480	18760	130		19115	18320	18715	220	100.1	sed. carbon
R_Date WW 6422	23870	100	365	28170	27690	27915	120		28170	27690	27915	120		sed. carbon
R_Date WW 3576	28289	120	375	32685	31640	32155	275		32680	31635	32155	275		sed. carbon
R_Date WW 6423	29490	190	380	34050	33305	33685	180		34050	33305	33685	180		sed. carbon
R_Date WW 8454	22770	120	400	27425	26720	27115	175		27465	26430	27000	335	95.8	sed. carbon
R_Date WW 8455	21440	100	440	25955	25555	25760	100		25955	25550	25760	100	1.4	sed. carbon
R_Date AZ 120	26800	900	470	33170	29125	31020	1000		32080	29365	30720	665	118.2	sed. carbon
R_Date WW 8456	29880	280	535	34530	33555	34010	240		34500	33310	33895	295	102.6	sed. carbon
R_Date A 9359	32565	2885	610	36655	36220	36430	105		36730	36035	36385	175	100.4	sed. carbon
R_Date WW 3364	28600	140	665	33195	31990	32640	290		33195	31990	32640	290		sed. carbon
R_Date A 9770	42400	1000	910	48255	44080	45990	1040		49995	45185	47245	1190	62.3	sed. carbon
Boundary									49995	45185	47245	1190		
P_Sequence Lake Cuitzeo														
Too old to calibrate														
R_Date WW 3365	45110	940	870	--	--	--	--		--	--	--	--	--	--

Melrose, Pennsylvania

Except for the age model and data table below, the following information was extracted from Bunch et al. (17) and Wittke et al. (19) with minor modifications. Detailed stratigraphic information is presented in Bunch et al. (17) and Wittke et al. (19). See main manuscript **Table 1** and **Tables S1-S2** for other site information. During the last Glacial Maximum, the Melrose area in northeastern Pennsylvania lay beneath 0.5 to 1 km of glacial ice that retreated rapidly after ≈18,000 Cal B.P. (114). Surficial sediments at Melrose are represented by unconsolidated latest Quaternary alluvium/colluvium overlying glacial till that, in turn, overlies the Devonian Catskill Formation. A shallow trench was excavated, and five contiguous samples were taken from 5 to 48 cmbs. The sedimentary section consists of fine-grained, humic colluvium to 38 cmbs, resting on distinctive end-Pleistocene glacial till (diamicton). The YDB layer is marked by a remarkable diversity of proxies with abundance peaks in melt-glass (0.8 g/kg), impact-related spherules (3100/kg), carbon spherules, nanodiamonds (66 ppb), charcoal, and osmium (see main paper). This layer occurs in the interval between 15 and 23 cmbs, ≈15 cm above the till, consistent with deposition during the deglacial episode, after the ice sheet retreated from this area (<18,000 Cal B.P.).
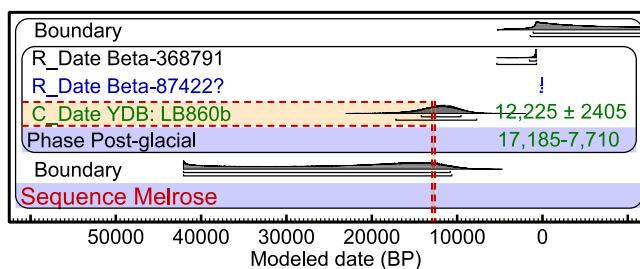

Fig. S19. Melrose age-sequence model, including a new date (Beta-368791) at 10 cmbs. The YDB has a modeled age based on an OSL date from just beneath the YDB layer. This age has high uncertainties that overlap the YDB age range.

Table S23. Melrose, Pennsylvania. Radiocarbon dates Beta-368791 and Beta-87422 are new. The latter date on a carbon spherule was rejected by OxCal as anomalously young. The LB860b OSL date of 11,700 Cal B.P. (before 2012) from Kinzie et al. (20) has been converted and rounded to 11,640 Cal B.P. (before 1950) to match the age scale used for the radiocarbon dating.

Laboratory #	Type	μ	σ	Depth (cm)	UNMODELED (BP) 95.4% range		μ	σ	Modelled (BP) 95.4% range		μ	σ	Amodel=98.9 Aoverall=98.9	
Boundary									1425	-20065	-7420	6750		
R_Date Beta-368791	14C	850	30	10	900	690	760	40	5355	695	1640	1305	99.6	charcoal
R_Date Beta-87422	14C	-5	25	18	245	35	65	45	245	35	65	45		charcoal
C_Date YDB: LB860b	OSL	11700	1850	28	15325	7955	11640	1845	17185	7710	12255	2405	98.5	quartz grains
Phase Post-glacial														
Boundary									42075	10610	24075	9660		
Sequence Melrose														

Mucuñuque (MUM7b), Venezuela

Except for the age model and data table below, the following information was extracted from Mahaney et al. (30-36) with minor modifications. See main manuscript **Table 1** and **Tables S1-S2** for other site information. This site is on a small glaciolacustrine plain at 3800 masl elevation in the Venezuelan Andes. The 2.5-m-thick sampled section is comprised of imbricated outwash, overlying a succession of stratified sand, gravel, and a manganese-rich black mat layer. These deposits were correlated with deposits further down the valley, representing a re-advance of the glacier during the early Younger Dryas episode. The stratigraphy is described in detail in Mahaney et al. (30-36). The YDB layer immediately is coincident with the dark layer, as it does at some other YDB sites.
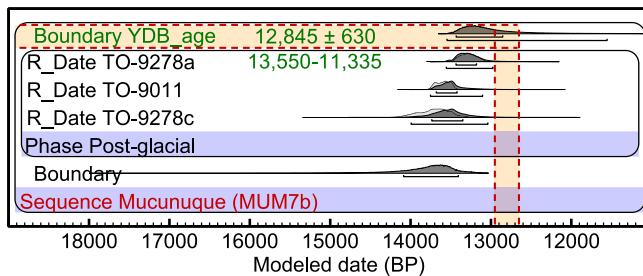
Fig. S20. Mucuñuque age-sequence model. The available dates are from layers of alluvial clay and peat, ≈20 cm below the YDB layer. There was no datable material in the YDB layer, glacial outwash, or moraine at this site, although the outwash was correlated by Mahaney et al. (31) with nearby deposits that are of Younger Dryas age.

Table S24. Mucuñuque, Venezuela. Radiocarbon dates are from Mahaney et al. (31).

Laboratory #	μ	σ	Depth (cm)	UNMODELED (BP) 95.4% range		μ	σ	Modelled (BP) 95.4% range		μ	σ	Amodel=99.2 Aoverall=99.3	
Boundary YDB_layer								13550	11335	12845	630		
R_Date TO-9278a	11440	100	232	13460	13095	13285	100	13560	12885	13250	190	94.2	charcoal
R_Date TO-9011	11760	80	235	13755	13445	13595	85	13765	12995	13465	215	100.5	charcoal
R_Date TO-9278c	11850	180	235	14125	13310	13720	215	14045	12960	13510	265	104.2	charcoal
Phase Post-glacial													
Boundary								15820	12890	14000	775		
Sequence Mucunuque													

Ommen, Netherlands

Except for the age model and data table below, the following information was extracted from Wittke et al. (19). See Lingen discussion above, main manuscript **Table 1** and **Tables S1-S2** for more information. Seven 5-cm-thick continuous samples of bulk sediment were from a 50-cm-thick sequence between 92.5 and 142.5 cmbs. The 5-cm-thick YDB layer, from 115 to 120 cmbs, displays a peak in impact-related spherules (5/kg) and nanodiamonds (1439 ppb) within carbon spherules (458/kg).
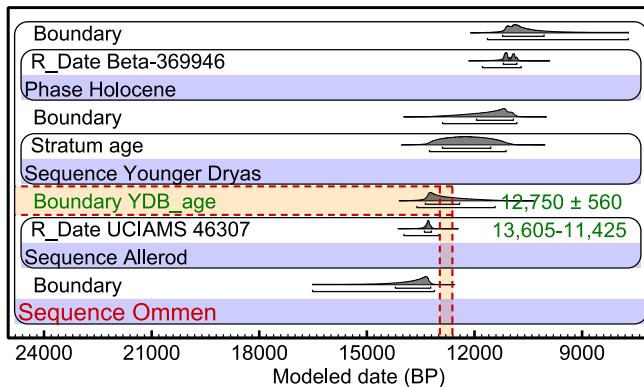

Fig. S21. Ommen age-sequence model. YDB corresponds to charcoal layer.

Table S25. Ommen, Netherlands. The date UCIAMS 46307 is from Wittke et al. (19) and Beta-369946 is new.

Laboratory #	μ	σ	Depth (cm)	UNMODELED (BP) 95.4% range		μ	σ	Modelled (BP) 95.4% range		μ	σ	Amodel=99.7 Aoverall=99.7	
Boundary								11640	7710	10395	855		
R_Date Beta-369946	9640	40	112.5	11190	10785	10995	120	11780	10695	11080	250	100	charcoal
Phase Holocene													
Boundary Transition								12890	10815	11660	570		
Stratum age								13255	11115	12205	595		
Phase Younger Dryas													
Boundary YDB_age								13605	11425	12750	560		
R_Date UCIAMS 46307	11440	35	117.5	13390	13185	13280	50	13970	12985	13325	195	99	charcoal
Phase Allerød													
Boundary								16515	13115	13990	800		
Sequence Ommen													

UNMODELED SITES

There are nine unmodeled sites:

1. Chobot, Alberta, Canada;
2. Gainey, Michigan;
3. Kangerlussuaq, Greenland;
4. Kimbel Bay, North Carolina;
5. Morley, Alberta, Canada;
6. Mt. Viso, France/Italy;
7. Newtonville, New Jersey;
8. Paw Paw Cove, Maryland; and
9. Watcombe Bottom, United Kingdom.

For detailed site descriptions, see Bunch et al. (17), Wittke et al. (19), and Kinzie et al. (20), partially summarized in **Tables S1-S2** above. Even though dating is insufficient for robust Bayesian analysis, a wide range of evidence indicates that all nine are YDB sites. Each contains one or more proxies, including impact-related spherules, melt-glass, carbon spherules, glass-like nanodiamonds, and/or geochemical anomalies. On the other hand, there are few to no proxies above and below the YDB layer. In addition, a YDB age for the proxy-rich layers is supported by biostratigraphy, archaeostratigraphy, climatology, and/or palynology. Because these nine sites contain the same abundance peaks in proxies that are found at well-dated YDB sites, we have proposed that they are of YDB age.
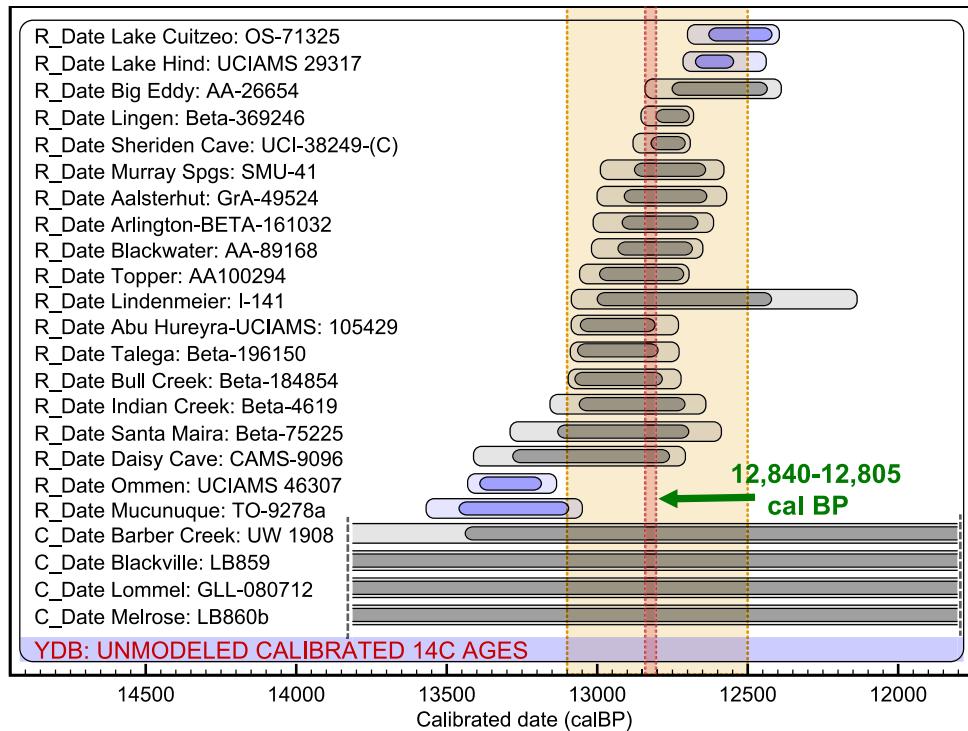
Fig. S22. Unmodeled, calibrated ^{14}C and OSL ages for 23 YDB sites. Dates used are directly from the YDB layer or were the closest in age to 12,800 ± 150 Cal B.P. To improve readability, horizontal gray error bars were used, rather than probability distribution curves; light gray bars represent 99% CI and dark gray equals 95%. The complete bars for the lower 4 OSL dates extend off the scale. The red vertical dashed lines and bar represent the common overlap of 35 years from 12,840 to 12,805 Cal B.P. The orange vertical dashed lines and bar represent 12,800 ± 300 Cal B.P. at 95% CI. Of the 23 dates, 22 (96%) fall within the YDB range at 99% CI; 19 of 23 dates (83%) overlap from 12,840 to 12,805 Cal B.P. at 95% CI. This indicates that the results from simply calibrating a group of YDB dates are not substantially different from using Bayesian-modeling for YDB dates.

Table S26. Unmodeled, calibrated dates for 23 YDB sites used in Fig S22 above. The date chosen for each site is either from within the YDB layer or represents the temporally closest date to 12,800 ± 150 Cal B.P.

Calibration (IntCal-13) unmodeled YDB ages and layers	μ	σ	68.2% range		95.4% range	
R_Date Lake Cuitzeo: OS-71325	12520	60	12580	12425	12630	12415
R_Date Lake Hind: UCIAMS 29317	12605	35	12635	12565	12675	12545
R_Date Big Eddy: AA-26654	12640	65	12715	12595	12755	12435
R_Date Lingen: Beta-369246	12745	30	12765	12705	12805	12690
R_Date Sheriden Cave: UCI-38249-(C)	12765	30	12795	12730	12825	12705
R_Date Murray Spgs: SMU-41	12745	55	12780	12690	12880	12640
R_Date Aalsterhut: GrA-49524	12750	60	12785	12690	12910	12635
R_Date Arlington-BETA-161032	12760	60	12790	12700	12920	12665
R_Date Blackwater: AA-89168	12780	65	12805	12705	12935	12680
R_Date Topper: AA100294	12835	80	12890	12730	12995	12710
R_Date Lindenmeier: I-141	12700	140	12805	12565	13000	12420
R_Date Abu Hureyra-UCIAMS: 105429	12935	70	13015	12860	13060	12805
R_Date Talega: Beta-196150	12930	75	13020	12855	13065	12795
R_Date Bull Creek: Beta-184854	12930	80	13020	12850	13075	12780
R_Date Indian Creek: Beta-4619	12875	100	12960	12740	13060	12705
R_Date Santa Maira: Beta-75225	12905	120	13015	12760	13135	12695
R_Date Daisy Cave: CAMS-9096	13025	135	13160	12865	13285	12760
R_Date Ommen: UCIAMS 46307	13280	50	13330	13235	13390	13185
R_Date Mucunuque: TO-9278a	13285	100	13395	13180	13460	13095
C_Date Barber Creek: UW 1908	12040	700	12745	11340	13440	10640
C_Date Blackville: LB859	12900	1190	14090	11705	15275	10520
C_Date Lommel: GLL-080712	12340	900	13240	11435	14135	10540
C_Date Melrose: LB860b	11640	1845	13485	9790	15325	7955
YDB: UNMODELED CALIBRATED 14C AGES						

35

ONSET AGE OF YOUNGER DRYAS CLIMATE EPISODE

It is widely accepted that the onset of the Younger Dryas climate episode occurred synchronously across the Northern Hemisphere, based on correlations among high-resolution records from the Cariaco Basin (115), Santa Barbara Basin (116, 117, 118), the Greenland ice sheet (119), and elsewhere. Even though the onset of the Younger Dryas episode was abrupt, not every associated climate change proxy responded synchronously across wide areas (120). For example, Lane et al. (121) and Muschitiello and Wohlfarth (122) investigated the Younger Dryas onset in laminated varve sequences, concluding that the pollen response was diachronous across Europe. In another example, Steffensen et al. (119), documented high resolution climatic records for the Greenland (NGRIP) ice core, concentrating on the Younger Dryas episode and its associated climate proxies (**Table S27**). Those workers placed the abrupt onset of the Younger Dryas episode at 12,896 ±1.5 years, consistent with the age of the peak in platinum in the GISP2 Greenland ice core (53, 123). The date of the Younger Dryas onset is based on a sharp change in deuterium excess (isotopic fractionation; $d = \delta D - 8(\delta^{18}O)$), a climate proxy that revealed an abrupt shift in atmospheric circulation patterns and changes in related moisture sources that contributed to Greenland's snowpack (119). This change in atmospheric circulation occurred within a span of approximately one year at the Younger Dryas onset (119). This was followed by a succession of changes in Younger Dryas-related proxies that lagged the shift in the deuterium record by up to ≈184 years (**Table S27**). That temporal lag in climate proxies, including a drop in Greenland temperatures, can probably be attributed to a succession of climatic feedbacks in the atmospheric-oceanic system early in the Younger Dryas episode.

Table S27. Age of onset for the Younger Dryas climate episode, using various proxies. From Steffensen et al. (119).

Steffensen et al. (2008)	Deuterium excess (d)	Annual ice thickness (λ)	Calcium ions (Ca^{2+})	Dust content	Stable oxygen isotope ($\delta^{18}O$)
Onset age	12,896 ±1.5	12,787 ±24	12,737 ±8.9	12,735 ±8.9	12,712 ±74

Table S28. Calculations for testing synchroneity (16, 124). Dates from 30 sites: 1 site with the Greenland platinum record, 6 for Younger Dryas climate onset, and 23 for the YDB (grouped by quality). The Bayesian modeled ages for the 30 records are separated by a minimum of zero (statistically calculated as "-5") years at 68%, 95%, and 99% ("Difference L" row in green). The maximum statistical difference is 130 years at 95% CI. Using the Date code, the length of the overlap among 30 sites was modeled from the Start and End Boundaries (two green highlighted dates), between which all dates fall, producing a modeled age range of 12,820 to 12,740 Cal B.P. at 95% (bottom row highlighted in green). Age model is in **Fig. 9** in the main manuscript.

Difference Code: modeled YDB ages and layers	Prior ages μ	σ	Common μ	σ	95.4% range		68.2% range		95.4% range		99.7% range		Amodel=188 Aoverall=190.7
Difference L			45	40			-5	60	-5	130	-5	215	
Boundary End			12760	25			12790	12740	12805	12710	12820	12665	
AGE OF YOUNGER DRYAS ONSET													
C_Date GRIP GICC05 ice model	12845	140	12785	25	13125	12570	12810	12760	12840	12735	12885	12700	127
C_Date GISP2 ice model	12840	260	12785	25	13360	12320	12810	12760	12835	12735	12885	12695	137.7
C_Date GISP2 platinum peak	12840	260	12785	25	13360	12315	12810	12760	12835	12735	12885	12695	138.1
C_Date Cariaco Basin varves	12770	30	12780	20	12835	12710	12805	12760	12820	12740	12840	12720	114.9
R_Date Late glacial tree-rings, GER	12810	50	12785	20	12920	12720	12810	12765	12830	12745	12865	12725	126.5
C_Date Hulu speleothems, CHN	12770	60	12785	20	12895	12650	12805	12760	12830	12735	12865	12705	130.5
C_Date Meerfelder Maar	12680	125	12785	25	12935	12425	12805	12760	12835	12735	12875	12695	101.4
YDB: HIGH QUALITY													
Prior Abu_Hureyra_UCIAMS_105429	12825	55	12790	25	12935	12705	12810	12765	12840	12740	12880	12715	92.1
Prior Arlington_Cyn_YDB_layer	12805	55	12785	20	12925	12695	12810	12765	12835	12740	12875	12715	129.1
Prior Aalsterhut_YDB_layer	12780	35	12780	20	12845	12725	12800	12760	12820	12745	12845	12730	106.5
Prior Big_Eddy_YDB_layer	12770	85	12785	20	12935	12580	12805	12760	12835	12740	12870	12705	143.4
Prior Bull_Creek_YDB_layer	12840	75	12790	20	12995	12710	12810	12765	12835	12740	12880	12715	122.3
Prior Daisy_Cave_YDB_age	12730	320	12785	25	13320	12050	12810	12760	12840	12735	12885	12695	141.4
Prior Lake_Hind_YDB_UCIAMS_29317	12745	180	12785	25	13190	12550	12810	12760	12835	12730	12880	12685	37.8
Prior Lingen_YDB_Beta_369246	12735	85	12780	20	12910	12520	12805	12760	12820	12730	12855	12700	87.7
Prior Sheriden_Cave_YDB_layer	12840	120	12785	20	13110	12625	12805	12765	12835	12740	12880	12710	146.1
YDB: MEDIUM QUALITY													
Prior Barber_Creek_YDB_age_UW_1908	12865	535	12785	25	13945	11865	12810	12760	12835	12735	12885	12695	138.4
Prior Blackwater_YDB_age	12775	365	12785	25	13510	12090	12810	12760	12840	12735	12885	12695	135
Prior Indian_Creek_YDB_age	12750	425	12785	25	13495	11805	12810	12760	12840	12735	12890	12700	120.8
Prior Lindenmeier_YDB_I_141	12775	180	12785	25	13195	12440	12805	12760	12835	12735	12880	12695	131.4
Prior Murray_Springs_YDB_layer	12750	235	12785	25	13195	12255	12810	12760	12840	12735	12885	12700	147.4
Prior Santa_Maira_YDB Beta-75225	12785	295	12785	25	13265	12070	12805	12760	12835	12735	12885	12705	147.6
Prior Talega_YDB_Beta_196150	12860	150	12790	25	13075	12545	12810	12765	12845	12740	12890	12710	62.7
Prior Topper_YDB_AA100294	12785	185	12785	20	13085	12365	12805	12760	12835	12735	12880	12710	158.9
YDB: LOWER QUALITY													
Prior Blackville_YDB_age_LB859	12820	1080	12785	25	15015	10705	12805	12760	12835	12735	12885	12695	142.8
Prior Lake_Cuitzeo_YDB_layer	12850	570	12785	25	14265	12195	12805	12760	12835	12730	12880	12690	60.3
Prior Lommel_YDB_age	12735	790	12785	25	14410	11325	12810	12760	12835	12735	12885	12695	120.4
Prior Melrose_YDB_LB860b	12255	2405	12785	25	17185	7710	12810	12760	12840	12735	12885	12695	129.2
Prior Mucunuque_YDB_age	12845	630	12785	25	13550	11335	12810	12760	12840	12735	12890	12700	59.7
Prior Ommen_YDB_age	12750	560	12785	25	13605	11425	12810	12760	12840	12735	12885	12695	94.3
Phase													
Boundary Start			12810	25			12830	12775	12865	12760	12920	12745	
Sequence YDB SYNCHRONICITY													
Prior Boundary Start to Boundary End													
Synchronicity_layer			12785	25			12805	12760	12835	12735	12880	12700	

Bayesian analyses. The OxCal program is used in many disciplines, e.g., by Huysecom et al. (79), who correlated ages of pottery at 26 sites in several countries across northern Africa. OxCal also has been employed to evaluate archaeological site usage in the Middle East (80), Central America (81, 82); and the U.S.A. (125). Bayesian analysis has limited previous usage for dating YDB sites (9, 13, 18, 20, 63). OxCal also has been used to produce age models of spatially scattered historic and prehistoric earthquakes along the San Andreas Fault (126).

For performing Bayesian analyses on a group of ^{14}C dates from a site, OxCal uses the Markov chain Monte-Carlo (MCMC) algorithm, which can analyze millions of possible age-depth permutations. The following is a simplified description of the process. OxCal calibrates all dates, and then at every available depth, it selects one age from all the possibilities in each probability distribution (127). Next, it combines all the ages for all depths, and this assemblage of

dates becomes one single iteration of an age-depth model. OxCal repeats this process many times, often calculating tens of millions of iterations. Once those calculations are completed, OxCal *(i)* rejects those iterations that contradict prior information, such as stratigraphic-chronological ordering, *(ii)* finds the mean of the various iterations, and *(iii)* calculates the final range of uncertainties. Each date and the overall model are ranked on an Agreement Index, where a value of >60% approximately corresponds to a chi-squared distribution of >95% probability (128).

In OxCal, if the Agreement Index drops below 60% (<95% CI), then that date is a potential outlier, i.e., either too old or too young for the model, and thus, a candidate for rejection. However, Bronk Ramsey (16), stated that the rejection of a date should be based on other criteria, such as the Agreement Index or the entire age model (A_{model}). If the model's Agreement Index is above 60% (>95% CI), then no samples need be rejected, even though index values of

individual dates fall below 60%. In some cases, a date is anomalously old and thus, is a candidate for rejection because of the old wood effect. To counter this, OxCal utilizes what is called the "Charcoal Outlier" coding, and because most dates were on charcoal, we used this coding for most sites. After performing outlier testing, we rejected only those dates for which the Agreement Index values for both the individual and the model fell below 60% (<95% CI). All rejected dates are marked in blue in the site tables (**SI Appendix—Tables S3-S28**).

Date sources. All dates and data are available from previously published source papers, as cited in each site's discussion and in Table S1.

Calculations and coding. The coding for each site is shown in **SI Appendix—Code.** The general types of OxCal coding used in this contribution include the following:

1) CALIBRATION. OxCal's "R_Date" code calibrates radiocarbon ages using the IntCal13 calibration curve (10) through conversion of radiocarbon years to calendar years. The code "C_Date" is used for OSL, varve, and ice layer dates that do not need calibration.

2) AGE-DEPTH MODELS. For three sites, we used the "P_Sequence" code that produces models from groups of dates for which depth relationships are known. In this OxCal model, the rigidity of the curves in the output model is determined by the "k" parameter (127). Higher k values produce a more rigid model that assumes more uniform deposition rates with lower uncertainties; this type of model typically deviates the most from existing dates. For example, if k = 100, then it is assumed that the deposition rate remains essentially unchanged throughout the sequence, an unlikely assumption, causing the resulting plot to be straight with low uncertainties. On the other hand, lower k values produce a model that allows for more variable deposition rates, but with higher uncertainties. The resulting plot is similar to a linear interpolation (regression), except that uncertainties become larger in the undated layers between radiocarbon dates. For the three sites, an inspection of the available radiocarbon dates and depths indicated variable deposition rates, and therefore, we used low k values of 0.03 to 0.1.

3) AGE-SEQUENCE MODELS. The "Sequence" code computes age models from groups of dates that are in chronological order, because depth correlations are uncertain or unavailable.

4) AGE-PHASE MODELS. The "Phase" code calculates age models from groups of dates that are in stratigraphic order, but for which precise depth correlations are uncertain or unavailable.

5) SYNCHRONEITY TEST. The "Phase" and "Difference" codes were used to compare dates from different sites to assess potential synchroneity (16, 124). Because of uncertainties inherent in all dating techniques, it is simply not possible to "prove" or "disprove" that all YDB dates are from an impact or any other event that occurred instantly. On the other hand, Bayesian analysis can determine whether YDB dates are statistically likely to be synchronous or diachronous. To do so, we placed all dates into a single group, called a Phase, and then used the Difference command to determine the span of the phase in years. If the minimum span was greater than zero, then the dates are diachronous. If the minimum span included zero years, then the dates could be isochronous.

6) OUTLIER CODE. Most dates, whether radiocarbon and OSL, are older than their parent stratum (16). On the other hand, some datable material may move downward through redeposition, making a stratum appear younger than its true age. To account for these effects, an Outlier Model was used for all sites. For sites with only charcoal dates, we named the code "Charcoal." Where dates were acquired on charcoal and sedimentary carbon, we used the same code, but named the model "Carbon." When OSL dates were used or radiocarbon dates were acquired on a mix of charcoal, wood, sedimentary carbon, and bone, we used the same code, but named it "General."

OxCal's outlier code has several variables, and their selection was based on balancing several objectives: achieving the highest model Agreement Index; producing the lowest age uncertainties; maintaining consistency with existing unmodeled ages; and rejecting the fewest outliers, based on the assumption that accepting more dates is preferable. To test the robustness of the variable selection, we *(i)* compiled all calibrated ^{14}C dates (IntCal13) acquired directly on the YDB layer; *(ii)* added the dates that were stratigraphically closest to the proxy-rich YDB layer for those sites with no direct ^{14}C dates; and *(iii)* used all YDB OSL dates as published. The results in **Fig. S22** and **Table S27** show that 91% of dates (39 of 43) share a common age range of 12,840 to 12,805 Cal B.P. at 99% CI and 81% of dates (35 of 43) overlap within the 95% CI range. Compared to the Combine test above with an age range of 12,815 to 12,755 Cal B.P. at 95% CI, the results indicate that Bayesian modeling does not negatively affect a comparison of the 30 YDB records.

(7) DATE CODE. When modeling sites, another factor was considered, the stratigraphic thickness of the YDB samples, which varied widely. Typically, stratigraphic intervals across the YDB were less than 5-cm thick, but sometimes they were thicker, mainly because we were unable to sample the sites directly, and instead, acquired archival samples from independent investigators. These thicker samples represent a temporal span that was short if deposition was rapid, but long if deposition was slow. Thus, it was not possible to determine if the entire thick sample represented the YDB layer or whether the YDB occurred only across a smaller percentage of the width. Consequently, a single calibrated radiocarbon date acquired from within that thick sample may or may not adequately represent the age of the YDB – the available date might be older or younger. This means that all we can conclude is that the age of the YDB falls somewhere within the age range of the entire sample, which must be calculated.

To compensate for sampling difference, we used the "Date" coding in two ways. For sites such as Arlington Canyon and Aalsterhut, there were multiple varying dates within the YDB layer. In those cases, we chose not to use the Combine code because that would have produced an age with a misleadingly low uncertainty. Instead, we inserted Boundary codes for "YDB_base" and "YDB_top," and after obtaining those values, we performed a second calculation using the modeled Boundary age data from previously calculated files called "priors." This calculation produces a modeled age for the entire stratum that contains the YDB layer. It is possible to incorporate such coding into the original age modeling, but for simplicity and clarity, we chose to perform the calculations in two separate steps, as shown in **SI Appendix—Code**.

REFERENCES

01. Telford RJ, Heegaard E, Birks HJB (2004a) The intercept is a poor estimate of a calibrated radiocarbon age. *The Holocene* 14(2):296–298.
02. Telford RJ, Heegaard E, Birks HJB (2004b) All age–depth models are wrong: but how badly? *Quaternary Science Reviews* 23 (2004) 1–5.
03. Andressen CS, et al. (2000) What do $\delta^{14}C$ changes across the Gerzensee oscillation/GI-1b event imply for deglacial oscillations? *J Quat Sci* 15(3):203–214.
04. Firestone RB, et al. (2007) Evidence for an extraterrestrial impact 12,900 years ago that contributed to the megafaunal extinctions and the Younger Dryas cooling. *Proc Natl Acad Sci USA* 104(41):16016–16021.
05. Overholt AC, Melott AL (2013) Cosmogenic nuclide enhancement via deposition from long-period comets as a test of the Younger Dryas impact hypothesis. *Earth Planet Sci Lett* 377–378:55–61.
06. Philippsen B (2013) The freshwater reservoir effect in radiocarbon dating, *Heritage Sci* 1:24.
07. Mahaney WC, Terasmae J (1988) Notes on radiocarbon dated Holocene soils in Rouge River basin, south-central Ontario. *Acta Geologica Hungarica* 31(1–2):153–163.
08. Blaauw M., et al. (2011) High-resolution ^{14}C dating of a 25,000-year lake-sediment record from equatorial East Africa. *Quaternary Science Reviews*, 30, 3043-3059.
09. Kennett DJ, et al. (2008) Wildfire and abrupt ecosystem disruption on California's northern channel islands at the Ållerød–Younger Dryas boundary (13.0–12.9 ka). *Quat Sci Rev* 27(27–28):2530–2545.
10. Reimer PJ, et al. (2013) IntCal13 and Marine13 radiocarbon age calibration curves 0-50,000 Years Cal B.P. *Radiocarbon* 55(4):1869–1887.
11. Sarnthein M, Grootes PM, Kennett JP, Nadeau M-J (2007) 14C reservoir ages show deglacial changes in ocean currents and carbon cycle, in Ocean Circulation: Mechanisms and Impacts - Past and Future Changes of Meridional Overturning (eds A. Schmittner, J. C. H. Chiang and S. R. Hemming), American Geophysical Union, Washington, D.C. doi: 10.1029/173GM13
12. Sarnthein M, Balmer S, Grootes PM, Mudelsee M (2015) Planktic and Benthic 14C Reservoir Ages for Three Ocean Basins, Calibrated by a Suite of 14C Plateaus in the Glacial-to-Deglacial Suigetsu Atmospheric 14C Record. Radiocarbon, 57, 1, 129-151.
13. Meltzer DJ, Holliday VT, Cannon MD, Miller DS (2014) Chronological evidence fails to support claim of an isochronous widespread layer of cosmic impact indicators dated to 12,800 years ago. *Proc Natl Acad Sci USA* 111(21):E2162–E2171.
14. Casson MA and Feathers JK. (2001) The Application of Luminescence Dating to Cultural Resource Management. Society for American Archaeology, New Orleans, LA.
15. Erlandson JM, Braje TJ, Graham MH (2008) How old is MVII?: seaweeds, shorelines, and chronology at Monte Verde, Chile. *J Island and Coastal Archaeol* 3(2):277–281.
16. Bronk Ramsey C (2009) Bayesian analysis of radiocarbon dates. *Radiocarbon* 51(1):337–360.
17. Bunch TE, et al. (2012) Very high-temperature impact melt products as evidence for cosmic airbursts and impacts 12,900 years ago. *Proc Natl Acad Sci USA* 109(28):11066–11067.
18. van Hoesel A, et al. (2012) Nanodiamonds and wildfire evidence in the Usselo Horizon postdate the Allerød-Younger Dryas boundary. *Proc Natl Acad Sci USA* 109(2):7648–7653.
19. Wittke JH, et al. (2013) Evidence for deposition of 10 million tonnes of cosmic impact spherules across four continents 12,800 years ago. *Proc Natl Acad Sci USA* 110(23):E2088–E2097.
20. Kinzie CR, et al. (2014) Nanodiamond-rich layer across three continents consistent with major cosmic impact at 12,800 Cal B.P. *J Geol* 122(5):475–506.
21. Tankersley KB, Ford K, McDonald G, Genheimer R, Hendricks R (1997a) Late Pleistocene archaeology of Sheriden Cave, Wyandot County, Ohio. *Curr Res Pleist* 14:81–83.
22. Tankersley KB, Sheriden B (1997b) A Clovis cave site in eastern North America. *Geoarch* 12(6):713–724.
23. Tankersley KB, Landefeld CS (1998) Geochronology of Sheriden Cave, Ohio: the 1997 field season. *Curr Res Pleist* 15:136–138.
24. Tankersley KB, Redmond BG (1999a) Fluoride/radiocarbon dating of late Pleistocene bone from Sheriden Cave, Ohio. *Curr Res Pleist* 16:107–108.
25. Tankersley KB, Redmond BG (1999b) Radiocarbon dating of a projectile point from Sheriden Cave, Ohio. *Curr Res Pleist* 16:76–77.
26. Tankersley KB, Redmond BG, Grove T (2001) Radiocarbon dates associated with a single-beveled bone projectile point from Sheriden Cave, Ohio. *Curr Res Pleist* 18:61–63.
27. Tankersley KB, Sheriden B (1999c) A stratified Pleistocene-Holocene cave site in the Great Lakes region of North America. *Zooarchaeology of the Pleistocene/Holocene Boundary*, ed Driver JC (Archaeopress, Oxford), BAR International Series 800, pp 67–75.
28. Redmond BG, Tankersley KB (2005) Evidence of Early Paleoindian bone modification and use at the Sheriden Cave Site (33WY252), Wyandot County, Ohio. *Amer Antiq* 70(3):503–526.
29. Redmond BG, Tankersley KB. (2012) Species response to the theorized Clovis Comet impact at Sheriden Cave, Ohio. *Curr Res Pleist* 28:141–143.
30. Mahaney WC, et al. (2008) Evidence for a Younger Dryas glacial advance in the Andes of northwestern Venezuela. *Geomorph* 96(1):199–211.
31. Mahaney WC, et al. (2010) Evidence from the northwestern Venezuelan Andes for extraterrestrial impact: the black mat enigma. *Geomorph* 116(1–2):48–57.
32. Mahaney WC, et al. (2011a) Fired glaciofluvial sediment in the northwestern Andes: biotic aspects of the Black Mat. *Sedimentary Geol* 237(1–2):73–83.
33. Mahaney WC, et al. (2011b) Notes on the black mat sediment, Mucuñuque catchment, northern Mérida Andes, Venezuela. *J Adv Microscop Res* 6(3):177–185.
34. Mahaney WC, Keiser L (2012) Weathering rinds—unlikely host clasts for an impact-induced event. *Geomorph* 184:74–83.
35. Mahaney WC, Krinsley D, Kalm V (2010b) Evidence for a cosmogenic origin of fired glaciofluvial beds in the northwestern Andes: correlation with experimentally heated quartz and feldspar. *Sedimentary Geol* 231(1–2):31–40.

36. Mahaney WC, Krinsley D (2012) Extreme heating events and effects in the natural environment: implications for environmental geomorphology. *Geomorph* 139–140:348–35937.
37. Israde-Alcántara I, et al. (2012) Evidence from Central Mexico supporting the Younger Dryas extraterrestrial impact hypothesis. *Proc Natl Acad Sci USA* 109(13):E738–E747.
38. Kurbatov AV, et al. (2011) Discovery of a nanodiamond-rich layer in the Greenland ice sheet. *J Glaciol* 56:749–759.
39. Mahaney WC, et al. (2013) Weathering rinds as mirror images of palaeosols: examples from the western Alps with correlation to Antarctica and Mars. *J Geol Soc* 170(5):833–847.
40. LeCompte MA, et al. (2012) Independent evaluation of conflicting microspherule results from different investigations of the Younger Dryas impact hypothesis. *Proc Natl Acad Sci USA* 109(44):E2960–E2969.
41. Firestone RB (2009) The case for the Younger Dryas extraterrestrial impact event: mammoth, megafauna, and Clovis extinction, 12,900 years ago. *J Cosmol* 2:256–285.
42. Firestone RB, et al. (2010) Analysis of the Younger Dryas impact layer. *Eng Techn* 1(3):30–62.
43. Firestone RB (2014) Observation of 23 supernovae that exploded <300 pc from earth during the past 300 kyr. *Astrophys J* 789(29):1–11.
44. Kennett DJ, et al. (2009a) Nanodiamonds in the Younger Dryas boundary sediment layer. *Science* 323(5910):94.
45. Kennett DJ, et al. (2009b) Shock-synthesized hexagonal diamonds in Younger Dryas boundary Sediments. *Proc Natl Acad Sci USA* 106 (31):12623–12628.
46. Haynes CV, Jr, et al. (2010) The Murray Springs Clovis site, Pleistocene extinction, and the question of extraterrestrial impact. *Proc Natl Acad Sci USA* 107(9):4010–4015.
47. Fayek M, Anovitz LM, Allard LF, Hull S (2012) Framboidal iron oxide: chondrite-like material from the black mat, Murray Springs, Arizona. *Earth Planet Sci Lett* 319:251–258.
48. Baker DW, Miranda PJ, Gibbs KE (2008) Montana Evidence for Extra-Terrestrial Impact Event That Caused Ice-Age Mammal Die-Off. *Amer Geophys Union Abstract* P41A–05.
49. Tian H, Schryvers D, Claeys P (2011) Nanodiamonds do not provide unique evidence for a Younger Dryas impact. *Proc Natl Acad Sci USA* 108(1):40–44.
50. Bement LC, Madden AS, Carter BJ, Simms AR, Swindle AL, Alexander HM, Fine S, Benamara M (2014) Quantifying the distribution of nanodiamonds in pre-Younger Dryas to recent age deposits along Bull creek, Oklahoma Panhandle, USA. *Proc Natl Acad Sci USA* 111(5):1726–1731.
51. Andronikov AV, Lauretta DS, Andronikva IE, Maxwell RJ (2011) On the possibility of a late Pleistocene, extraterrestrial impact: LA-ICP-MS analysis of the Black Mat and Usselo Horizon samples. Abstract for a poster presented at the 74th Meteorit Soc Meeting, London UK.
52. Marshall W, Head K, Clough R, Fisher A (2011) Exceptional iridium concentrations found at the Allerød-Younger Dryas transition in sediments from Bodmin Moor in southwest England. Paper #2641, XVIII INQUA-Congress, Bern, Switzerland.
53. Petaev MI, Huang S, Jacobsen SB, Zindler A (2013) Large Pt anomaly in the GISP2 ice core points to a cataclysm at the onset of Younger Dryas. *Proc Natl Acad Sci USA* 110(32):12917–12920.
54. Beets C, Sharma M, Kasse K, Bohncke S (2008) Search for Extraterrestrial Osmium at the Allerod - Younger Dryas Boundary. *Amer Geophys Union Abstract* V53A–2150.
55. Sharma M, Chen C, Jackson BP, Abouchami W (2009) High resolution osmium isotopes in deep-sea ferromanganese crusts reveal a large meteorite impact in the Central Pacific at 12 ± 4 ka. *Amer Geophys Union Abstract* PP33B-06.
56. Wu Y, Sharma M, LeCompte MA, Demitroff M, Landis JD (2013) Origin and provenance of spherules and magnetic grains at the Younger Dryas boundary. *Proc Natl Acad Sci USA* 110(38):E3557–E3566.
57. Melott A, Thomas BC, Dreschhoff G, Johnson CK (2009) Cometary airbursts and atmospheric chemistry: Tunguska and a candidate Younger Dryas event. *Geol* 38(4):355–358.
58. Surovell TA, et al. (2009) An independent evaluation of the Younger Dryas extraterrestrial impact hypothesis. *Proc Natl Acad Sci USA* 104(43):18155–18158.
59. Pinter N, et al. (2011) The Younger Dryas impact hypothesis: a requiem. *Earth Sci Rev* 106:247–264.
60. Pigati JS, et al. (2012) Accumulation of impact markers in desert wetlands and implications for the Younger Dryas impact hypothesis. *Proc Natl Acad Sci USA* 109(19):7208–7212.
61. Boslough MB, et al. (2012) Arguments and evidence against a Younger Dryas impact event. *Climates, Landscapes, and Civilizations*, eds Giosan L, Fuller DQ, Nicoll K, Flad RK, Clift PD (Amer Geophys Union, Washington, DC), Geophys Monograph Ser Vol 198, pp 13–26.
62. Scott AC, et al. (2010) Fungus, not comet or catastrophe, accounts for carbonaceous spherules in the Younger Dryas "impact layer." *Geophys Res Lett* 37(14):L14302.
63. van Hoesel A, et al. (2014) The Younger Dryas impact hypothesis: a critical review. *Quat Sci Rev* 83(1):95–114.
64. Daulton T, Pinter N, Scott A (2010) No evidence of nanodiamonds in Younger-Dryas sediments to support an impact event. *Proc Natl Acad Sci USA* 107(37):16043–16047.
65. Paquay FS, Goderis S, Ravizza G, Vanhaeck F, Boyd M, Surovell TA, Holliday VT, et al. (2009) Absence of geochemical evidence for an impact event at the Bølling–Allerød/Younger Dryas transition. *Proc Natl Acad Sci USA* 106(51):21505–21510.
66. Moore AMT, Hillman GC, Legge AJ (2000) *Village on the Euphrates* (Oxford Univ Press, New York).
67. Moore AMT, Kennett DJ. (2013) Cosmic impact, the Younger Dryas, Abu Hureyra, and the inception of agriculture in Western Asia. *Eurasian Prehistory*, 10, 1–2, 57–66.
68. Hillman G, Hedges R, Moore A, Colledge S, Pettitt P (2001) New evidence of late glacial cereal cultivation at Abu Hureyra on the Euphrates. *The Holocene* 11(4):383–393.
69. Hajic ER, Mandel RD, Ray JH, Lopinot NH (2007) Geoarchaeology of stratified Paleoindian deposits at the Big Eddy site, southwest Missouri, U.S.A. *Geoarch* 22(8):891–934.
70. Lopinot NH, Ray JH, Conner MD (1998) *The 1997 Excavations at the Big Eddy Site (23CE426) in Southwest Missouri* (Special Publication 2, Center for Archaeological Research, Southwest Missouri State University, Springfield, MO).
71. Lopinot NH, Ray JH, Conner MD (2000) *The 1999 Excavations at the Big Eddy Site (23CE426)* (Special Publication 3, Center for Archaeological Research, Southwest Missouri State University, Springfield, MO).
72. Bement LC, Carter BJ, Varney RA, Cummings LS, Sudbury JB (2007) Paleo-environmental reconstruction and bio-stratigraphy, Oklahoma Panhandle, USA. *Quat Internatl* 169–170:39–50.

73. Conley TO (2010) Buried soils of late Pleistocene to Holocene ages accented in stacked soil sequences from the southern High Plains of the Oklahoma Panhandle. MS thesis (Oklahoma State University, Stillwater, OK).

74. Erlandson JM, et al. (1996) An archaeological and paleontological chronology for Daisy Cave (CA-SMI-261), San Miguel Island, California. *Radiocarbon* 38(2):355–373.

75. Haynes CV, Jr, Huckell BB (2007) *Murray Springs: A Clovis Site with Multiple Activity Areas in the San Pedro Valley, Arizona* (Univ of Arizona Press, Tucson).

76. Haynes CV, Jr (2008) Younger Dryas "black mats" and the Rancholabrean termination in North America. *Proc Natl Acad Sci USA* 105(18):6520–6525.

77. Haynes CV, Jr. (1998) Arizona's Famous Clovis Sites Could be Displayed for Public. Mammoth Trumpet 13(2), p. 3.

78. Anderson DG, Goodyear AC, Kennett J, West A. (2011) Multiple lines of evidence for possible human population decline/settlement reorganization during the early Younger Dryas. Quatern. Int. 242 570-583.

79. Huysecom E, et al. (2009) The emergence of pottery in Africa during the 10th millennium cal BC: new evidence from Ounjougou (Mali). *Antiquity* 83(322):905–917.

80. Finkelstein I and Piasetzky E (2010) Radiocarbon dating the Iron Age in the Levant: a Bayesian model for six ceramic phases and six transitions. *Antiquity* 84(324):374–385.

81. Bachand BR (2008) Bayesian refinement of a stratified sequence of radiometric dates from Punta de Chimino, Guatemala. *Radiocarbon* 50(1):19–51.

82. Kennett DJ, et al. (2013) Correlating the Ancient Maya and Modern European Calendars with High-Precision AMS ^{14}C Dating. *Sci Rep* 3(1597):1–5.

83. Haynes V., Haas H. (1974) Southern Methodist University, Radiocarbon Date List I. *Radiocarbon*, 16, 3, 368-380.

84. Waters MR, Stafford TW, Jr, Redmond BG, Tankersley KB (2009) The age of the Paleoindian assemblage at Sheriden Cave, Ohio. *Amer Antiq* 74(1):107–111.

85. McDonald HG (1994) Late Pleistocene Vertebrate Fauna of Ohio: Coinhabitants with Ohio's Paleoindians. *The First Discovery of America*, ed Dancey WS (Ohio Archeological Council, Columbus) pp 23–42.

86. Daniel IR, Jr (2002) Stratified early-middle Holocene remains in the North Carolina Coastal Plain. *Southeast Archaeol Conf Spec Pub* 7:6–11.

87. Daniel IR, Jr, Seramur KC, Potts TL, Jorgenson MW (2008) Searching a sand dune: shovel testing the Barber Creek site. *N Carolina Archaeol* 57:50–77.

88. Daniel IR, Jr, Moore CR (2011) Current research into the Paleoindian and Archaic periods in the North Carolina Coastal Plain. *The Archaeology of North Carolina: Three Archaeological Symposia*, eds Ewen CR, Whyte T, Davis RPS, Jr (North Carolina Archaeological Council Publication No 30), pp 93–117.

89. McFadden P (2009) *Geoarchaeological Investigations of dune formation and artifact deposition at Barber Creek (31PT259).* MA thesis (East Carolina University, Greenville, NC).

90. Moore CR (2009) *Late Quaternary geoarchaeology and geochronology of stratified eolian deposits, Tar River, North Carolina.* PhD dissertation (East Carolina University, Greenville NC).

91. Moore CR, Daniel IR, Jr (2011) Geoarchaeological investigations of stratified sand ridges along the Tar River, North Carolina. *North Carolina Archaeology: Three Archaeological Symposia*, eds Ewen CR, Whyte T, Davis RPS, Jr. (North Carolina Archaeological Council Publication 30), pp 1–42.

92. Choate BC (2011) Stratigraphic investigations at Barber Creek (31PT259): reconstructing the culture-history of a multicomponent site in the North Carolina Coastal Plain. MA thesis (East Carolina University, Greenville, NC).

93. Haynes CV, Jr (1995) Geochronology of paleoenvironmental change, Clovis type site, Blackwater Draw, New Mexico. *Geoarch* 10(5):317–388.

94. Kilby D, Crawford G. (2013) Current Research and Investigations at Blackwater Draw, NM. *NewsMAC: Newsletter of the New Mexico Archaeological Council* 2013-2.

95. Davis LB, Greiser ST (1992) Indian Creek Paleoindians: early occupation of the Elkhorn Mountains' southeast flank, west-central Montana. *Ice Age Hunters of the Rockies*, eds Stanford DJ, Day JS (Univ Press of Colorado, Boulder, CO), pp. 225–283.

96. Running GL IV, Havholm KG, Boyd M, Wiseman DJ (2002) Holocene stratigraphy and geomorphology of Flintstone Hill, Lauder Sandhills, Glacial Lake Hind Basin, southwestern Manitoba. *Géographie Physique et Quaternaire* 56(2–3):291–303.

97. Boyd M, Running GL, Havholm K (2003) Paleoecology and Geochronology of Glacial Lake Hind During the Pleistocene-Holocene Transition: A Context for Folsom Surface Finds on the Canadian Prairies. *Geoarchaeology* 18(6):583-607.

98. Wilmsen EN, Roberts FHH, Jr (1978) *Lindenmeier, 1934–1974: Concluding Report on Investigations.* Contributions to Anthropology 24, Smithsonian Institution Press, Washington, D.C.

99. Haynes CV, Jr, Beukens RP, Jull AJT, Davis OK (1992) New radiocarbon dates from some old Folsom sites: accelerator technology. *Ice Age Hunters of the Rockies*. eds Stanford DJ, Day JS (Univ Press of Colorado, Boulder, CO), pp 83–100.

100. Hoek WZ (1997) Late-glacial and early Holocene climatic events and chronology of vegetation development in the Netherlands. *Veget Hist Archaeobot* 6(4):197–213.

101. Vanmontfort B, Van Gils M, Paulissen E, Bastiaens J, Meirsman E, De Bie M (2010) Landscape evolution and hunter-gatherer occupation in the Liereman landscape. *J Archaeol Low Countries* 2(2):31–51.

102. Derese C, Vandenberghe DAG, Van Gils M, Mees F, Paulissen E, Van den haute P (2012) Final Palaeolithic settlements of the Campine region (NE Belgium) in their environmental context: optical age constraints. *Quat Internatl* 251:7–21.

103. Aura JE, Carrion Y, Estrelles E, and Jorda JP (2005) Plant economy of hunter-gatherer groups at the end of the last Ice Age: plant macroremains from the cave of Santa Maira (Alacant, Spain) ca. 12000—9000 B.P. *Veget Hist Archaeobot* 14(4):542–550.

104. Bergin KA, et al. (2011) *The Archaeology of the Talega Site (CA-ORA-907), Orange County, California: Perspective on the Prehistory of Southern California* (Viejo California Associates, Mission Viejo, CA).

105. Waters MR, Forman S, Stafford TW, Jr, Foss J (2009a) Geoarchaeological investigations at the Topper and Big Pine Tree sites, Allendale County, South Carolina. *J Archaeol Sci* 36(7):1300–1311.

106. Blaauw M, Holliday VT, Gill JL, Nicoll K (2012) Age models and the Younger Dryas impact hypothesis. *Proc Natl Acad Sci USA* 109(34):E2240.

107. Israde-Alcántara I, et al. (2010) Evolución paleolimnologica del Lago Cuitzeo, Michoacán, durante el Pleistoceno–Holoceno (Paleolimnologic evolution of Lake Cuitzéo, Michoacán, during the Pleistocene–Holocene). *B Soc Geol Mex* 62:345–357.

108. Hooghiemstra H, Cleef AM, Noldus CW, Kappelle M (1992) Upper Quaternary vegetation dynamics and palaeoclimatology of the La Chonta bog area (Cordillera de Talamanca, Costa Rica). *J Quaternary Sci* 7:205–225.

109. Bush MB, et al. (1992) A 14,300-yr paleoecological profile of a lowland tropical lake in Panama. *Ecol Monogr* 62:251–275.

110. Correa-Metrio A (2010) Cimate and vegetation of the Yucatan Peninsula during the Late Pleistocene. PhD dissertation (Florida Institute of Technology, Melbourne FL), p 194.

111. Hodell DA, et al. (2008) An 85-ka record of climate change in lowland Central America. *Quat Sci Rev* 27:1152–1165.

112. Haug GH, et al. (2001) Southward Migration of the Intertropical Convergence Zone through the Holocene. Science 293, 1304-1308.

113. Piper DZ, Dean WE (2002) Trace-Element Deposition in the Cariaco Basin, Venezuela Shelf, under Sulfate-Reducing Conditions: A History of the Local Hydrography and Global Climate, 20 ka to the Present (USGS, Washington, DC), Prof. paper 1670.

114. Colgan PM, Mickelson DM, Cutler PM (2003) Ice-marginal terrestrial landsystems: southern Laurentide ice sheet. *Glacial Landsystems,* eds Evans DA, Rea BR (Edwin Arnold, London), pp 111–142.

115. Haug GH, Hughen KA, Peterson LC, Sigman DM, Röhl U (2001) Cariaco Basin Trace Metal Data (NOAA/NGDC), IGBP PAGES/World Data Center A for Paleoclimatology Data Contribution Series #2001-12628.

116. Kennett JP, Ingram BL (1995) A 20,000 year record of ocean circulation and climate change from the Santa Barbara Basin. *Nature* 377:510-514.

117. Behl RJ, Kennett JP (1996) Brief interstadial events in the Santa Barbara Basin, NE Pacific, during the past 60 kyr. *Nature* 379: 243-246

118. Hendy IL, Kennett JP (1999) Latest Quaternary North Pacific surface-water responses imply atmosphere-driven climate instability. *Geology* 27:291-294.

119. Steffensen JP, et al. (2008) High-Resolution Greenland Ice Core Data Show Abrupt Climate Change Happens in Few Years. *Science*, 321: 650-1.

120. Blaauw M, Mauquoy D. (2012) Signal and variability within a Holocene peat bog—chronological uncertainties of pollen, macrofossil and fungal proxies. *Review of Palaeobotany and Palynology* 186:5–15.

121. Lane CS, Brauer A, Blockley SPE, Dulski P. (2013) Volcanic ash reveals time-transgressive abrupt climate change during the Younger Dryas. First published online October 30, 2013, doi: 10.1130/G34867.1

122. Muschitiello F, and Wohlfarth B. (2015) Time-transgressive environmental shifts across Northern Europe at the onset of the Younger Dryas. Quat Sci Rev, 109, 49–56.

123. Meese DA, et al. (1997) The Greenland Ice Sheet Project 2 depth-age scale: methods and results. *J Geophys Res* 102(C12):26411–26423.

124. Parnell AC, et al. (2008) A flexible approach to assessing synchroneity of past events using Bayesian reconstructions of sedimentation history. *Quat Sci Rev,* 27:19-20, 1872-1885.

125. Steponaitis VC, Scarry CM. (2015) New directions in Moundville research. *Rethinking Moundville and its Hinterland,* ed Steponaitis VC, Scarry CM (University Press of Florida, Gainesville, FL), in press.

126. Lienkaemper JL, Williams PL, Guilderson TP (2010) Evidence for a twelfth large earthquake on the southern Hayward Fault in the past 1900 years. *Bull Seismol Soc Amer* 100(5A):2024–2034.

127. Bronk Ramsey C, Lee S (2013) Recent and planned developments of the program OxCal. *Radiocarbon* 55(2–3):720–730.

128. Ward GK, Wilson SR (1978) Procedures for comparing and combining radiocarbon age determinations: a critique. *Archaeometry* 20(1):19–31.

For the code for individual sites shown below, OxCal's Options generally were as follows:

```
Options()
 {
 Resolution=5;
 Curve="IntCal13";
 Cubic=TRUE;
 RawData=FALSE;
 UseF14C=FALSE;
 BCAD=FALSE;
 PlusMinus=FALSE;
 Intercept=FALSE;
 Floruit=FALSE;
 SD1=TRUE;
 SD2=TRUE;
 SD3=FALSE;
 ConvergenceData=TRUE;
 UniformSpanPrior=TRUE;
 kIterations=100;
 };
```

Occasionally, we used the "General" outlier code, as follows:

Outlier_Model("General", T(5), U(0,3),"t");

For most sites, we used the outlier model "Charcoal," on the assumption that all wood burned at a site is, by definition, older than the age of the fire. Typical code is as follows:

Outlier_Model("Carbon",Exp(1,-10,0),U(0,4),"t");

We used the same code for those sites where dates were acquired on charcoal and sedimentary carbon, except that we named the model "Carbon." When dates were acquired on charcoal, wood, sedimentary carbon, and bone, we used the same code, but named it "Multi."

The outlier code has multiple variables for specifying the constraints for accepting or rejecting outliers, e.g., "Exp(1,-10,n)." For the first two variables, we always used "1" and "-10. For the third exponential variable, "n," we used values ranging from 0 to 10 based on the degree of variation in dates, whenever there were multiple radiocarbon date reversals in a stratigraphic sequence. Usually, that variable was tuned to minimize rejection of radiocarbon dates, based on the assumption that using more radiocarbon dates is preferable to using fewer ones.

The individual code is provided below for each site in alphabetical order:

AALSTERHUT, NETHERLANDS.
AGE-SEQUENCE MODEL:

```
Plot()
 {
Outlier_Model("Charcoal",Exp(1,-10,3),U(0,3),"t");
Sequence("Aalsterhut")
  {
   Boundary();
   Phase("ND-rich layer")
{
R_Date("GrA-49524",11020,75){Outlier("Charcoal",1);};
R_Date("GrA-49509",10865,55){Outlier("Charcoal",1);};
R_Date("GrA-49515",10840,75){Outlier("Charcoal",1);};
};
   Boundary();
   Phase("Above NDs")
{
R_Date("GrA-49575",10900,50){Outlier("Charcoal",1);};
R_Date("GrA-49569",10895,45){Outlier("Charcoal",1);};
R_Date("GrA-49514",10880,110){Outlier("Charcoal",1);};
R_Date("GrA-49527",10960,60){Outlier("Charcoal",1);};
R_Date("GrA-49507",10920,50){Outlier("Charcoal",1);};
R_Date("GrA-49573",10860,45){Outlier("Charcoal",1);};
R_Date("GrA-49574",10845,45){Outlier("Charcoal",1);};
};
   Boundary();
   Phase("Later fire")
```

```
{
R_Date("GrA-49516",10765,50){Outlier("Charcoal",1);};
R_Date("GrA-49529",10755,55){Outlier("Charcoal",1);};
R_Date("GrA-49521 ",10765,50){Outlier("Charcoal",1);};
R_Date("GrA-49570 ",10735,45){Outlier("Charcoal",1);};
 };
   Boundary("");
 };
};
```

ABU HUREYRA
AGE-SEQUENCE MODEL

```
Plot()
 {
Outlier_Model("Multi",Exp(1,-10,1),U(0,3),"t");
Sequence("Abu Hureyra")
  {
   Boundary("Transition");
   Phase("Start Phase 1")
{
R_Date("OxA-883",11450, 300){Outlier("Multi",1);};
R_Date("OxA-468",11090, 150){Outlier("Multi",1);};
R_Date("OxA-387",11070, 160){Outlier("Multi",1);};
R_Date("OxA-469",10920, 140){Outlier("Multi",1);};
R_Date("OxA-172",10900, 200){Outlier("Multi",1);};
R_Date("OxA-470",10820, 160){Outlier("Multi",1);};
};
   Boundary("Transition");
   Phase("Transition Phase 1-2; YDB")
{
R_Date("UCIAMS-105429",11070, 40){Outlier("Multi",1);};
};
   Boundary("Top of YDB");
   Phase("Start Phase 2")
{
R_Date("BM-1718R",11140, 140){Outlier("Multi",1);};
R_Date("OxA-430",11020, 150){Outlier("Multi",1);};
R_Date("OxA-6685",10930, 120){Outlier("Multi",1);};
R_Date("OxA-474",10930, 150){Outlier("Multi",1);};
R_Date("OxA-472",10750, 170){Outlier("Multi",1);};
R_Date("OxA-431",10680, 150){Outlier("Multi",1);};
R_Date("OxA-171",10600, 200){Outlier("Multi",1);};
R_Date("OxA-434",10490, 150){Outlier("Multi",1);};
R_Date("OxA-435",10450, 180){Outlier("Multi",1);};
R_Date("OxA-397",10420, 140){Outlier("Multi",1);};
};
   Boundary("Transition");
   Phase("Start Phase 3")
{

R_Date("OxA-386",10800, 160){Outlier("Multi",1);};
R_Date("OxA-471",10620, 150){Outlier("Multi",1);};
R_Date("OxA-8719",10610, 100){Outlier("Multi",1);};
R_Date("OxA-170",10600, 200){Outlier("Multi",1);};
};
   Boundary("Transition");
   Phase("Late Phase 3")
{
R_Date("OxA-408",10250, 160){Outlier("Multi",1);};
R_Date("OxA-407",10050, 180){Outlier("Multi",1);};
R_Date("OxA-473",10000, 170){Outlier("Multi",1);};
 };
   Boundary("");
 };
};
```

ARLINGTON CANYON
AGE-SEQUENCE MODEL

```
Plot()
{
Outlier_Model("Charcoal",Exp(1,-10,0),U(0,3),"t");
Sequence("Arlington Canyon")
{
Boundary("");
Phase("Proxy-rich Phase")
{
R_Date("UCIAMS-36304",11020,25){Outlier("Charcoal",1);};
R_Date("UCIAMS-36305",11235,25){Outlier("Charcoal",1);};
R_Date("UCIAMS-36306",11375,25){Outlier("Charcoal",1);};
R_Date("BETA-161032",10860,70){Outlier("Charcoal",1);};
R_Date("UCIAMS-36959",11075,30){Outlier("Charcoal",1);};
R_Date("UCIAMS-36962",11110,35){Outlier("Charcoal",1);};
R_Date("UCIAMS-36960",11185,30){Outlier("Charcoal",1);};
R_Date("UCIAMS-36961",11440,90){Outlier("Charcoal",1);};
R_Date("UCIAMS-36307",11070,25){Outlier("Charcoal",1);};
R_Date("UCIAMS-42816",11095,25){Outlier("Charcoal",1);};
R_Date("UCIAMS-36308",11095,25){Outlier("Charcoal",1);};
R_Date("UCIAMS-47239",11105,30){Outlier("Charcoal",1);};
};
Boundary("Transition");
Phase("Upper Phase")
{
R_Date("UCIAMS-47238",11105,30){Outlier("Charcoal",1);};
R_Date("UCIAMS-47237",10895,35){Outlier("Charcoal",1);};
R_Date("UCIAMS-47236",12095,40){Outlier("Charcoal",1);};
R_Date("UCIAMS-47235",11040,30){Outlier("Charcoal",1);};
};
Boundary();
 };
 };
```

BARBER CREEK
AGE-SEQUENCE MODEL

```
Plot()
 {
Sequence("Barber Creek")
  {
   Boundary("");
   Phase("Allluvial Phase")
{
C_Date("FS2511",calBP(2009-16800), 1900);
C_Date("UW 1909",calBP(2009-14500), 1000);
};
   Boundary();
   Phase("YDB Layer")
{
C_Date("UW 1908",calBP(2009-12100), 700);
};
   Boundary("");
   Phase("Eolian Phase")
{
R_Date("Beta-188956",10500, 50);
R_Date("Beta-166238",9860, 60);
R_Date("Beta-166237",9280, 60);
R_Date("Beta-188955",8950, 40);
R_Date("Beta-150188",8940, 70);
C_Date("FS2476",calBP(2009-9740), 590);
C_Date("UW 1907",calBP(2009-9200), 700);
C_Date("UW1963",calBP(2009-9100), 700);
R_Date("Beta-166239",8440, 50);
 };
  Boundary("");
 };
 };
```

AGE-DEPTH MODEL

```
Plot()
 {
Outlier_Model("Charcoal",Exp(1,-10,0.5),U(0,3),"t");
P_Sequence("Big Eddy",0.03,0.01)
  {
Boundary();

R_Date("AA-27484",12700,180){z=396.0;Outlier("Charcoal",1);};
R_Date("AA-34590",12590,85){z=386.0;Outlier("Charcoal",1);};
R_Date("AA-27483",11910,440){z=384.0;Outlier("Charcoal",1);};
         R_Date("AA-34589",11375,80){z=383.0;Outlier();color="red";};
R_Date("AA-34588",12250,100){z=375.0;Outlier("Charcoal",1);};
R_Date("AA-72613",11960,270){z=373.0;Outlier("Charcoal",1);};
R_Date("AA-34587",11930,110){z=364.0;Outlier("Charcoal",1);};
R_Date("AA-34586",12320,130){z=358.0;Outlier("Charcoal",1);};
R_Date("AA-26655",10940,80){z=347.0;Outlier("Charcoal",1);};
R_Date("AA-72608",12450,300){z=347.0;Outlier("Charcoal",1);};
R_Date("AA-27482",11190,75){z=338.0;Outlier("Charcoal",1);};

Date("Base of YDB"){z=335.0;Outlier("Charcoal",1);};
R_Date("AA-26654",10710,85){z=333.0;Outlier("Charcoal",1);};
R_Date("AA-27486",11900,80){z=331.0;Outlier("Charcoal",1);};
            R_Date("AA-25778",10260,85){z=328.0;Outlier();color="red";};
Date("Top of YDB"){z=327.0;Outlier("Charcoal",1);};

R_Date("AA-27481",11160,75){z=326.0;Outlier("Charcoal",1);};
R_Date("Beta-230984",10940,60){z=322.0;Outlier("Charcoal",1);};
R_Date("AA-72612",10959,54){z=322.0;Outlier("Charcoal",1);};
R_Date("AA-27485",11280,75){z=322.0;Outlier("Charcoal",1);};
R_Date("AA-27488",10470,80){z=321.0;Outlier("Charcoal",1);};
R_Date("AA-72607",9960,920){z=317.0;Outlier("Charcoal",1);};
R_Date("AA-75720",10896,54){z=315.0;Outlier("Charcoal",1);};
R_Date("AA-29022",10430,70){z=313.0;Outlier("Charcoal",1);};
R_Date("AA-27480",10340,100){z=308.0;Outlier("Charcoal",1);};
R_Date("AA-27487",10400,75){z=306.0;Outlier("Charcoal",1);};
R_Date("AA-75719",10506,53){z=303.0;Outlier("Charcoal",1);};
R_Date("AA-26653",10185,75){z=298.0;Outlier("Charcoal",1);};
R_Date("AA-72610",10440,160){z=294.0;Outlier("Charcoal",1);};
R_Date("AA-72609",9924,50){z=286.0;Outlier("Charcoal",1);};
R_Date("AA-72611",9751,64){z=285.0;Outlier("Charcoal",1);};
R_Date("AA-35462",9835,70){z=283.0;Outlier("Charcoal",1);};

Boundary();
 };
 };
```

Because the YDB sample at this site spanned 8 cm, we interpolated the ages of the upper and lower boundary of that layer. Then, we combined those dates with the all dates (except one rejected Outlier) that fell within the interval to model the YDB age. To do that, we saved the data from running the age-depth model as *.prior files and then called out those files for the Combine code below. This procedure was followed for all other sites below where *.prior files are called out.

COMBINE

```
Plot()
  {
   Combine("Big Eddy")
  {
Prior("Base_of_YDB");
Prior("AA_26654");
Prior("AA_27486");
//OUTLIER Prior("AA_25778");
Prior("Top_of_YDB");
  };
 };
 };
```

AGE-SEQUENCE MODEL

```
Plot()
 {
Sequence("Blackville")
  {
   Boundary("Unconformity");
{
C_Date("LB859",calBP(2011-12960),1190);
         C_Date("LB861",calBP(2011-18540),1680){Outlier();color="red";};
C_Date("LB862",calBP(2011-11500),1030);
R_Date("Beta 307821",830,30);
};
   Boundary("Top");
  };
 };
```

BLACKWATER DRAW
AGE-SEQUENCE MODEL

```
Plot()
  {
Outlier_Model("Carbon",Exp(1,-10,2),U(0,4),"t");
   Sequence("Blackwater, Locality 1")
   {
    Boundary("Transition");
    Phase("Level B")
    {
R_Date("AA-2262",11810, 90){Outlier(Carbon,1);};
R_Date("AA-1375",11380, 150){Outlier(Carbon,1);};
R_Date("AA-87917",10933, 56){Outlier(Carbon,1);};
R_Date("AA-30454",10914, 72){Outlier(Carbon,1);};
    };
    Boundary("Transition");
    Phase("Level C: Clovis")
    {
R_Date("A-491",11630, 400){Outlier(Carbon,1);};
R_Date("A-481",11170, 360){Outlier(Carbon,1);};
R_Date("A-490",11040, 500){Outlier(Carbon,1);};
R_Date("AA-89168",10884, 67){Outlier(Carbon,1);};
R_Date("SMU-1880",10780, 110){Outlier(Carbon,1);};
R_Date("AA-1360",10580, 100){Outlier(Carbon,1);};
    };
    Boundary("Transition C-D1= YDB");
    Phase("Level D1: Black Mat")
    {
R_Date("AA-1362",10740, 100){Outlier(Carbon,1);};
R_Date("AA-39843",10526, 70){Outlier(Carbon,1);};
R_Date("A-4701",10470, 580){Outlier(Carbon,1);};
R_Date("AA-1364",10210, 110){Outlier(Carbon,1);};
R_Date("AA-1363",10160, 120){Outlier(Carbon,1);};
    };
    Boundary("Transition");
    Phase("Level D2")
    {
R_Date("A-380",10600, 320){Outlier(Carbon,1);};
R_Date("A-492",10490, 200){Outlier(Carbon,1);};
R_Date("A-386",10490, 900){Outlier(Carbon,1);};
R_Date("AA-87335",10376, 50){Outlier(Carbon,1);};
R_Date("AA-86575",10281, 58){Outlier(Carbon,1);};
R_Date("AA-1370",10260, 230){Outlier(Carbon,1);};
R_Date("A-1372",10250, 200){Outlier(Carbon,1);};
R_Date("A-488",10200, 250){Outlier(Carbon,1);};
R_Date("AA-2261",9950, 100){Outlier(Carbon,1);};
R_Date("A-379",9900, 320){Outlier(Carbon,1);};
    };
    Boundary("Transition");
    Phase("Level E")
    {
R_Date("A-489",9890, 290){Outlier(Carbon,1);};
R_Date("A-4703",10000, 910){Outlier(Carbon,1);};
```

```
R_Date("AA-87338",9889, 50){Outlier(Carbon,1);};
R_Date("AA-87337",9820, 110){Outlier(Carbon,1);};
R_Date("A-4705",9260, 320){Outlier(Carbon,1);};
    };
   Boundary("");
  };
 };
```

AGE-DEPTH MODEL
```
Plot()
 {
Outlier_Model("General", T(5), U(0,3),"t");
P_Sequence("Bull Creek",0.05,0.5)
  {
Boundary();

R_Date("Beta-184854",11070, 60){z=307.0;Outlier(0.05);};
R_Date("Beta-262540",10870, 70){z=293.5;Outlier(0.05);};
Date("Top of YDB"){z=289;Outlier(0.05);};
         R_Date("Beta-184853",10350, 210){z=270.5;Outlier();color="red";};
R_Date("Beta-262539",10640, 70){z=256;Outlier(0.05);};
R_Date("Beta-262538",10750, 70){z=239;Outlier(0.05);};
R_Date("Beta-180546",10850, 210){z=238;Outlier(0.05);};
R_Date("Beta-262537",10410, 70){z=226.5;Outlier(0.05);};
R_Date("Beta-184852",10400, 120){z=224.5;Outlier(0.05);};
R_Date("Beta-184851",9850, 90){z=156;Outlier(0.05);};
R_Date("Beta-191040",8670, 990){z=119;Outlier(0.05);};
R_Date("Beta-184850",7660, 80){z=82;Outlier(0.05);};
R_Date("Beta-191039",6200, 90){z=55;Outlier(0.05);};
Boundary();
  };
 };
```

COMBINE
```
Plot()
 {
Combine("Bull Creek")
  {
Prior("Bull_Creek_BETA_184854");
Prior("Bull_Creek_Beta_262540");
Prior("Bull_Creek_Top");
  };
 };
 };
```

AGE-SEQUENCE MODEL
```
Plot()
 {
Outlier_Model("Charcoal",Exp(1,-10,0),U(0,4),"t");
  Sequence("Daisy Cave")
  {
Boundary("Stratum K; bottom");
Phase("Lower section")
{
   R_Date("Stratum J: CAMS-14369", 11700, 70){Outlier("Charcoal",1);};
};
Boundary("Transition J to I");
Phase("Black mat section")
{
   R_Date("Stratum I: CAMS-9096", 11180, 130){Outlier("Charcoal",1);};
Boundary("Strata I1 and I2: YDB layer");};
Boundary("Stratum H");
Phase("Upper section")
{
   R_Date("Stratum G: CAMS-9094",10390,130){Outlier("Charcoal",1);};
   R_Date("Stratum F3: CAMS-8863",8810,80){Outlier("Charcoal",1);};
```

```
    R_Date("Stratum F1: CAMS-8867 ",8600,60){Outlier("Charcoal",1);};
    R_Date("Stratum E4: CAMS-8865",8040,60){Outlier("Charcoal",1);};
    R_Date("Stratum E1: CAMS-8866",7810,60){Outlier("Charcoal",1);};
    R_Date("Stratum C: CAMS-8862",6000,70){Outlier("Charcoal",1);};
    R_Date("Stratum A3: CAMS-9095",3110,60){Outlier("Charcoal",1);};
    R_Date("Stratum A1: CAMS-8864",3220,70){Outlier("Charcoal",1);};
   };
Boundary("Top");
  };
 };
```

INDIAN CREEK
AGE-SEQUENCE MODEL
```
Plot()
 {
Sequence("Indian Creek")
  {
Phase("Glacier Peak Tephra")
{
   R_Date("Beta-4951",11125,130);
};
Boundary("Transition");
Phase("Reworked tephra")
{
Boundary("Proxy-rich layer");
};
Phase("Upper section")
{
R_Date("Beta-4619",10980,110);
R_Date("Beta-4620",10160,80);
R_Date("RL-7753",9870,130);
R_Date("Beta-7752",9290,120);
R_Date("Beta-7751",8340,100);
R_Date("Lab # n/a",7980,80);
R_Date("Beta-5117",7210,110);
  };
Boundary("Top");
  };
 };
```

LAKE CUITZEO
AGE-DEPTH MODEL
```
Plot()
 {
Outlier_Model("Carbon",Exp(1,-10,10),U(0,4),"t");
P_Sequence("Lake Cuitzeo",0.1,0.1)
  {
Boundary();

R_Date("A 9770",42400,1000){z=910;Outlier("Carbon",1);};
        R_Date("WW 3364",28600,140){z=665;Outlier();color="red";};
R_Date("A 9359",32565,2885){z=610;Outlier("Carbon",1);};
R_Date("WW 8456",29880,280){z=535;Outlier("Carbon",1);};
R_Date("AZ 120*",26800,900){z=470;Outlier("Carbon",1);};
        R_Date("WW 8455",21440,100){z=440;Outlier();color="red";};
R_Date("WW 8454",22770, 120){z=400;Outlier("Carbon",1);};
        R_Date("WW 6423",29490,190){z=380;Outlier();color="red";};
        R_Date("WW 3576",28289,120){z=375;Outlier();color="red";};
        R_Date("WW 6422",23870,100){z=365;Outlier();color="red";};
R_Date("T11-M47",15500,130){z=335;Outlier("Carbon",1);};
        R_Date("WW 3375",32940,190){z=310;Outlier();color="red";};
Date("Proxies:282.5 cm"){z=282.5;Outlier("Carbon",1);};
Date("Proxies:277.5 cm"){z=277.5;Outlier("Carbon",1);};
R_Date("OS-71325 ",10550, 35){z=277;Outlier("Carbon",1);};
        R_Date("WW 3363",27360,130){z=275;Outlier();color="red";};
        R_Date("OS 7133C",21600,100){z=255;Outlier();color="red";};
        R_Date("WW 3362",21730,70){z=245;Outlier();color="red";};
        R_Date("T7-M31",17605,215){z=225;Outlier();color="red";};
```

```
              R_Date("WW 3361",14720,50){z=205;Outlier();color="red";};
R_Date("A 9354",8830,215){z=195;Outlier("Carbon",1);};
R_Date("A 9353",6165,70){z=135;Outlier("Carbon",1);};
R_Date("A 9352",1755,115){z=85;Outlier("Carbon",1);};

Boundary();
 };
 };
```

DATE CODE

For the date code below, we set boundaries and calculated the dates for the upper and lower depths of the YDB layer. Then, we used the "Date" code to calculate the age between them, based on the assumption that the true YDB date occurs between the two dates.

```
Plot()
 {
Sequence("Lake Cuitzeo")
 {
Boundary();

Prior("Cuitzeo_Proxies_282_cm");
   Date("YDB age");
Prior("Cuitzeo_Proxies_277_cm");

Boundary();
 };
 };
```

AGE-SEQUENCE MODEL

```
Plot()
 {
Outlier_Model("Carbon",Exp(1,-10,5),U(0,4),"t");
Sequence("Lake Hind")
 {
Boundary("Bottom");
Phase("Glaciated section")
{
         R_Date("Beta-375046",43500,300){Outlier();color="red";};
         R_Date("Beta-375047",36830,310){Outlier();color="red";};
};
Boundary("Transition 1");
Phase("Younger Dryas section")
 {
R_Date("UCIAMS 29317",10610,25){Outlier("Carbon",1);};
R_Date("Beta 116994",10420,70){Outlier("Carbon",1);};
};
   Boundary("Transition 2");
   Phase("Holocene section")
 {
R_Date("TO-7692",9250,90){Outlier("Carbon",1);};
R_Date("Beta 111142",6700,70){Outlier("Carbon",1);};
R_Date("Beta 165741",5760,50){Outlier("Carbon",1);};
R_Date("Beta 165740",5780,50){Outlier("Carbon",1);};
R_Date("Beta 109530",5350,50){Outlier("Carbon",1);};
R_Date("Beta 109900",4090,70){Outlier("Carbon",1);};
R_Date("Beta 109529",3250,70){Outlier("Carbon",1);};
R_Date("Beta 111143",2500,40){Outlier("Carbon",1);};
 };
Boundary("Top");
 };
 };
```

LINDENMEIER
AGE-SEQUENCE MODEL

```
Plot()
 {

Sequence("Lindenmeier")
```

```
  {
Boundary("Bottom");
Phase("Level B")
  {
R_Date("AA-51988",12170,80);
  };
Boundary("Transition 1");
Phase("Level C")
  {
Boundary("Interpolated");
  };
R_Date("Transition 2; I-141, YDB",10780,135);

Phase("Level D: Black Mat,Folsom")
  {
R_Date("TO-337",10560,110);
R_Date("TO-342",10500,80);
R_Date("TO-338",10040,80);
R_Date("TO-339",9880,100);
R_Date("TO-341",9690,60);
R_Date("TO-340",9330,70);
  };
Boundary("Transition 3");
Phase("Level F")
  {
        R_Date("TO-344",10060,100){Outlier();color="red";};
R_Date("A-749 AB",9440,180);
  };
  Boundary("Top");
 };
 };
```

AGE-SEQUENCE MODEL
```
Plot()
 {
Sequence("Lingen")
 {
Boundary("Bottom");
Phase("Prior to Younger Dryas")
{
R_Date("Oldest Dryas-1a (Ua-382)",12930,210);
R_Date("Bølling-1b (UtC-3196)",12480,90);
R_Date("Older Dryas-1c (GrN-926)",12065,120);
R_Date("Allerød-2a1 (GrN-10833)",11960,60);
R_Date("Allerød-2a2 (GrN-10883)",11600,50);
R_Date("Allerød-2b (GrN-925)",11305,120);
        R_Date("UCIAMS 46302",11310,60);
        R_Date("Beta-369246",10870,40);
R_Date("Allerod-2b, end (GrN-11569)",10880,50);
 };
Boundary("Transition=YDB");
Phase("Younger Dryas and Holocene")
{
R_Date("Younger Dryas-3a (GrN-6063)",10940,60);
R_Date("Younger Dryas-3b (GrN-17030)",10450,260);
R_Date("Younger Dryas-4a (GrN-12825)",10150,90);
R_Date("Holocene-4b (GrN-7756)",9850,90);
R_Date("Holocene-4c (IRPA-185)",9740,295);
R_Date("Holocene-5 (GrN-6035)",9530,55);
};
Boundary("Top");
 };
 };
```

AGE-SEQUENCE MODEL
```
Plot()
```

```
 {
Sequence("Lommel")
  {
Boundary();
   Phase("End Glacial")
{
C_Date("GLL-080704",calBP(2012-15300),1100);
C_Date("GLL-080714",calBP(2012-14500),1100);
};
   Boundary("Transition");
   Phase("B-A Coversands")
{
C_Date("GLL-080708",calBP(2012-14000),1000);
C_Date("GLL-080713",calBP(2012-13700),1000);
C_Date("GLL-080716",calBP(2012-13300),1000);
C_Date("GLL-080703",calBP(2012-13300),900);
C_Date("GLL-080715",calBP(2012-12700),900);
        C_Date("GLL-080707",calBP(2012-12400),900);
};
   Boundary("Transition");
   Phase("Usselo Horizon")
{
C_Date("GLL-080712",calBP(2012-12400),900);
        C_Date("GLL-080711",calBP(2012-10600),700){Outlier();color="red";};
R_Date("UCIAMS 46303",11480,100);
};
C_Date("Transition from Usselo",calBP(1950-12811),48);
   Phase("Coversands II")
{
C_Date("GLL-080706",calBP(2012-12300),800);
C_Date("GLL-080701",calBP(2012-12000),900);
C_Date("GLL-080705",calBP(2012-11700),800);
C_Date("GLL-080702",calBP(2012-11600),800);
C_Date("GLL-080710",calBP(2012-11500),800);
C_Date("GLL-080709",calBP(2012-11000),700);
};
Boundary();
 };
 };
```

MELROSE
AGE-SEQUENCE MODEL
```
Options()
 {
 BCAD=FALSE;
 kIterations=30;
};
Plot()
 {
Sequence("Melrose")
  {
C_Date("LB860b",calBP(2012-11701),1846);
R_Date("Beta-87422",-5,25){Outlier();color="red";};
R_Date("Beta-368791",850,30);
 };
 };
```

MUCUNUQUE
AGE-SEQUENCE MODEL
```
Plot()
 {
Sequence("Mucunuque (MUM7b)")
  {
Boundary();
{
R_Date("TO-9278c",11850,180);
R_Date("TO-9011",11760,80);
R_Date("TO-9278a",11440,100);
```

```
Prior("Mucunuque_5_lakes");
 };
Boundary();
 };
 };
```

COMBINE YD ONSET IN 5 AREA LAKES
```
Plot()
 {
COMBINE("MUM7b, nearby lakes")
{
R_Date("Valle Laguna Victoria",11045, 90);
R_Date("Paramo de Miranda",10954, 163);
R_Date("Lake Chonita",11005, 45);
R_Date("Laguna Verde Alta",11038, 165);
C_Date("Laguna de Los Anteojos",calBP(1950-12924), 80);

 };
 };
```

AGE-SEQUENCE MODEL
```
Plot()
 {
  Sequence("Murray Springs")
  {
   Boundary("");
   Phase("Unit E")
   {
R_Date("SMU-34",13980,190);
R_Date("TX-1235",13310,190);
R_Date("I-4562",12310,170);
R_Date("SMU-33",11880,250);
R_Date("SMU-18",11190,180);
};
   Boundary();
   Phase("Unit F")
   {
R_Date("TX-1044",12600,2440);
R_Date("A-805A/805B",11220,330);
R_Date("SMU-28",11210,200);
R_Date("SMU-43",11160,110);
R_Date("SMU-1463",10900,200);
R_Date("SMU-29",10790,150);
   };
   Boundary();
   Phase("Unit F, Clovis surface")
   {
R_Date("TX-1413",11080,180);
R_Date("TX-1462",10930,170);
R_Date("SMU-27",10890,180);
R_Date("SMU-41",10840,70);
R_Date("SMU-42",10840,140);
R_Date("A-1045",10760,100);
R_Date("SMU-19",10740,190);
R_Date("TX-1459",10710,160);
   };
   Boundary();
   Phase("Unit F2, Black mat at base")
   {
R_Date("AA-26212",10628,60);
R_Date("A-989b",10360,90);
R_Date("AA-26211",10325,44);
R_Date("A-977",10250,170);
R_Date("AA-26210",9823,46);
R_Date("TX-1460/1461",9820,110);
R_Date("TX-1184/1185",9820,110);
R_Date("TX-1238",9810,150);
```

```
      };
    Boundary("");
   };
  };
```

COMBINE

```
Plot()
{
Outlier_Model("Charcoal",Exp(1,-10,5),U(0,3),"t");
COMBINE("Murray Springs")
{
Prior("A_1045"){Outlier("Charcoal",1);};
Prior("SMU_19"){Outlier("Charcoal",1);};
Prior("SMU_27"){Outlier("Charcoal",1);};
Prior("SMU_41"){Outlier("Charcoal",1);};
Prior("SMU_42"){Outlier("Charcoal",1);};
Prior("TX_1413"){Outlier("Charcoal",1);};
Prior("TX_1459"){Outlier("Charcoal",1);};
Prior("TX_1462"){Outlier("Charcoal",1);};
  };
 };
```

OMMEN

AGE-SEQUENCE MODEL

```
Plot()
 {
Sequence("Ommen")
  {
Boundary("Bottom");
Phase("Prior to Younger Dryas")
{
R_Date("Oldest Dryas-1a (Ua-382)",12930,210);
R_Date("Bolling-1b (UtC-3196)",12480,90);
R_Date("Older Dryas-1c (GrN-926)",12065,120);
R_Date("Allerod-2a1 (GrN-10833)",11960,60);
R_Date("Allerod-2a2 (GrN-10883)",11600,50);
         R_Date("UCIAMS 46307",11440,35);
R_Date("Allerod-2b (GrN-925)",11305,120);
R_Date("Allerod-2b, end (GrN-11569)",10880,50);
 };
Boundary("Transition");
Phase("Younger Dryas and Holocene")
{
R_Date("Younger Dryas-3a (GrN-6063)",10940,60);
R_Date("Younger Dryas-3b (GrN-17030)",10450,260);
R_Date("Younger Dryas-4a (GrN-12825)",10150,90);
R_Date("Holocene-4b (GrN-7756)",9850,90);
R_Date("Holocene-4c (IRPA-185)",9740,295);
         R_Date("Beta-369946",9640,40);
R_Date("Holocene-5 (GrN-6035)",9530,55);
};
Boundary("Top");
 };
 };
```

SANTA MAIRA

AGE-SEQUENCE MODEL

```
Plot()
  {
  Sequence("Santa Maira")
  {
  Boundary("");
  Phase("Levels 4B and II")
   {
R_Date("Beta-75226",14310, 190);
R_Date("UCIAMS-52623",12615, 99);
R_Date("Beta-156023",11920, 40);
R_Date("Beta-131579",11620, 150);
R_Date("Beta-149948",11590, 70);
```

```
};
    Boundary("");
    Phase("YDB; Transition to YD")
    {
R_Date("Beta-75225",11020, 140);
};
    Boundary("");
    Phase("Levels 4A and I")
    {
R_Date("Beta-158014",9820, 40);
R_Date("Beta-131578",9760, 40);
R_Date("Beta-156021",9370, 40);
R_Date("Beta-156022",9220, 40);
R_Date("Beta-75224",5640, 140);
    };
    Boundary();
  };
 };
```

AGE-SEQUENCE MODEL

```
Plot()
 {
Outlier_Model("Carbon",Exp(1,-10,0),U(0,3),"t");
Sequence("Sheriden Cave")
  {
   Boundary("");
   Phase("Unit 5A, lower")
   {
R_Date("Beta-127908b-(E)",12840,100){Outlier("Carbon",1);};
R_Date("Beta-127908a-(E)",12590,450){Outlier("Carbon",1);};
R_Date("Beta-127907-(E)",12520,170){Outlier("Carbon",1);};
R_Date("Beta-139687-(E)",11860,40){Outlier("Carbon",1);};
R_Date("CAMS-12845-(E)",11610 70){Outlier("Carbon",1);};
R_Date("CAMS-12839-(E)",11570,70){Outlier("Carbon",1);};
R_Date("CAMS-33968-(E)",11570,50){Outlier("Carbon",1);};
R_Date("CAMS-12837-(E)",11480,60){Outlier("Carbon",1);};
};
   Boundary();
   Phase("Unit 5A upper; YDB charcoal")
   {
R_Date("Beta-127910",10960,60){Outlier("Carbon",1);};
R_Date("Beta-127909",10840,80){Outlier("Carbon",1);};
R_Date("UCI-38249-(C)",10915,30){Outlier("Carbon",1);};
   };
   Boundary();
   Phase("Unit 5B")
   {
R_Date("CAMS-10349-(E)",11060,60){Outlier("Carbon",1);};
   };
   Boundary();
   Phase("Unit 5C")
   {
R_Date("Beta-117607",10970,70){Outlier("Carbon",1);};
R_Date("Beta-117601",10940,70){Outlier("Carbon",1);};
R_Date("Beta-117602",10850,70){Outlier("Carbon",1);};
R_Date("CAMS-26783-(E)",10850,60){Outlier("Carbon",1);};
R_Date("AA-21710",10680,80){Outlier("Carbon",1);};
R_Date("Beta-117606",10620,70){Outlier("Carbon",1);};
R_Date("Beta-117603",10600,60){Outlier("Carbon",1);};
R_Date("Beta-117605",10570,70){Outlier("Carbon",1);};
R_Date("Beta-117604",10550,70){Outlier("Carbon",1);};
R_Date("Beta-139686",10440,40){Outlier("Carbon",1);};
};
   Boundary();
   Phase("Unit 6")
   {
R_Date("AA-21706",10020,115){Outlier("Carbon",1);};
```

```
R_Date("AA-21705",9775,70){Outlier("Carbon",1);};
R_Date("CAMS-24127",9190,60){Outlier("Carbon",1);};
R_Date("CAMS-24126",9170,60){Outlier("Carbon",1);};
   };
   Boundary("");
  };
 };
         COMBINE
Plot()
  {
Outlier_Model("Carbon",Exp(1,-10,0),U(0,3),"t");
COMBINE("Sheriden Cave")
  {
Prior("Beta_127909"){Outlier("Carbon",1);};
Prior("Beta_127910"){Outlier("Carbon",1);};
  };
 };
```

TALEGA
AGE-SEQUENCE MODEL

```
Plot()
  {
Outlier_Model("Charcoal",Exp(1,-10,0),U(0,3),"t");
Sequence("Talega")
  {
   Boundary("");
   Phase("Level 15-13")
   {
R_Date("Beta-196153",14980,70){Outlier("Charcoal",1);};
R_Date("Beta-192337",13070,40){Outlier("Charcoal",1);};
R_Date("Beta-192338",12310,10){Outlier("Charcoal",1);};
};
   Boundary();
   Phase("Level 12, YDB")
   {
R_Date("Beta-196150",11070,50){Outlier("Charcoal",1);};
R_Date("Beta-196151",11060,60){Outlier("Charcoal",1);};
};
   Boundary();
   Phase("Level 10-6")
   {
R_Date("Beta-196155",10540,50){Outlier("Charcoal",1);};
R_Date("Beta-196154",9830,50){Outlier("Charcoal",1);};
C_Date("Beta-196152",calBP(1950-10990),220){Outlier("Charcoal",1);};
C_Date("Beta 176904",calBP(1950-10960),220){Outlier("Charcoal",1);};
C_Date("Beta-176903",calBP(1950-8885),145){Outlier("Charcoal",1);};
C_Date("Beta-172976",calBP(1950-8820),200){Outlier("Charcoal",1);};
C_Date("Beta-194724",calBP(1950-8795),205){Outlier("Charcoal",1);};

   };
   Boundary();
  };
 };
```

TOPPER
AGE-SEQUENCE MODEL

```
Plot()
  {
  Sequence("Topper")
  {
  Boundary("");
  Phase("Level 2b")
  {
C_Date("UIC764",calBP(2009-14800),1500);
C_Date("UIC837",calBP(2009-14000),1200);
};
   Boundary();
   Phase("Level 3b base, Clovis")
```

```
    {
R_Date("AA100294",10958, 65);
};
    Boundary();
    Phase("Level 3b")
    {
C_Date("UIC763",calBP(2009-13200),1300);
C_Date("UIC1114",calBP(2009-13000),900);
C_Date("UIC1115",calBP(2009-11000),800);
C_Date("UIC836",calBP(2009-8000),800);
C_Date("UIC1229",calBP(2009-8000),500);
C_Date("UIC835",calBP(2009-7600),900);
C_Date("UIC782",calBP(2009-7300),800);
C_Date("UIC1228",calBP(2009-4300),300);
    };
    Boundary();
  };
 };
```

SYNCHRONEITY-SEQUENCE MODEL

```
Plot()
{
Outlier_Model("OLD",Exp(1,-10,1),U(0,3),"t");

Sequence("SYNCHRONICITY of YDB SITES")
    {
    Boundary("S");
    Phase()
    {
C_Date("Meerfelder Maar",calBP(1950-12680),127){Outlier("OLD",1);};
C_Date("Hulu speleothems, CHN",calBP(2000-12820),60){Outlier("OLD",1);};
R_Date("Late glacial tree-rings, GER",10980,20){Outlier("OLD",1);};
C_Date("Cariaco Basin varves",calBP(2000-12820),30){Outlier("OLD",1);};
C_Date("GISP2 platinum peak",calBP(2000-12887),260){Outlier("OLD",1);};
C_Date("GISP2 ice model",calBP(2000-12890),260){Outlier("OLD",1);};
C_Date("GRIP GICC05 ice model",calBP(2000-12896),138){Outlier("OLD",1);};

Label("AGE OF YOUNGER DRYAS ONSET");

Prior("Santa_Maira_MD"){Outlier("OLD",1);};
Prior("Ommen_MT"){Outlier("OLD",1);};
Prior("Mucunuque_5_lakes"){Outlier("OLD",1);};
Prior("Melrose_UD"){Outlier("OLD",1);};
Prior("Lake_Cuitzeo_YDB_age"){Outlier("OLD",1);};
Prior("Blackville_MD"){Outlier("OLD",1);};

Label("YDB: LOWER QUALITY");

Prior("Topper_MD"){Outlier("OLD",1);};
Prior("Talega_OMD"){Outlier("OLD",1);};
Prior("Lommel_MT"){Outlier("OLD",1);};
Prior("Lingen_MT"){Outlier("OLD",1);};
Prior("Lindenmeier_MD"){Outlier("OLD",1);};
Prior("Lake_Hind_MD"){Outlier("OLD",1);};
Prior("Indian_Creek_MT"){Outlier("OLD",1);};
Prior("Blackwater_MT"){Outlier("OLD",1);};
Prior("Barber Creek-MD"){Outlier("OLD",1);};

Label("YDB: MEDIUM QUALITY");

Prior("Sheriden_Cave_MOC"){Outlier("OLD",1);};
Prior("Murray_Springs_OMC"){Outlier("OLD",1);};
Prior("Daisy_Cave_MT"){Outlier("OLD",1);};
Prior("Bull_Creek_MC"){Outlier("OLD",1);};
Prior("Big Eddy-MC-allx1"){Outlier("OLD",1);};
Prior("Aalsterhut_MOT"){Outlier("OLD",1);};
Prior("Arlington-MT"){Outlier("OLD",1);};
Prior("Abu_Hureyra_MD"){Outlier("OLD",1);};
```

```
Label("YDB: HIGH QUALITY");
    };
    Boundary("E");
    };
  Difference("L","E","S");
};
```

DATE CODE for SYNCHRONICITY TEST

For the Date code below, we used the prior files for the upper and lower boundaries for the synchronicity plot of the 30 dates. Then, we used the "Date" code to calculate the age between them, based on the assumption that the true YDB date falls between the upper and lower age boundaries.

```
Plot()
 {
Sequence("Synchronicity")
 {
Boundary();

Prior("SYNCH_START");
   Date("LENGTH OF OVERLAP");
Prior("SYNCH_END");

Boundary();
 };
 };
```